UNIVERSITAT POLITÈCNICA DE VALÈNCIA

ESCUELA TÉCNICA SUPERIOR INGENIERÍA INDUSTRIAL VALENCIA

CHEMICAL ENGINEERING MASTERS THESIS

OPTIMISATION OF THE ANODIC HALF-CELL IN THE DANIELL CELL

AUTHOR: SUSAN WOODHOUSE
TUTOR: PROF. EMMA MARIA ORTEGA NAVARRO
COTUTOR: DR JUAN JOSÉ GINER SANZ

ACADEMIC YEAR: 2021-22

ACKNOWLEDGEMENTS

Firstly, I would like to thank all involved at both Strathclyde and UPV for their time and contribution to enabling the feasibility of this Erasmus placement.

I would like to express my gratitude to my project supervisors, Dr Juan José Giner Sanz and Prof. Emma Maria Ortega Navarro, for their consistent support, feedback and expert knowledge and advice throughout the completion of the project. I would also like to thank my other colleagues within the IEC department at UPV for being extremely welcoming and helpful.

I would like to thank my academic supervisor, Dr Edward Brightman, for the guidance and constructive feedback provided for this thesis development.

Lastly, I would like to thank my family and friends, especially my parents, my brothers and Jay, for their continual encouragement and support throughout the completion of this thesis and importantly the duration of my degree.

RESUMEN

Se requieren sistemas de almacenamiento de energía rentables y ecológicos para resolver la crisis energética actual. En 1836, el químico británico John Frederic Daniell inventó el modelo básico de la batería de zinc-cobre, conocida hoy como celda de Daniell. Inicialmente, esta batería se utilizó sustancialmente como batería estacionaria para repetidores de telegrafía remotos. Sin embargo, con la invención de las baterías modernas, ha quedado relegada, y hoy en día es solo una batería de demostracin, utilizada en las clases de química de todo el mundo para ilustrar la química redox. A pesar de perder su supremacía en el campo de las baterías, la batería de zinc-cobre presenta varias características (por ejemplo, costo, seguridad, impacto ambiental, densidad de energía, etc.) que la convierten en un sistema de almacenamiento de energía muy prometedor, siempre que se resuelvan sus inconvenientes.

El objetivo de este proyecto es optimizar la reacción de la semicelda andica de una celda Daniel. Para lograr esto, se probaron diferentes electrolitos utilizando voltametr as cíclica y lineal, y Espectroscop a de Impedancias Electroqu micas.

Para conseguirlo, se llev a cabo una optimización inicial del procedimiento de medida para intentar crear un montaje experimental estable y reproducible. Diversos factores, incluidos el rango de voltaje, la velocidad de barrido, el pretratamiento de los electrodos y la nitrogenación del electrolito, se modificaron para identificar formas de hacer que las mediciones de la celda sean reproducibles y fiables entre experimentos.

Post eriormente, se probaron electrolitos ácidos, neutros y alcalinos donde se utilizaron técnicas analíticas, incluido el análisis de Tafel y el análisis de Koutecky-Levich, para determinar cuantitativamente los parámetros cinticos en los diferent es medios. En base a estos result ados, se seleccion el medio ptimo.

Palabras clave: Ánodo, Baterías de zinc, Constantes de velocidad, Electrolito acuoso, Rendimiento electroquímico.

RESUM

Es requerixen sistemes d'emmagatzemament d'energia rendibles i ecològics per a resoldre la crisi energètica actual. En 1836, el químic britànic John Frederic Daniell va inventar el model bàsic de la bateria de zinc-coure, coneguda hui com a cel·la de Daniell. Inicialment, esta bateria es va utilitzar substancialment com a bateria estacionària per a repetidors de telegrafia remots. No obstant això, amb la invenció de les bateries modernes, ha quedat relegada, i hui en dia és només una bateria de demostracin, utilitzada en les classes de química de tot el món per a il·lustrar la química redox. A pesar de perdre la seua supremacia en el camp de les bateries, la bateria de zinc-coure presenta diverses característiques (per exemple, cost, seguretat, impacte ambiental, densitat d'energia, etc.) que la convertixen en un sistema d'emmagatzemament d'energia molt prometedor, sempre que es resolguen els seus inconvenients.

L'objectiu d'este projecte és optimitzar la reacció de la semicelda andica d'una cel·la Daniel. Per a aconseguir açò, es van provar diferents electròlits utilitzant voltametr as cíclica i lineal, i Espectroscop a d'Impedàncies Electroqu miques.

Per a aconseguir-ho, es llev a cap una optimització inicial del procediment de mesura per a intentar crear un muntatge experimental estable i reproduïble. Diversos factors, inclosos el rang de voltatge, la velocitat d'agranat, el pretractament dels elèctrodes i la nitrogenación de l'electròlit, es van modificar per a identificar formes de fer que els mesuraments de la cel·la siguen reproduïbles i fiables entre experiments.

Post eriormente, es van provar electròlits àcids, neutres i alcalins on es van utilitzar tècniques analítiques, inclòs l'anàlisi de Tafel i l'anàlisi de Koutecky-Levich, per a determinar quantitativament els paràmetres cinticos en els diferent és mitjans. Basant-se en estos result ados, se selecció el mig ptimo.

Paraules clau: Ànode, Bateries de zinc, Constants de velocitat, Electròlit aquós, Rendiment electroquímic.

ABSTRACT

Cost-effective and eco-friendly energy storage systems are required to solve the actual energy crisis. In 1836, the British chemist John Frederic Daniell invented the basic model of the zinc-copper battery, known today as the Daniell cell. Initially, this battery was substantially used as a stationary battery for power remote telegraphy repeaters. However, with the invention of modern batteries, it has been relegated, and today it is just a reference standard battery, used in all-around-the-World chemistry classes to illustrate redox chemistry. Despite losing its supremacy in the battery field, the zinc- copper battery presents several characteristics (e.g., cost, safety, environment impact, energy density, etc.) that make it a very promising energy storage system, provided that its drawbacks are solved.

The aim of this project is to optimise the anodic half-cell reaction in a Daniel cell. To achieve this, different supporting electrolytes will be tested of varying pH using cyclic and linear voltammetry and electrochemical impedance spectroscopy. The use of a rotating disc electrode (RDE) will be used to examine the effect of mass transfer limitations within the reaction.
To achieve this, initial optimisation of the measurements of the half-cell will be carried out to try to create a stable and reproduceable experimental set-up. Varying factors including voltage range, scan rate, pre-treatment of the electrodes, nitrogenation of the electrolyte, will be altered to identify ways to make the cell measurements reproducible and reliable between experiments.

Acidic, neutral, and alkaline electrolytes will be tested where analytical techniques, including Tafel analysis and Koutecky-Levich analysis, will be used to quantitively determine kinetic and mass transfer reaction parameters enabling comparison between the different medias tested. A discussion of the electrolyte media which best supports the anodic half-cell will be concluded.

Key words: anode, aqueous electrolyte, electrochemical performance, rate constants, zinc batteries.

INDEX

INDEX OF THE MAIN DOCUMENT

INDEX OF BUDGET

COVER OF THE REPORT

The energy crisis, climate change and environmental pollution are issues directly related to the increasing energy demands. Renewable energy appears to be the best solution; however, the lack of efficient energy storage systems currently inhibits their full development.

The Daniell Cell was one of the first batteries to be developed, once broadly used in the telegraph industry, however now, it is used as an educational concept. It was replaced by rechargeable, more powerful batteries. Due to the advantageous properties of zinc, revival of the Daniell cell has been ignited in research.

In this work, voltammetric experiments were completed to calculate the important kinetic parameters of the electrochemical reaction, i.e., the Tafel slope and the exchange current density. Firstly, the experimental setup was optimised by varying different experimental parameters, e.g., voltage range, scan rate, need of nitrogenation, to improve the reproducibility of the experiments. A voltage range of -1.5 to -0.5 V and a scan rate of 10 mV/s were selected. it was concluded that nitrogenation was unnecessary. Secondly, different electrolytes (HCl, H_2SO_4, CH_4O_3S, NaOH, NaCl and Na_2SO_4) were tested, obtaining the kinetic parameters of the reaction in each of them. The concentration of Zn^{2+} was found to affect the reaction kinetic parameters, therefore a fixed concentration of 1 M was chosen to be added to the electrolytes. This enabled investigation of two concepts: a new cell representing a "fully charged" cell - where no zinc ions are present; and a used cell representing a "partially discharged" cell - where zinc ions are present due to its use.

For a "fully charged" cell, the NaCl electrolyte was found to best optimise the anodic reaction due to its high conductivity (152 ± 0.4 mS/cm), low anodic Tafel slope (80 ± 24 mV/dec) and relatively high anodic exchange current density (1.7 ± 0.01 mA/cm^2).

For a "partially discharged" cell, no electrolyte media appeared outrightly advantageous. The NaCl electrolyte media was also found to have the greatest conductivity (142 ± 0.1 mS/cm). However, the anodic Tafel slope was minimal in the acidic media – H_2SO_4 (68 ± 3 mV/dec) and CH_4O_3S (70 ± 1 mV/dec), but with low exchange current density (4.4 ± 0.01 mA/cm^2 and 1.3 ± 0.01 mA/cm^2, respectively). The greatest anodic exchange current density was found in HCl media (19 ± 0.01 mA/cm^2). The lowest cathodic Tafel slope was found for CH_4O_3S media (62 ± 4 mV/dec), while HCl enabled the greatest cathodic exchange current density (18 ± 0.01 mA/cm^2).

A similar investigation could be completed for the cathodic half-cell and combined with this works findings resulting in complete optimisation of the full Daniell cell.

Chapter 1. Introduction

1.1 Introduction

The world requires to change in order to solve the problems of climate change, environmental pollution and energy resources. Fossil fuels – including oil, coal, and natural gas – have been energising economies for over 150 years and currently supply approximately 80% of the world's energy according to the Environmental and Energy Study Institute (EESI) (1). However, due to their negative impact on the environment and diminishing supplies, alternative energy sources must be found.

Renewable energies appear to be the best possible solution to reduce society's dependence on non-renewable sources and would improve society's sustainability. In comparison to non-renewable energies, renewable energy is much more inconsistent and requires an efficient energy storage system to allow surplus energy to be used later. Batteries are the primary method of energy storage, but their technology lags behind the advances of wind and solar production.

Batteries have been a key invention, as without them modern comforts including computers, vehicles and communication devices may not have been possible. Luigi Galvani – an Italian scientist – discovered electricity in the 1740s through the experimentation with frogs' legs, noticing that their muscles contract when in contact with copper and iron as long as the iron and copper are also connected. This is the first documented electric circuit. Although at the time, Galvani was unsure of what he had discovered – this observation laid the fundamentals of battery technology and the basis of converting chemical energy into electrical energy. This type of device is known today as a galvanic cell. Alessandro Volta – an Italian physicist – developed the voltaic pile in the 1800s by investigating the contact voltage of various metals creating the galvanic voltage series. The development of the galvanic cell and voltaic pile triggered the development of electrochemistry in the 19th century (2). Table 1. 1 displays the timeline of battery evolution.

The world demand for primary and secondary batteries is predicted to grow by 8.1% per year to a worth of $156 billion in 2024. Growth specifically is focused in secondary (rechargeable) batteries due to their use in mobile phones and tablets (3). Figure 1. 1 shows an overview of the revenue contributions from different battery chemistries, where it can be seen Li-ion batteries dominate today.

Performance of a battery is characterised by its specific energy, where greater specific energy translates to longer runtime; and specific power that enables producing higher currents (Figure 1. 2). Figure 1. 2 shows the different battery technologies in terms of specific energy and specific power.

Table 1. 1 - Timeline of key battery developments (2,4)

Year(s)	Development/Use	Characteristics
1740s	1st electro-chemical battery	Luigi Galvani, experimentation with frogs' legs using copper, iron, and an electrolyte.
1800s	Voltaic pile	Alessandro Volta, creation of the voltaic pile by layering copper and zinc plates with layers of cardboard soaked in brine. 1st continuous source of electricity.
1802	1st rechargeable battery	Johann Wihelm Ritter – German physicist – developed the first rechargeable battery using copper and cardboard sheets layered soaked in salt.
1854	1st Lead-Acid battery	Wihelm Josef Sinsteden – German physicist - created the first lead acid battery by placing two large lead plates in diluted sulphuric acid.
1899	Idea of a gas-tight battery using nickel-cadmium	Waldermar Junger – Swedish inventor – thought of keeping the electrolyte unchanged during charging and discharge, unlike all previous cells, enabling the gas-tight cells.
1950 – 1990s	Large production of gas-tight batteries	Their use in new portable applications like cordless telephones and remote controls put them in high demand. They were faded out in the 1990s due to the toxicity of cadmium.
1991	1st Lithium-ion (Li) battery	Michael Stanely Whittingham – British chemist - patented the first viable Lithium-based battery in 1976 but John B Goodenough – American physicist – pursued its development. Sony brought to market the first lithium-ion battery offering high energy density, durability, and low weight.

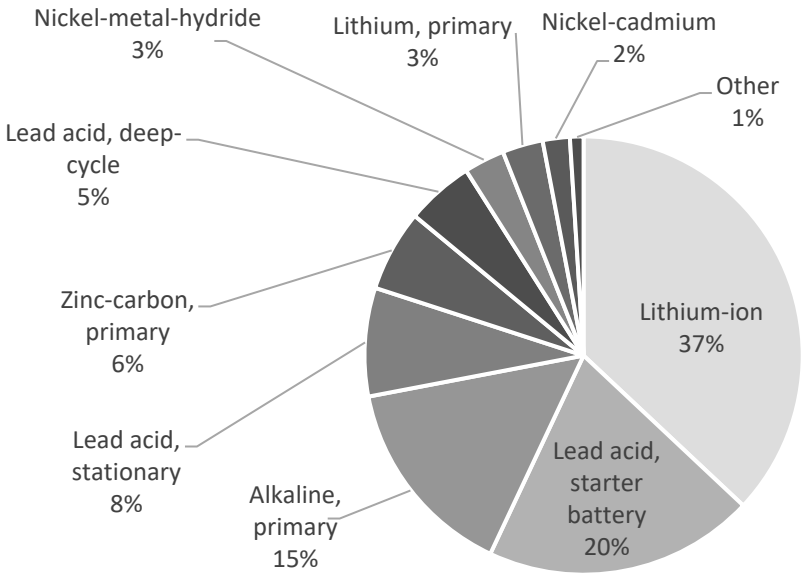

Figure 1. 1 – Revenues contributions from different battery chemistries (2).

Currently, the best performing battery based on specific energy and power is the secondary lithium metal (Li-metal). However, solid lithium is known to form metal dendrites – a tree-like structure of

crystals – causing short circuits and are therefore not used. Li-ion batteries are the next best (3), hence reinforcing their popularity in many applications.

Depletion of the lithium reserves, as well as the negative environmental impact and safety issues associated with lithium-ion batteries, has ignited the quest for alternative solutions. Zinc-based batteries have been identified as one of the most compelling substitutes due to their intrinsic safety, low cost, and high performance. Zinc is the 24th most frequent element on Earth, representing 76 ppm of the Earth's Crust and is deposited worldwide. It is completely recyclable, mainly with the help of the Waelz process (5).

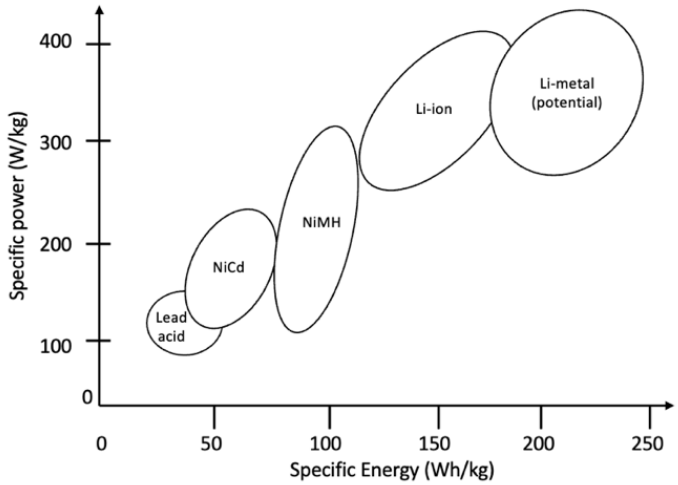

Figure 1. 2 – The specific energy (capacity a battery can hold in watt-hours per kilogram) and specific power of rechargeable batteries (the battery's ability to deliver power in watts per kilogram) (3)

The advantageous properties of zinc have sparked revival of the Daniell cell. The Daniell cell – created by John Frederick Daniell in 1836 – is a twist on the classic electrical cell to try to create a longer lasting source of power. It was the first highly reliable and practical electric battery, and broadly used in static machines, especially in the European telegraph industry (19th century).

The Daniell cell consists of two half-cells: the anodic half-cell consisting of zinc (the anode) in a zinc containing electrolyte, and the cathodic half-cell consisting of copper (the cathode) in a copper containing electrolyte. The standard potential of this cell is approximately 1.1 V at 25^{o}C. The half cells are separated by a porous material which allows the ions to exchange for electric continuity. Oxidation occurs at the zinc electrode where electrons are generated (anodic reaction), while reduction occurs at the copper electrode (cathodic reaction) where the electrons are consumed. They flow through an external electric circuit. The reactions occurring are shown below:

Anodic:	$Zn_{(s)} \rightarrow Zn^{2+}_{(aq)} + 2e^-$	$E^o = -0.7618$ V
Cathodic:	$Cu^{2+}_{(aq)} + 2e^- \rightarrow Cu_{(s)}$	$E^o = +0.340$ V
Global:	$Cu^{2+}_{(aq)} + Zn_{(s)} \rightarrow Zn^{2+}_{(aq)} + Cu_{(s)}$	$E_{cell} = 1.1018$ V

Due to the issues associated with its structure, e.g., liquid electrolyte spillages and breakages due to their glass structure, its use was not transferable to mobile machines. To date, its common use is for educational purposes to demonstrate how batteries work and teach the fundamentals of electrochemistry (6).

The Daniell cell is a primary battery and cannot supply a steady current for a long period of time. The goal is to develop a rechargeable Zn/Cu battery. However, there are two key obstacles preventing this: the tendency of zinc to electroplate as dendrites which inhibits the batteries' cyclic life, and the crossover of the copper ions (Cu^{2+}) to the anodic compartment during open circuit and recharging, causing the capacity loss of the battery.

Chapter 2. Objectives and Structure

2.1 Project Objectives and Learning Objectives

The project specific objectives include:

- Optimisation of the experimental procedure (including voltage range, scan rate, pre-treatment and nitrogenation) to maximise the reproducibility between experiments.
- Apply different analytical techniques to qualitatively and quantitively assess the reaction kinetics of the electrochemical reactions that take place in the anodic half-cell.
- Study the effect of the electrolyte on the anodic half-cell reaction kinetics.

In addition to the investigation aims, several personal learning objectives were set:

- Develop a widespread understanding of electrochemical techniques and the significance of the organisation's research.
- Improve practical analytical ability and gain experience working within a research team using advanced laboratory equipment.
- Apply theoretical knowledge to practical work, while learning independently and overcoming language and communication barriers.

2.2 Document Structure

This report will outline the purpose of the project providing background information for the reason of study. Project specific and personal objectives for the report will be stated. A review of similar battery chemistries will be detailed, highlighting the gap in literature, reinforcing the motive for this investigation. The underlying theoretical content will be provided, followed by the method used to collect and analyse data. The results collected from the experiments will be presented, where a discussion between the various electrolytes tested will provide comparison to identify the electrolyte conditions which best optimises the anodic half-cell. All findings will be concluded.

2.3 Purpose of Project

The main purpose of this project is to optimise the anodic half-cell of the Daniell cell by identifying which electrolyte favours the dissolution (oxidation) and deposition (reduction) of zinc. A variety of electrolytes will be tested to investigate their effect on the kinetics of these electrochemical reactions in a "fully charged" and "partially discharged" cell.

The ultimate aim of this work is to assist in the development of creating a rechargeable Daniell cell to help tackle the current energy crisis and support renewable energy technologies.

Chapter 3. Background

3.1 Literature Review

3.1.1 Developments of the Daniell Cell

The first zinc-based battery created was the voltaic pile in 1800, followed by the Daniell cell ($Zn_{(S)}|Zn^{2+}_{(aq)}||Cu^{2+}_{(aq)}|Cu_{(s)}$) in 1836. Since then, many Zn metal electrode batteries in varying types of electrolytes have been developed (see Figure 3. 1). The traditional telegraphic Daniell cell is a non-rechargeable primary cell - a primary cell describes a cell in which the electrical energy is generated within the cell itself and cannot be reused, whereas in a secondary cell the electrical energy is not generated within the cell itself but previously stored in it from an external source. The Daniell cell is not rechargeable as the porous barrier is unable to prevent the flow of copper ions into the anodic compartment (9).

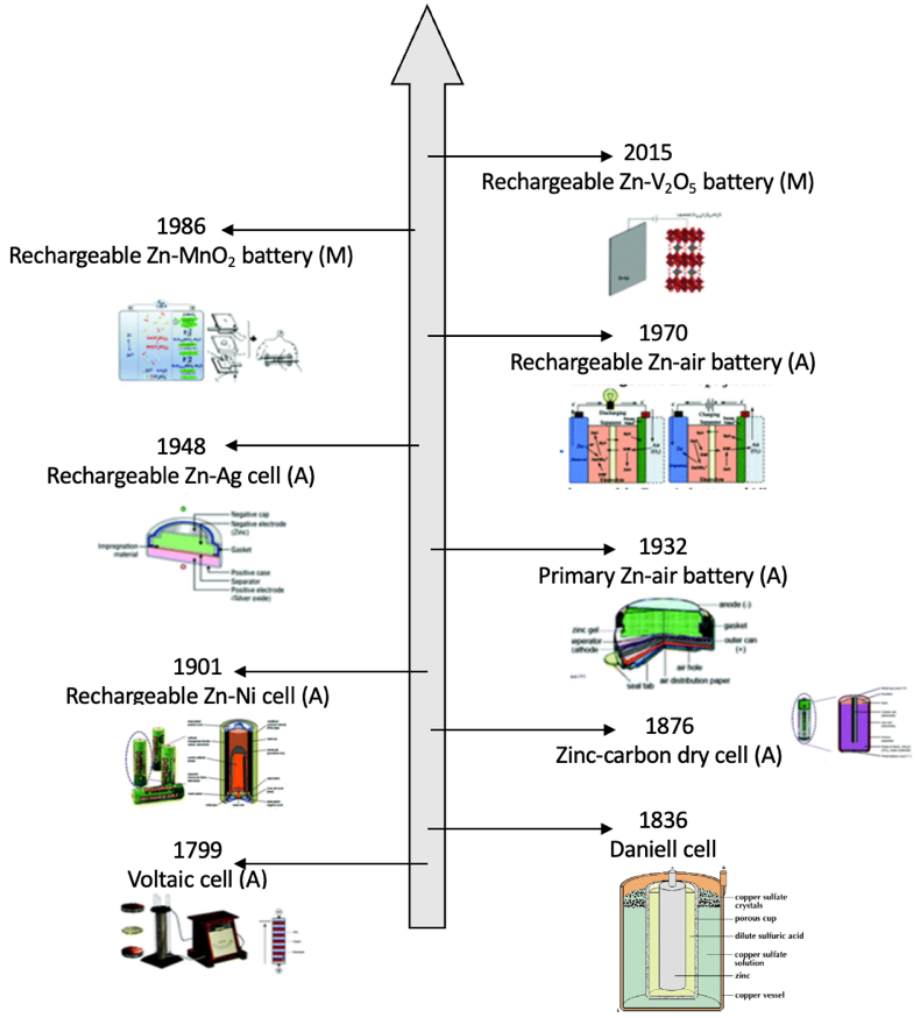

Figure 3. 1 – Timeline of the development of zinc metal electrode batteries used in different alkaline and mild electrolytes (9)

Reconsideration of the Daniell cell as candidate for large-scale energy storage has been proposed due to both Zn and Cu having low toxicity, as well as being renewable and reusable. The great challenge

of dealing with the Cu^{2+} crossover during the operating process still remains a large problem. Xiaoli Dong, Younggang Wang and Yongyao Xia from Fudan University in Shanghai (China) aimed to re-build the Daniell cell using a Li-ion exchange film. They used a ceramic lithium super-ionic conductor (LATSP, $Li_{1+x+y}Al_xTi_{2-x}Si_yP_{3-y}O_{12}$) thin film to separate both compartments to create a stable and rechargeable Zn-Cu battery. They found the battery could be recycled 150 times without obvious capacity fading and the open circuit voltage remained stable for over 100 hours without loss of capacity. They stated that the rechargeable Zn-Cu battery could be considered a promising power source for large-scale energy storage and has a theoretical energy density compatible with current aqueous rechargeable batteries. However, this technology may only be suitable for solar energy storage at this present stage due to its charge rate being limited by the low conductivity of the ceramic LATSP film. Further investigation of the conductivity of the ion-exchange membrane and optimisation of the operating temperature is still required (10).

Rafael Trócoli and Fabio La Mantia investigated an aqueous zinc-ion battery based on copper hexactanoferrate (CuHCF). They used a nontoxic, noncorrosive, and low-cost aqueous electrolyte (20 mM $ZnSO_4$), with an experimental set up containing a CuHCF working electrode, Zn foil counter electrode and a silver/silver chloride (Ag/AgCl) reference electrode. It was found to provide 90% of the theoretical capacity with a retention of 96.3% after 100 cycles with a current density equivalent to 1C and an average discharge potential of 1.73 V. [Note: a rate of nC in this study is defined as a full charge or discharge in 1/n hours]. The battery was found to generate a specific power at 10C comparable to organic batteries based on $Li_4Ti_5O_{12}$ and $LiFePO_4$. The performance, scalability, cost and safety of the cell were stated to make it optimal for stationary storage applications of renewable energies (11).

Sreemannarayana Mypati, Ali Khazaeli and Dominik P.J. Barz investigated a novel rechargeable zinc-copper battery without a separator, which is normally required to prevent copper ion crossover and for zinc dendrite growth. This research team proposed using electrolytes made from hydrogels. One of their hydrogels was formulated such that it coordinated the copper ions but allowed unhindered transfer of sodium ions which were exchanged between the electrodes to maintain electro-neutrality (12).

Jameson, Khazaeli and Barz modified the classic Daniell cell design by introducing a cation exchange membrane as a half-cell separator along with a sodium-based background electrolyte. This was attempted to prevent the copper ion crossover but enabled ion exchange. They also performed experiments to determine the superiority between sulphate-, chloride-, or nitrate-based electrolytes. Their study concluded the battery was able to charge and discharge for 100 cycles without significant degradation (13).

3.1.2 Other Zinc-Based Batteries

The development of rechargeable zinc – air batteries has been considered, as they are well-established primary cells, with common use in hearing aids and medical pagers. Their high energy density, safety and environmental benefits plus the abundance of air make them ideal candidates for large energy storage (14). Many investigated the effect of the electrolyte pH due to its link to zinc's reactivity (Table 3. 1 shows the variation in equilibrium potential with the media type).

Table 3. 1 – Examples of zinc half-cell reactions in aqueous electrolytes of different pH (14)

Aqueous electrolyte	Reaction on zinc electrode	E^0 (V)
Acid	$Zn_{(s)} \leftrightarrow Zn^{2+}_{(aq)} + 2e^-$	1.250
Neutral	$Zn_{(s)} \leftrightarrow Zn^{2+}_{(aq)} + 2e^-$	-0.762
Alkaline	$Zn_{(s)} + 2OH^-_{(aq)} \leftrightarrow ZnO_{(s)} + H_2O_{(l)} + 2e^-$	-0.762

In addition, aqueous Zn-ion batteries have also received attention due to their high energy density, ionic conductivity, safety, environment-friendliness, and low fabrication cost (3 – 5 times lower than lithium-ion batteries) (15). Many studies investigate the factors which impact their performance: cathode material, electrolyte, and separator, however often neglecting the impact of the Zn anode (16).

3.1.3 Conclusion to Literature Findings

From literature, it was apparent to the best of my knowledge, that no studies have been completed focusing on the optimisation of the anodic half-cell reaction of the Daniell cell through the variation of the electrolyte.

3.2 Theory

3.2.1 Aqueous Electrolytes

Aqueous rechargeable batteries are stated to be promising alternatives to Li-ion batteries (LIB) due to water being flame retardant (preventing the dangers of fire or explosion), lower in cost than organic solvents, can be assembled in air, display greater ionic conductivity and are environmentally benign. To date, aqueous Zn-based batteries are far from suitable, regardless of the electrolyte used. Poor reversibility of the Zn anode in an aqueous electrolyte causing a low coulombic efficiency (CE) – the ratio of the output of charge by a battery to the input of charge - has largely hindered their development (17). The few papers which have tested this have failed to distinguish the difference of Zn behaviour in mild and alkaline media, where it faces distinct reaction mechanisms and redox potentials. Different challenges are presented in the electrolyte type, i.e., issues associated with electrode shape change, dendrite growth, passivation and H_2 evolution in alkaline media, and alternative unwanted side reactions in mild electrolytes. Dendrite growth, electrode corrosion and H_2 are challenges both electrolyte medias face (9) – summarised in Figure 3. 2.

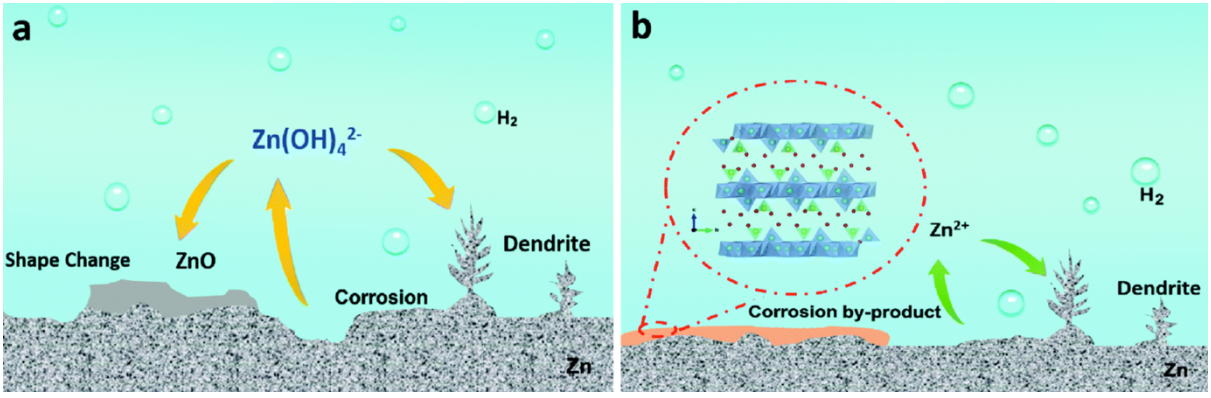

Figure 3. 2 - A schematic diagram of Zn electrode problems in (a) alkaline electrolytes and (b) mild electrolytes. In the alkaline media, the problems include corrosion, passivation, shape change, dendrite growth and H_2; and in mild media, the issues include electrode corrosion, H_2 evolution and dendrites formation. The corrosion product included is $Zn_4(OH)_6SO_4xH_2O$ which is a by-product in $ZnSO_4$ electrolyte (9)

Zn alkaline systems – for a typical rechargeable Zn-air battery – contain a Zn anode, an air electrode, an alkaline electrolyte, and a separator, where the electrolyte typically contains LiOH, NaOH and KOH, with KOH being the most tested one due to its fast electrochemical kinetics, high ionic conductivity of K^+ and high solubility of Zn. A mild Zn-ion battery (ZIB) usually consists of a Zn metal anode, cathode for hosting ions, a mild electrolyte containing soluble salt(s) like $ZnCl_2$, $ZnSO_4$, and a cathode of similar structure of a LIB (9).

The different electrolytes create different working environments causing the Zn electrode to experience differing reaction mechanisms (Table 3. 2). In alkaline systems, during discharge, the Zn electrode oxidises to form zincate ions ($Zn(OH)_4^{2-}$),converts to Zinc Oxide (ZnO), then vice versa when charging. In mild systems, only Zn plating and stripping occurs during the charging and discharging

process. The different reaction mechanisms affect the redox potentials impacting the output voltage (see Table 3. 1), energy densities and create different complications for the Zn electrode (9).

The performance of the Zn-based batteries is both dependent on the Zn electrode performance and the interaction between the electrolyte and electrode. To improve the performance of Zn-based batteries, electrolyte additives have been tested to suppress the issues previously stated. The addition of electrolyte salts have an impact on the pH, ionic conductivity, electrochemical stability, reaction kinetics and reversibility of the Zn anode. Although a variety of approaches have been investigated to improve the aqueous Zn-based battery, the Zn electrode behaviour is still inconclusive in mild and alkaline electrolytes (9).

Table 3. 2 – Reaction mechanisms with Zn anode in alkaline and mild electrolyte media (9)

Electrolyte Type	Discharge	Charge
Alkaline (pH > 7)	$Zn_{(S)} + 4OH^-_{(aq)} \rightarrow Zn(OH)^{2-}_{4\,(aq)} + 2e^-$ $Zn(OH)^{2-}_{4(aq)} \rightarrow ZnO_{(S)} + 2OH^-_{(aq)} + H_2O_{(l)}$	$ZnO_{(S)} + 2OH^-_{(aq)} + H_2O_{(l)} \rightarrow Zn(OH)^{2-}_{4\,(aq)}$ $Zn(OH)^{2-}_{4\,(aq)} + 2e^- \rightarrow Zn_{(S)} + 4OH^-_{(aq)}$
Mild (pH ~7, and slightly acidic)	$Zn_{(S)} \rightarrow Zn^{2+}_{(aq)} + 2e^-$	$Zn^{2+}_{(aq)} + 2e^- \rightarrow Zn_{(S)}$

3.2.2 Nernst Equation

The Nernst equation expresses the relationship between the cell potential to the standard potential and to the activities of the electrically active species:

$$E = E^0 + \frac{RT}{nF}\ln\left[\frac{C_O}{C_R}\right] \quad \text{Eq. 1}$$

Where E^0 is the standard reversible potential, R is the universal gas constant, T is the temperature, n is the number of electrons, F is Faraday's constant, C_O and C_R are the concentration of the oxidised and reduced species. The ratio of $[C_O/C_R]$ is usually in terms of activity, however it can be assumed equal to molar concentration at low concentrations.

It enables the determination of the maximum cell voltage, E. As current flows, polarisation losses occur, namely activation, mass transport, and ohmic, which reduces the cell voltage (18).

3.2.3 Conductivity and Resistivity

An important property of an electrolyte in a battery is its electrical conductivity and resistivity. The electrical transport properties dictate its electrical conductivity, with conductivity (σ) being inversely proportional to resistivity (ρ) (19).

3.2.4 Tafel Equation

The swiss chemist, Julius Tafel, empirically developed the Tafel equation (Eq. 2) in 1905. He summarised extensive experimental data for the hydrogen evolution reaction (HER) on metals observing the relationship of overpotential, opposed to the absolute potential, to the logarithm of the current density. At that time , Tafel was unaware of his contribution to the electrochemical field and of the physical meaning of his equation (20).

$$\eta = a + b\log(i) \qquad \text{Eq. 2}$$

Where η is the overpotential ($E - E^o$), i is the current, and a and b are Tafel constants.

It has since been shown that his empirical relationship is related to fundamental principles. The Butler-Volmer (BV) equation (Eq. 3) – a critical equation in electrochemistry which describes the relationship between the current density and the overpotential associated with overcoming the reaction barrier - was published near to 27 years after Tafel printed his work. The Tafel equation stems from fundamental electrochemical principles and can in fact be derived from the Butler-Volmer (BV) equation (20).

$$i = i_0 \exp\left[\frac{\alpha n F\eta}{RT} - \frac{(1-\alpha)nF\eta}{RT}\right] \qquad \text{Eq. 3}$$

Where i_0 is the exchange current density and α is the charge transfer coefficient. All other parameters are the same as previously defined.

To derive the Tafel equation from the BV equation, the system must be operating at large overpotentials (η > 50 -100 mV). In such conditions the second term in the BV equation can be neglected, simplifying to (21):

$$i = i_0 \exp\left[\frac{\alpha n F\eta}{RT}\right] \qquad \text{Eq. 4}$$

And therefore:

$$\eta = \frac{RT}{\alpha Fn}\ln(i) - \frac{RT}{\alpha Fn}\ln(i_0)$$

Herein, it can be seen the constants, a, and b, in Eq. 2 equal:

$$a = -\frac{2.303RT}{\alpha Fn}\log(i_0) \text{ and } b = -\frac{2.303RT}{\alpha Fn}$$

The Tafel equation enables determination of the exchange current density – the rate at which the oxidised and reduced species transfer electrons with the electrode providing information of the associated energy barrier in the reaction – through the intercept of the linear region on a Tafel plot (TP). The slope of this line (Tafel slope) provides information on how responsive the current is to a change in the applied potential due to the effect of voltage losses. These parameters are found using a Tafel plot (TP) (Figure 3. 3(a)).

As shown in Figure 3. 3(b)) curved TPs can occur. The curvature is a result of the depletion in the oxidised (O) and reduced (R) species at the surface of the electrode (i.e., mass transfer limitations). An assumption of the Tafel analysis is the concentration of the oxidised (C_O) and reduced (C_R) species are the same at the surface as in the bulk, where the composition of the solution remains unchanged. It is, therefore, essential to correct the data for concentration depletion before determining b and i_0. An appropriate mass transfer coefficient - also referred to as the Koutecky-Levich compensation (22) – is used to correct:

$$i_k = \frac{i_l i}{(i_l - i)} \qquad \text{Eq. 5}$$

Where i_K is the kinetic current density and i_l is the limiting current density.

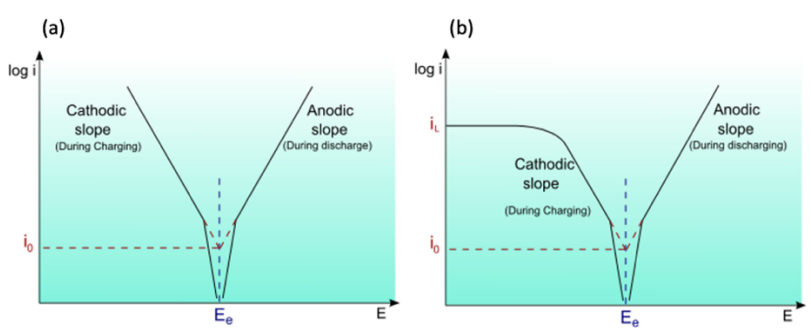

Figure 3. 3 - Typical Tafel Plots where log(i) is plotted against E. (a) Displays no mass transfer limitations (b) Displays a Tafel curve showing the diffusion limiting current (23).

Chapter 4. Methodology

4.1 Experimental Work

4.1.1 The Electrochemical Cell

All experiments were completed in a cell similar to the one shown in Figure 4. 1. A minor adjustment to the original cell was made, where the addition of a Luggin Capillary tube filled with the same electrolyte as the cell was used, as seen in the diagram, as opposed to the reference electrode (RE) directly immersed in the electrolyte in the cell. The reason for the change will be discussed in Section 5.1.4. Photographs of the experimental set up are shown in Appendix A.1.

The working electrode (WE) was a zinc 8 mm diameter electrode (99.99% Chempur). The WE was supported using a rotating disk electrode (RDE). A platinum (Pt) counter electrode (CE) was used to complete the electrical circuit and was selected due to its inertness. The area of the CE exceeded the area of the WE to avoid CE effects on the results. Silver/silver chloride (Ag/AgCl) electrode was used as the reference electrode (RE) due to its stable potential. Clamps were used to hold the RE and WE at a stable position. The tip of the Luggin capillary – RE system was held also by a clamp as close as 2 mm to prevent shielding of the electrode. All experiments were completed at room temperature.

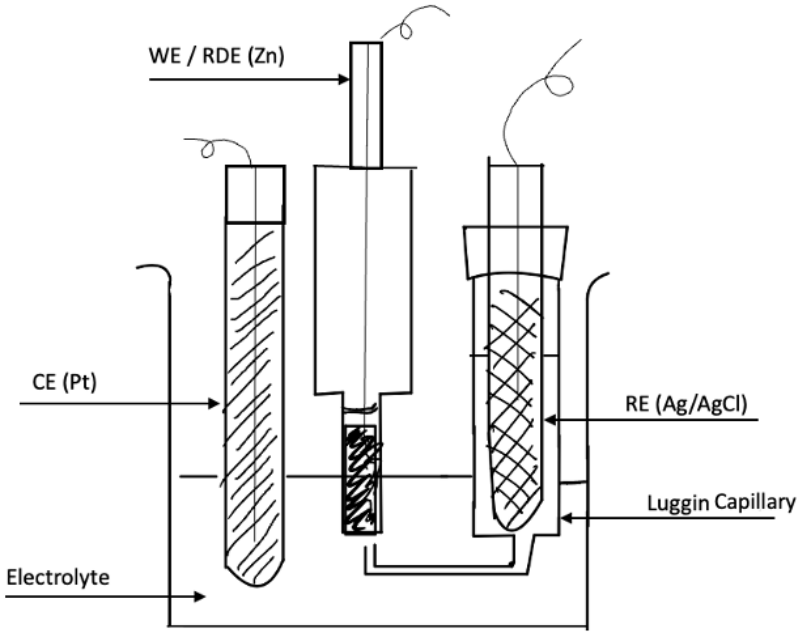

Figure 4. 1 – The electrochemical cell

4.1.2 Chemicals and Reagents

All solutions were prepared using deionised (DI) water. The list of chemicals used with their specifications and supplier are tabulated in Table 4. 1

Table 4. 1 - Chemical and reagents used in this work

Name of Chemical	Chemical Formula	Specifications	Origin
Zinc Chloride	$ZnCl_2$	97.0-100.5% Assay(titr.)	Panreac AppliChem
Zinc Sulfate Heptahydrate	$ZnSO_47H_2O$	ACS reagent, 99%	Sigma-Aldrich
Sodium Chloride	NaCl	ACS Specifications	J.T.Baker
Sodium Sulfate Anhydrous	Na_2SO_4	99.0% min assay	Panreac AppliChem
Hydrochloric Acid	HCl	ACS,ISO,Reag. Ph Eur, fuming 37%	Supelco
Sulphuric Acid	H_2SO_4	ISO, 96%	Panreac AppliChem
Methanesulfonic Acid	CH_4O_3S	70wt. % in H_2O	Sigma-Aldrich

4.1.3 Electrode Pre-treatment

The zinc working electrode was mechanically polished between experiments to keep the WE surface consistent throughout. Waterproof silicon carbide paper of three different roughness (e.g., P240, P500, P4000) enabled the mirror-like surface shown in Figure 4. 2. The steps taken are outlined in Appendix A.2. Once polished the electrode was carefully wrapped in Nafion enabling only the circular face to be active in the reaction.

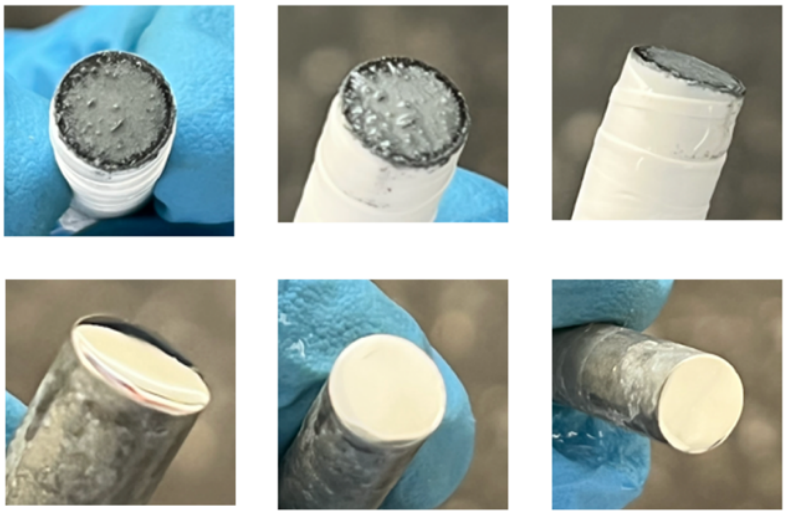

Figure 4. 2 - Comparison of before (top row) and after (bottom row) polishing the zinc electrode

After each experiment, the CE was chemically cleaned with 3 M H_2SO_4 if there was a noticeable colour change, which would remove any Zn deposited onto its surface. Thereafter it was cleaned and dried using DI water.

E After each experiment, the CE was chemically cleaned with 3 M H_2SO_4 if there was a noticeable colour change, which would remove any Zn deposited onto its surface. Thereafter it was cleaned and dried using DI water.

4.1.4 Electrolyte Section

The electrolytes selected for this project are listed in Table 4. 2, with their concentration range and reason for selection.

The solutes, $ZnCl_2$ or $ZnSO_4$, were added to the selected electrolytes to provide zinc ions to the solution. The purpose of testing two identical experiments – one with Zn^{2+} ions in the solution and one without – was to investigate the performance of the cell as "fully charged" i.e., new, and as "partially discharged" i.e., used, representing a cell that has been operating for a substantial period of time. Due to this, the cathodic kinetic parameters for solutions mimicking a "fully charged" cell (no Zn^{2+} ions initially present) is not required to be analysed.

Table 4. 2 – Electrolytes selected for this work including their concentration range and justification for selection (24)

Electrolyte Type	Concentration Range Tested (M)	Reason for Selection
Hydrochloric acid	0.001 – 0.01	Typically used in zinc electrodeposition studies
Sulphuric acid	0.0001 – 0.01	Historically, the anodic half-cell electrolyte of the Daniell cell uses zinc sulphate ($ZnSO_4$), however sometimes substituted for sulphuric acid
Methansulfonic acid	0.001 – 0.01	Few studies of zinc electrodeposition from methansulfonic acid (CH_4O_3S) electrolytes have recently been published, with patents suggesting CH_4O_3S can significantly decrease dendritic growth and therefore increase the life cycle in a zinc-based flow battery
Sodium Hydroxide	0.000001 – 0.5	Limited studies in literature for NaOH, more findings available for potassium hydroxide (KOH)
Sodium Chloride	0.5 – 3.3	To test an electrolyte with a neutral pH however differing conductivity to the others. Selected due to its chemical correspondence to $ZnCl_2$
Sodium Sulphate	0.1 - 1	To test an electrolyte with a neutral pH however differing conductivity to the others. Selected due to its chemical correspondence to $ZnSO_4$

4.1.5 Electrolyte Preparation

All apparatus and glassware used in the solution preparation were cleaned thoroughly using DI water and dried using paper towels or compressed air. For the preparation of electrolytes, containing HCl, H_2SO_4 and CH_4O_3S, a dilute mother solution was prepared for ease of further dilution.

4.1.6 Electrochemical Measurements

Electrochemical tests were performed using an Autolab High Performance Potentiostat and Galvanostat (PGSTAT12/30/302) instrument. Cyclic and linear voltammetry studies were carried out. Voltammetry refers widely to any method where the electrode potential is altered while the current is measured. Cyclic voltammetry (CV) involves a method where the electrode potential is swept repeatedly back and forth between two extreme limits, whereas linear voltammetry (LV) only sweeps to one extreme end (25). Initially, CV studies were used to detect possible side reactions and assess electrode stability (cycle repeatability). If any similarity, LV studies were completed due to time advantages.

The Autolab instrument was used to complete electrochemical impedance spectroscopy (EIS) studies, in which the resistance between WE-RE was estimated to verify it was negligible.

4.1.7 Temperature, pH and Conductivity Measurements

To measure the temperature, pH and conductivity of the electrolyte, a thermometer, a pH meter and a conductivity meter were used, respectively. The pH and conductivity meters were initially used to measure a known standard to confirm accuracy, and three measurements of each were taken to assess measurement uncertainty (95% confidence interval).

4.2 Data Analysis

4.2.1 Tafel Analysis

To determine the anodic and cathodic Tafel slopes (b_A and b_C, respectively) and the exchange current density of the oxidation and reduction reaction of Zn at the electrode surface ($i_{0,A}$ and $i_{0,C}$, respectively), various approaches in literature were initially reviewed to determine the most suitable way to accurately determine the linear Tafel region.

The approach used included initially plotting the measured current (I) against its corresponding voltage (E) obtained from the CV or LV study. The current was divided by the surface area of the WE to determine the current density (i). The equilibrium potential (E^0) was obtained using linear interpolation to the potential value at zero current. It was subtracted from each voltage point converting potentials into overpotentials (η). The logarithm of the current density was plotted against the overpotential to create a Tafel plot (TP). The data plotted was refined manually to portray a linear region originating from an overpotential of 50 mV. The gradient determined equalled the Tafel slope, where the exchange current density was found using:

$$i_0 = 10^{\frac{c}{-m}}$$ Eq. 6

Where c is the intercept and m is the slope of the line.

The errors associated with the calculated Tafel slopes and exchange current densities correlate to a 95% confidence interval of the linear regression coefficients. The uncertainty associated with the selection of the linear Tafel zone was not accounted for (see Section 5.4).

A detailed worked example for the estimation of the kinetic parameters (Tafel slope and exchange current density) and their respective errors for the aqueous electrolyte containing 0.05 M $ZnSO_4$ is presented in Appendix A.3.

4.2.2 Levich and Koutecky-Levich Analysis

Mass transfer limitations associated with the reaction were also assessed. This was completed using another electrochemical analysis technique - the Levich and Koutecky-Levich (KL) analysis.

Mass transfer limitations in the electrochemical reaction is associated with the rate at which the reactant species travels to the electrode surface from the bulk electrolyte. To study the effect of mass transport – specifically from forced convection (intentional mixing of an electrolyte from external mechanical means e.g., electrode rotation) – a common approach is using a rotating disk electrode (RDE). The use of the RDE enables kinetic information to be determined when the reaction is both limited by mass transfer and slow kinetics (26).

This was implemented into the experimental set – up where experiments were completed using aqueous electrolytes containing varying concentrations (0.1 to 1 M) of $ZnCl_2$. CV studies were completed at rotational rates ranging from 250 to 1500 rpm. The Levich and KL analysis was applied to the experimental data to estimate the diffusion coefficient of the reacting species and the kinetic current density.

The practical application of the technique was hindered by time limitations; therefore, focus was placed on the Tafel analysis. However, the underlying theory, experimental and analytical procedure details, and results determined for the aforementioned experiment, are provided in Appendix A.4.

Chapter 5. Results and Discussion

5.1 Optimisation of the Experimental Procedure

To ensure the system was reproducible, the procedure was first optimised.

5.1.1 Voltage Range

An optimal voltage range was identified by completing two CV studies using 2 voltage ranges: -2 to 0 V and -1.5 to -0.5 V, and an aqueous electrolyte containing 0.5 M of $ZnCl_2$. Hysteresis appeared with the greater voltage range (Figure 5. 2) therefore the smaller voltage range (-1.5 to 0.5 V) was selected. Noticeably in the larger voltage range study, many bubbles were visible on the WE, CE, and electrolyte, suggesting the hysteresis was due to gas evolution reactions occurring. Literature outlined similar findings: an electrolyte containing $ZnCl_2$ in aqueous HCl media, the gas evolution reaction occurred at -0.45 and -1.45 V (27).

5.1.2 Nitrogenation

In determining if nitrogenation was needed, a CV study was completed for an aqueous electrolyte containing 0.5 M of $ZnCl_2$ and repeated after bubbling nitrogen for 10 minutes to minimise the oxygen content. The reproducibility was seen to improve with the addition of nitrogen due to less variation being visible at negative currents (Figure 5. 1), however its impact was deemed insignificant and therefore considered unnecessary.

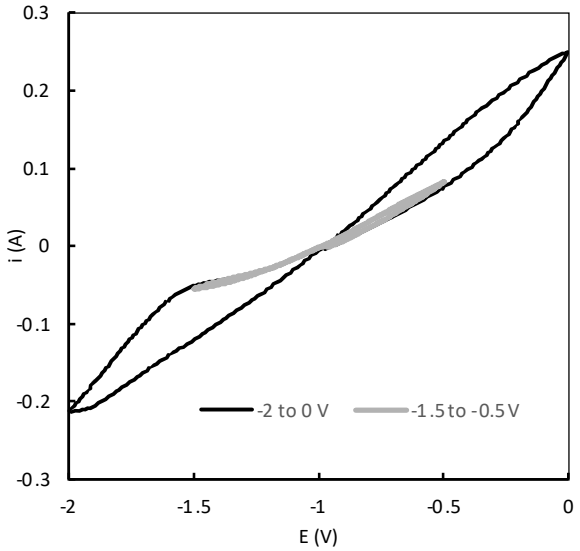

Figure 5. 2 – I-V curve at a scan rate of 100 mV/s for 2 voltage ranges

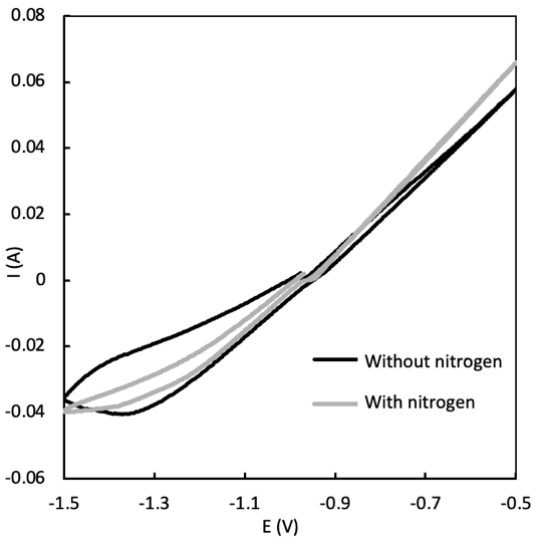

Figure 5. 1 – Comparison of CVs obtained for aqueous 0.5 M of $ZnCl_2$ with and without nitrogen

5.1.3 Scan Rate

To determine the optimal scan rate consecutive CV studies were completed using an aqueous electrolyte containing 0.5 M $ZnCl_2$ for scan rates starting at 10 mV/s, increasing in increments of 10 mV/s until 100 mV/s. Polishing of the WE was completed between scans. The results are shown in Figure 5. 3(a), where it can be seen the scan rate has a noticeable effect on the current measured. This observation is reiterated in Figure 5. 3(b), where the current measured at the upper and lower limits were plotted against the scan rate. It shows the minima and maxima reached varies at lower scan rates, as deviation is seen at scan rates lower than 40 mV/s.

Electrochemical kinetic parameters are determined based on the assumption of a steady-state system, therefore the lowest scan rate tested (10 mV/s) was selected , as lower rates extended the time to complete each experiment considerably.

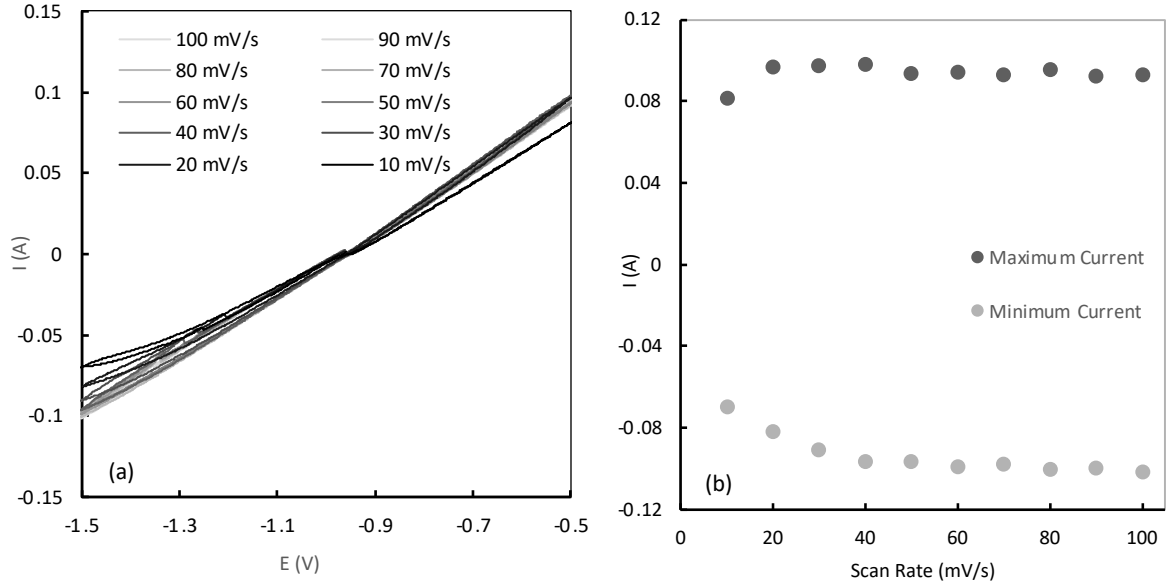

Figure 5. 3 – (a) Comparison of consecutive CV studies in aqueous 0.5 M $ZnCl_2$ for scan rates starting with 10 mV/s increasing in increments of 10mV/s until 100 mV/s, (b) Comparison of maximum and minimum current reached for different scan rates for an electrolyte containing 0.5 M $ZnCl_2$

5.1.4 Amplitude of the Perturbation for EIS Measurements

Five different amplitudes: 5, 10, 15, 25 and 281 mV were tested with the aim of finding the perturbation amplitude which maximises the signal-to-noise ratio without generating significant non-linear effects (28). Firstly, from the viewing the EIS spectra obtained for different perturbation amplitudes (Figure 5. 4, Nyquist plots), it was noticed the perturbation amplitude did not affect the high frequency real axis intercept, which corresponds to the uncompensated resistance (which is the parameter of interest). Therefore, from this work's perspective any perturbation amplitude could be

selected for use. However, in case the whole spectra were to be analysed, the amplitude was further optimised.

For each of the perturbation amplitudes, 5 frequency points were selected (25.6, 244, 1100, 22200, 82900 Hz). Figure 5. 5 shows the Lissajous figures for the 5 frequencies for each perturbation amplitude. The combination of a high frequency and low perturbation amplitude portrays the effect of noise most significant, while at a low frequency and high amplitude, non-linear effects are greatest. The optimum perturbation amplitude is 15 mV since it presents a good signal-to-noise ratio, while not generating significant non-linear effects.

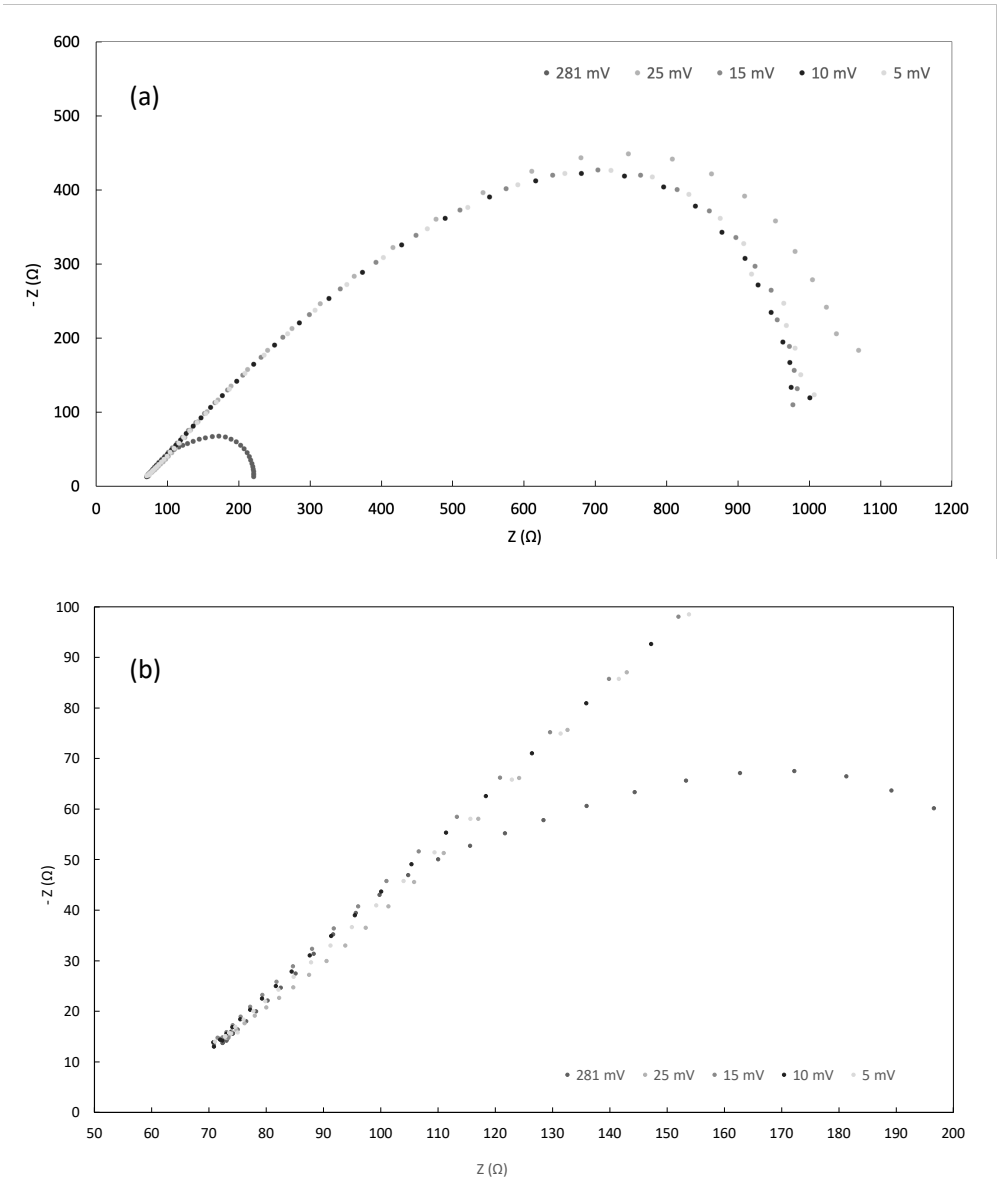

Figure 5. 4 –(a) Nyquist plot obtained for different perturbation amplitudes, (b) Zoomed in axis of Nyquist plot

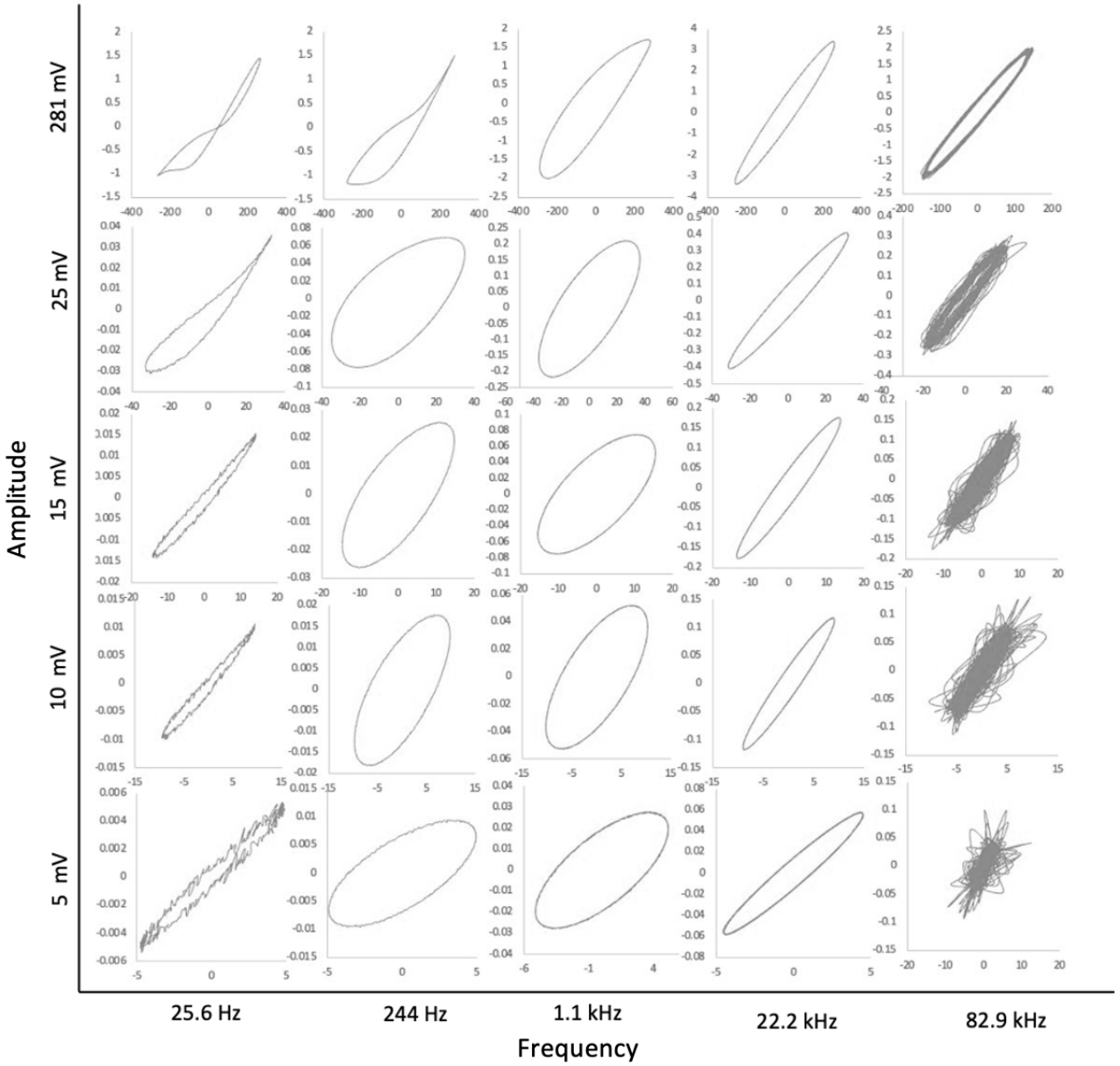

Figure 5. 5 - Lissajous curves at different frequencies for different perturbations amplitudes. Each individual plot has current (mA) on the y-axis against potential (mV) on the x-axis.

It should be noted, this study was completed with the RE immersed directly in the electrolyte as opposed to the Luggin capillary set-up, which explains why the resistance measured in Figure 5. 4 is not negligible.

It was discovered the resistance of the electrolyte measured by the EIS study, before and after the CV, was noticeably different. Uncertainty of what value to use to correct for the uncompensated resistance, initiated the use of the Luggin capillary. Further details of this experiment and outcome is listed in Appendix B.1

5.1.5 Reproducibility

To confirm the optimised system was reproducible a final experiment using a 1 M $ZnCl_2$ aqueous containing electrolyte was created – 100 ml of the solution was prepared and divided in half. Each half of the solution was tested with the cell cleaned using DI water, dried and after polishing the WE. The results were also compared to the same experiment on a different day.

The results collected from the three experiments are shown in Figure 5. 6. Noticeably, the current experimental set-up is extremely reproducible. Therefore, the experimental procedure yields sufficiently reproducible results for the purpose of this work.

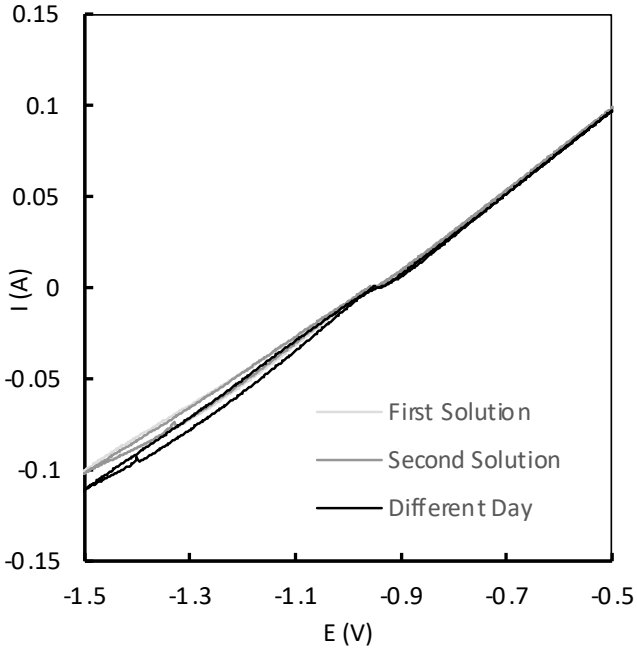

Figure 5. 6 – Reproducibility study of CVs obtained for aqueous 1 M $ZnCl_2$ electrolyte at 10mV/s. The 'first' and 'second' solution experiments were completed one after the other, with the different day experiment completed the following day.

5.2 Electrolyte Optimisation

5.2.1 Zinc Chloride

Aqueous electrolytes of six different $ZnCl_2$ concentrations – 0.05, 0.1, 0.25, 0.5, 0.75 and 1 M – were tested. Firstly, an EIS study was completed to check that the resistance between the WE and RE was negligible and that it did not change significantly during the experiments. This was followed by a CV study, then another EIS study for each concentration.

The results are presented in Figure 5. 7. The pH decreased for increasing concentrations of $ZnCl_2$, while the conductivity increased. The anodic and cathodic Tafel slopes (b_A and $-b_C$) initially increased for increasing concentrations of $ZnCl_2$ between a range of 0.05 to 0.25 M, then levelled off to a constant value of ~170 mV/dec and ~50 mV/dec, respectively. Both the experimental anodic ($i_{0,A}$) and cathodic ($i_{0,C}$) exchange current densities increased with increasing $ZnCl_2$ concentration but at a reducing rate.

From the limited values found in literature, the values in this work appeared larger in magnitude compared to published values. A source stated for concentrations of 0.5, 1 and 2 M of $ZnCl_2$ (pH = 2), i_0 equated to 1.36, 1.75 and 2.65 mA/cm^2 , also listing b_A and $-b_c$ to be 108.5, 94.4 and 90.6, and 139.5, 131.3 and 113.7, respectively (29). A possible explanation could be the difference in the electrolyte pH, which was much lower in literature sources. The increase in i_0 with increasing $ZnCl_2$ concentration is coherent with this works findings.

The electrode kinetics theory (Eq. 7) (30), relates i_0 to the concentration of the oxidising and reducing species. This expression suggests i_0 should increase with the concentration of Zn^{2+}.

This is coherent with the findings in this work (however it is noted this expression is for a single electron reaction at equilibrium which is not fully the case for the reaction in this work).

$$i_0 = FkC_O^{*(1-\alpha)}C_R^{*\alpha} \qquad \text{Eq. 7}$$

It was noticeable for lower concentrations of $ZnCl_2$, the aqueous electrolyte would appear cloudy (see Figure 5. 8)– no longer transparent like water. A literature report confirmed this behaviour stating as the zinc-chloride solution becomes diluted a precipitate ($ZnCl_25ZnO6H_2O$) becomes apparent (31).

This study does confirm the concentration of $ZnCl_2$ impacts the reaction kinetics and therefore for optimisation of the electrolyte a fixed concentration must be selected to get comparable results. A concentration of 0 M and 1 M of $ZnCl_2$ was selected, to represent “fully charged” and “partially discharged” cell, respectively.

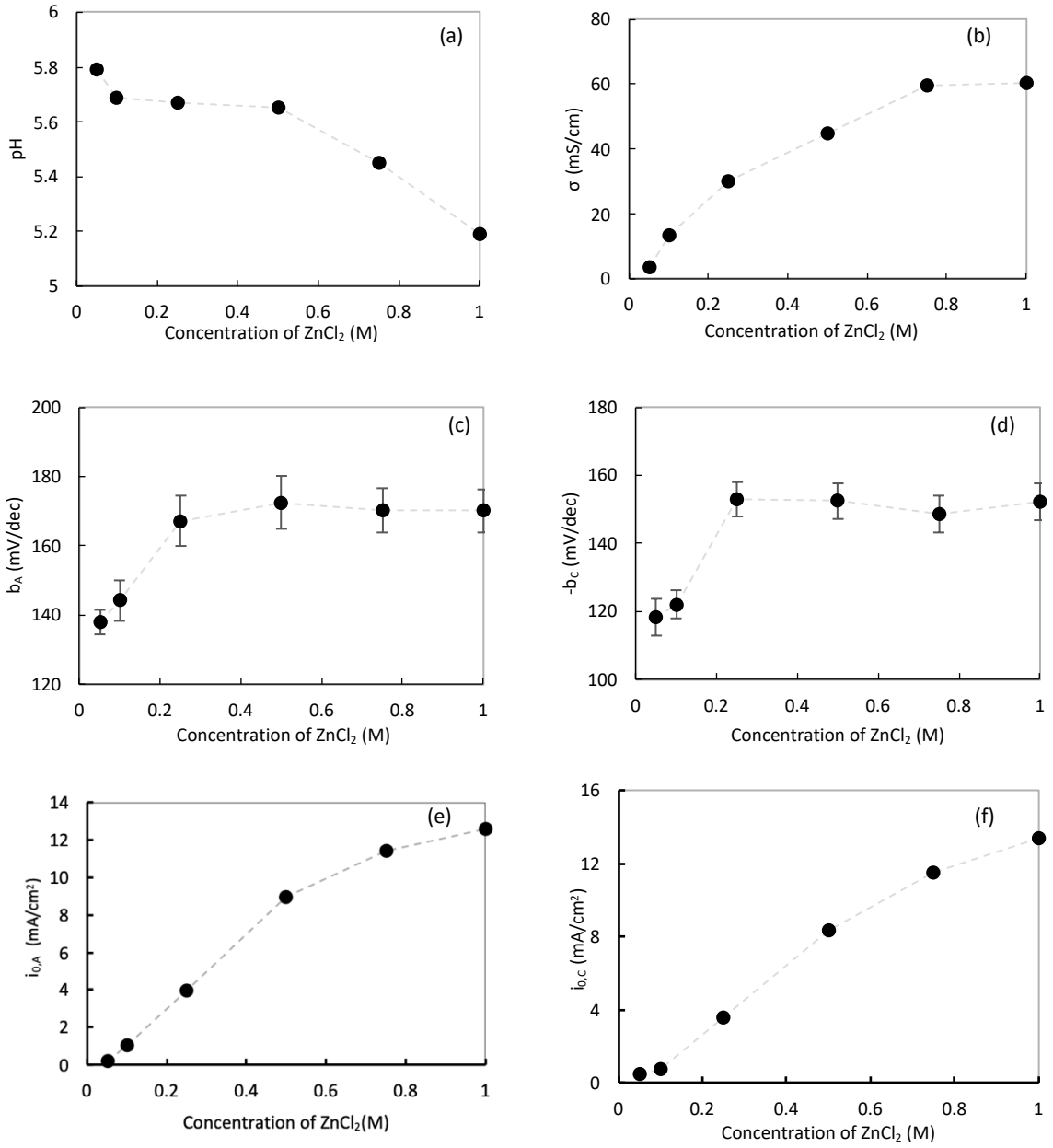

Figure 5. 7 – (a) pH (b) conductivity (c) anodic Tafel slope for varying concentration of aqueous $ZnCl_2$ (d) Corrected cathodic Tafel slope (e) anodic exchange current density (f) cathodic exchange current density, for different $ZnCl_2$ concentrations. All data plots include error bars, however in plots (a), (b), (e) and (f), the associated errors are too small to be seen. Dotted line included for visualisation purposes

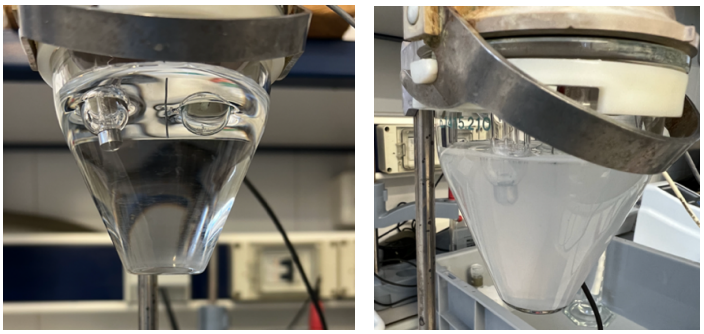

Figure 5. 8 – Aqueous electrolytes containing (a)1 M $ZnCl_2$ (transparent) (b)0.25 M $ZnCl_2$ (cloudy).

5.2.1.1 Open Cell Potential (OCP) Experiment

An OCP experiment (where the potential is measured when the applied current is off) was completed to compare the cell's E_{OCP} with the Nernst equation, allowing analysis of the maximum voltage achievable from the half-cell.

Details of the experiments and their results are presented in Appendix B.2, where it was concluded the experimental values displayed coherence with the theoretical values estimated using the Nernst equation from a concentration of 0.37 to 1.03 M.

As expected, deviations in the experimental values from Nernst were shown as the concentration increases. The Nernst equation used, is applicable for dilute solutions therefore it was suitable to assume the active coefficients were close to unity. At greater concentrations, the system is no longer dilute. Unexpected deviations were however seen at low concentrations. It can be assumed this is due to the precipitate formed (as discussed in Section 5.2.1) where the concentration tested did not equal the concentration prepared.

5.2.2 Hydrochloric Acid Media

The zinc working electrode was initially placed in 0.1 M of HCl and observed for 5 minutes. Bubbles were shown to form on the surface of the WE (see Figure 5. 9) highlighting 0.1 M HCl was too strong and was causing zinc to dissolve chemically, thus unsuitable for use as the battery would auto-discharge.

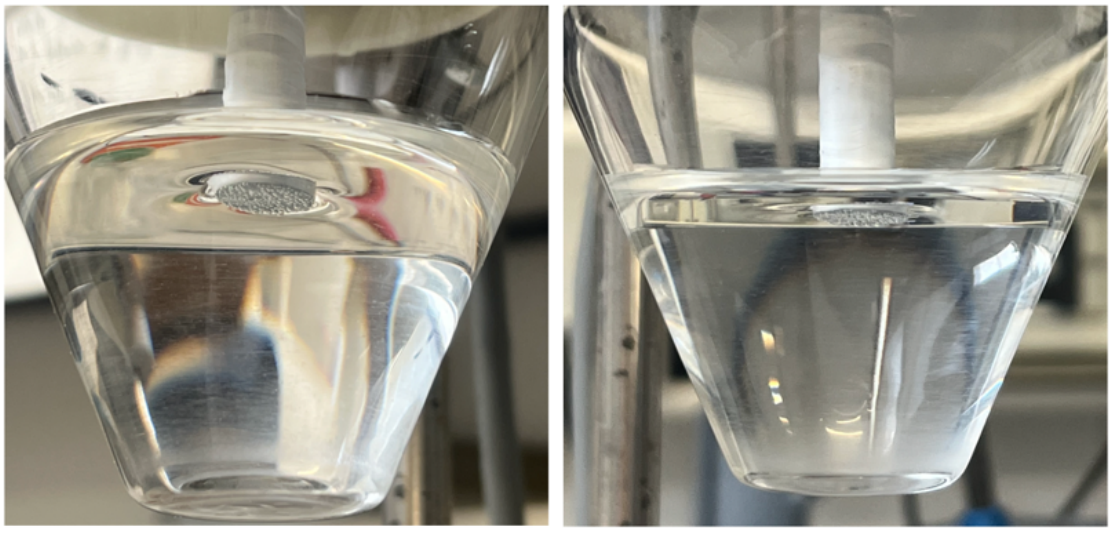

Figure 5. 9 – Formation of bubbles on the surface of the zinc working electrode surface when placed in a 0.1 M HCl solution

CV studies were completed for acid concentrations of 0.1, 0.01 and 0.005M to observe if any unusual behaviour is shown at this concentration (Figure 5. 10). Observing the 0.1M HCl solution independently, noise was shown at the lower voltage range. The working electrode at this point had

accumulated a surface covered in bubbles providing explanation to the noise seen in the CV study. The bubbles are due to gas evolution. The results collected for the acid concentrations 0.01 M and 0.005 M were very similar, resulting in additional CV studies being completed for HCl concentrations of: 0.001, 0.003, 0.007 and 0.009 M – to further investigate the effect of the acid concentration. For each acid concentration studied, an equivalent experiment was completed with the inclusion of 1 M $ZnCl_2$. The results are shown in Figure 5. 11.

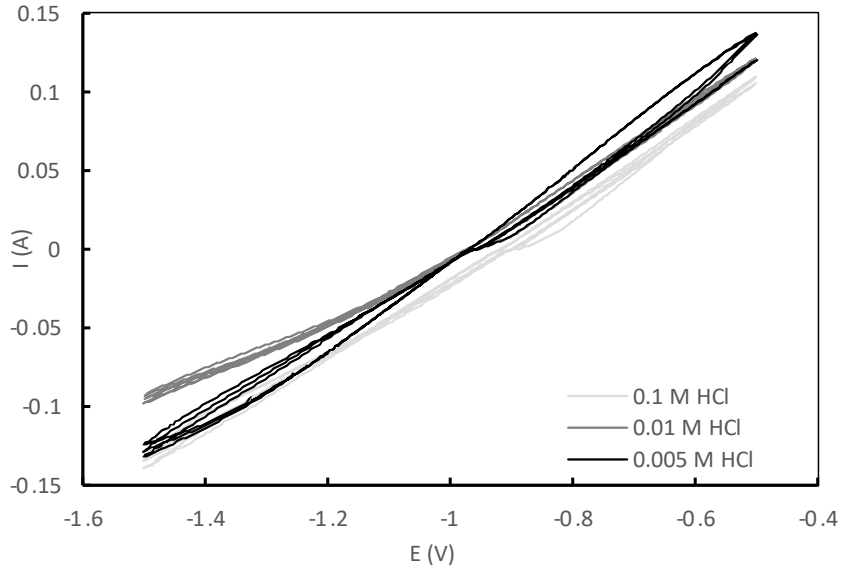

Figure 5. 10 - CVs for 0.1M, 0.01M and 0.005M of HCl with 1 M $ZnCl_2$

For the pure acid solutions , as the acid concentration increased, the pH decreased, the conductivity increased, b_A decreased slightly, and $i_{0,A}$ increased. Literature b_A values of 90 and 25 mV/dec for 0.06 and 1 M HCl concentrations were found (32), which is consistent with the study results. .

For the electrolytes containing 1 M $ZnCl_2$, the pH decreased for increasing acid concentration while the conductivity fluctuated. The Tafel slopes generally decreased, and both $i_{0,A}$ and $i_{0,C}$ had similar magnitudes, being independent of acid concentration, all excluding the data point of water (0 M HCl).

For a “fully charged” cell greater concentrations favour larger conductivity, lower b_A and larger $i_{0,}$. For a “partially discharged” cell, generally the acid concentration slightly impacts the reaction parameters, where only a greater acid concentration promotes a lower b_A and $-b_C$.

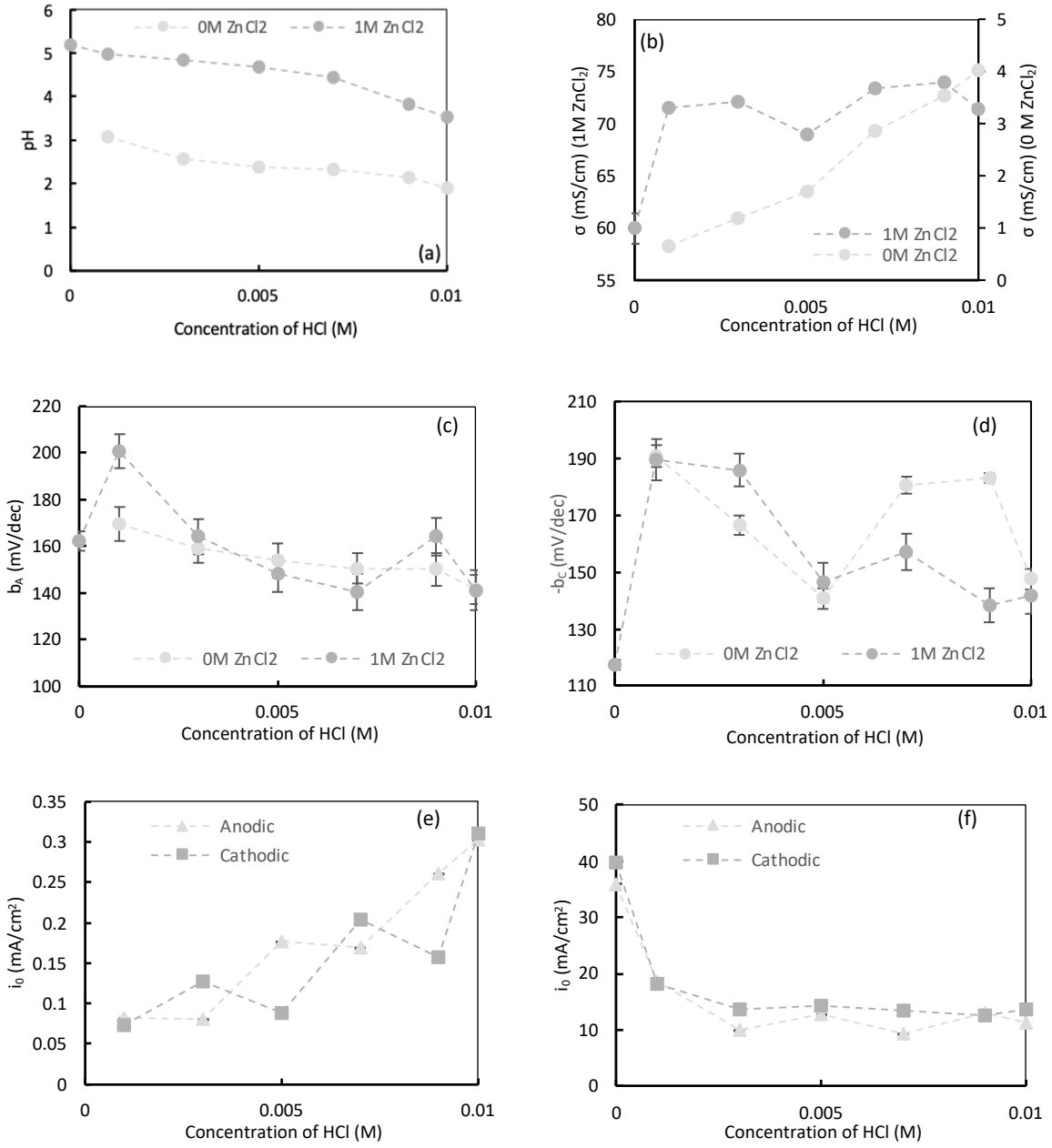

Figure 5. 11 – (a) pH (b) conductivity (c) anodic Tafel slope (d) cathodic Tafel slope, for different concentrations of HCl acid for solutions containing 0 M and 1 M of $ZnCl_2$. (e) exchange current density for electrolytes containing 0 M, (f) exchange current density for electrolytes containing 1 M, of $ZnCl_2$. Inclusion of error bars in all figures, where dotted lines are used as a visual graphical aid

5.2.3 Zinc Sulphate

Similar experiments to those completed with $ZnCl_2$ were carried out using $ZnSO_4$.

Aqueous – $ZnSO_4$ electrolytes of concentrations: 0.05, 0.1, 0.25, 0.5, 0.75 and 1 M, were tested. It was noticed in the initial CV studies that the system was reproducible, therefore LV studies – anodic and cathodic - were used instead. A comparison of these LV studies is shown in Figure 5. 12, where current magnitudes were greater for larger concentrations of $ZnSO_4$. Conductivity, pH and Tafel analysis parameters are shown in Figure 5. 13. No correlation between the pH and concentration of $ZnSO_4$

was found, however the conductivity increased. The order of magnitude of the electrolyte conductivity is coherent with literature, which states in a patent 'for the development of an aqueous zinc sulphate (II) rechargeable cell that zinc sulphate has an electrical conductivity of around 50 mS/cm at room temperature' (33).

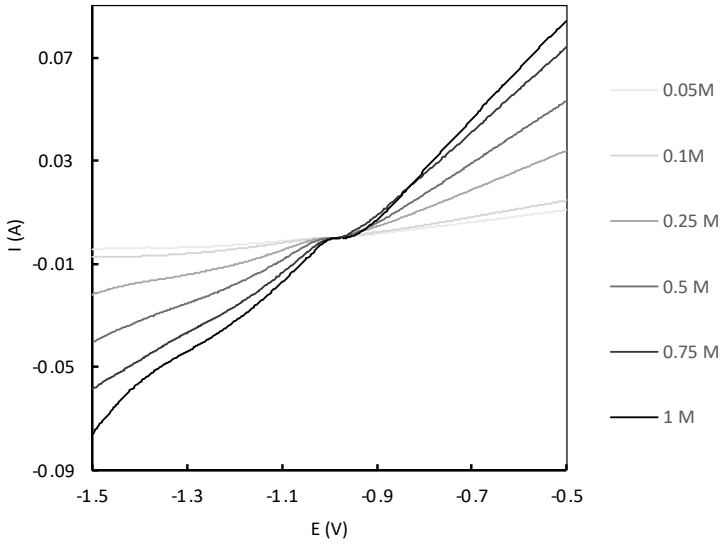

Figure 5. 12 - LV measurements for 0.05, 0.1, 0.25, 0.5, 0.75, 1 M of $ZnSO_4$ solutions

For increasing concentrations of $ZnSO_4$, b_A decreased, $-b_C$ initially decreased then increased for concentrations above 0.25 M, and $i_{0,A}$ and $i_{0,C}$ generally increased (aligns with literature, see Eq. 7). A literature source listed b_A and $i_{0,A}$ values of 120 mV/dec and 200 mA/cm^2 respectively for a concentration of 1 M $ZnSO_4$ (32). The b_A determined in this work is relatively coherent. Acknowledging that the concentration of $ZnSO_4$ influences the reaction kinetics, a fixed concentration of 1 M $ZnSO_4$ was used in further tests.

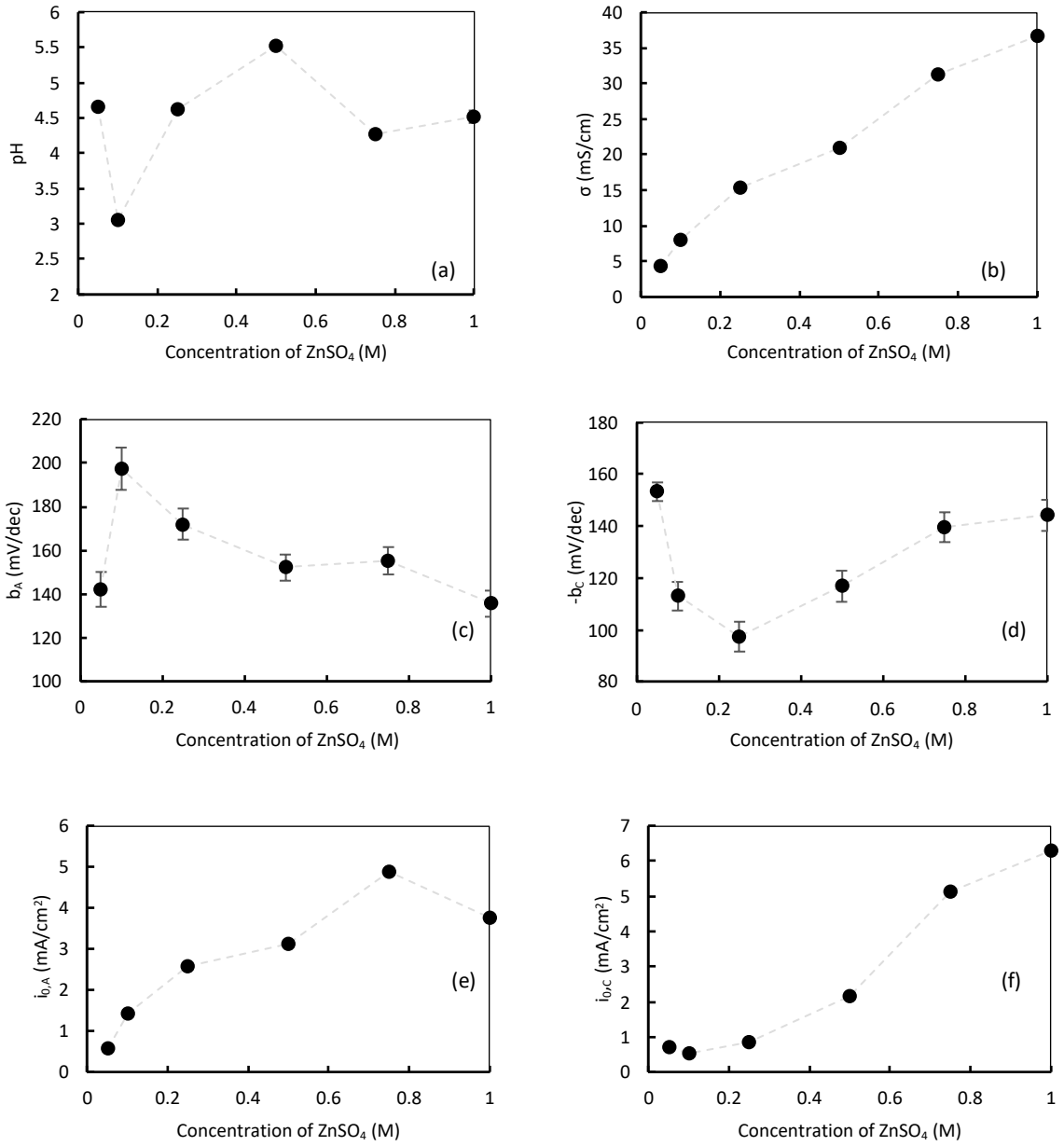

Figure 5. 13 –(a) pH (b) conductivity (c) anodic Tafel slope (d) cathodic Tafel slope (e) anodic exchange current density (f) cathodic exchange current density, for electrolytes of varying concentration of $ZnSO_4$. All data plots include error bars, however for plots (a),(b),(e),(f), the associated error bars are too small to be seen. The dotted line is included for visualisation purposes.

5.2.4 Sulphuric Acid Media

The WE was placed in 0.1 M of H_2SO_4 and left immersed in the solution for 5 minutes. Similar to the outcome for HCl, bubbles had formed covering the WE surface (see Figure 5. 9) highlighting the acid was too strong. The process was repeated for a 10-fold dilution of the acid concentration (0.01 M). No bubbles were visible at this concentration and therefore deemed suitable for use .

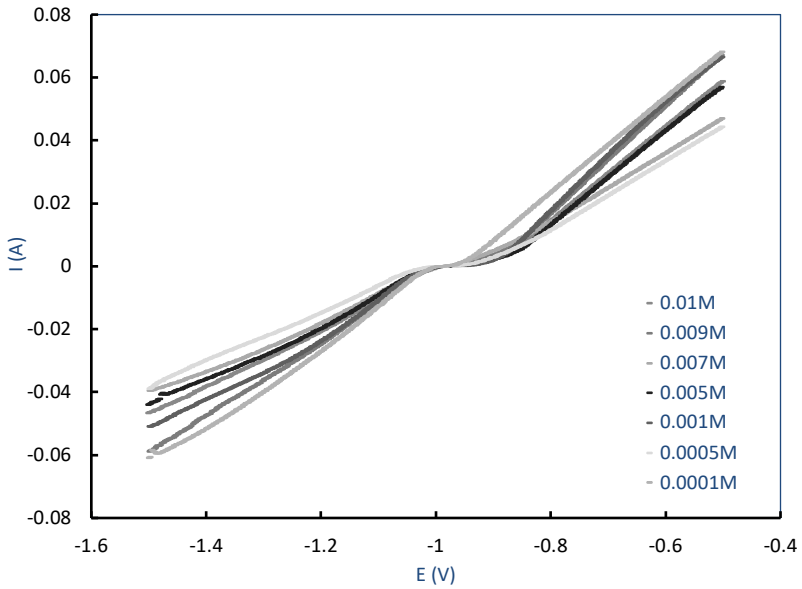

Figure 5. 14 – LV studies for electrolytes containing 1 M $ZnSO_4$ in different concentrations of H_2SO_4

The H_2SO_4 concentrations tested include 0.0001, 0.0005, 0.001, 0.005, 0.007, 0.009 and 0.01 M, and were repeated with the addition of 1 M $ZnSO_4$. The results of the LV studies are shown in Figure 5. 14, where no correlation was seen for the varying electrolyte (containing 1 M $ZnSO_4$) acid concentration. The pH, conductivity, and Tafel analysis results are shown in Figure 5. 15.

For the pure acid solutions and increasing acid concentration, pH decreased, conductivity increased slightly, b_A appeared independent, and $i_{0,A}$ increased slightly.

For the 1 M $ZnSO_4$ tests and increasing acid concentration, the pH decreased, the conductivity increased slightly, b_A increased and $-b_C$ fluctuated around a constant value of 100 mV/dec. No trend was obvious for $i_{0,A}$ and $i_{0,C}$. No real benefit to using 1 M $ZnSO_4$ was found.

The values calculated from this study exceed those found in literature – 60 mV/dec and 30 mV/dec for neutral and acidic electrolytes, respectively. This could be due to differences in the experimental conditions as the literature study used an electrode where zinc was deposited onto the RDE (34), or possibly due to the limited pH range tested, but lower pH electrolytes (higher H_2SO_4 concentrations) could not be examined due to the Zn electrode chemically dissolving.

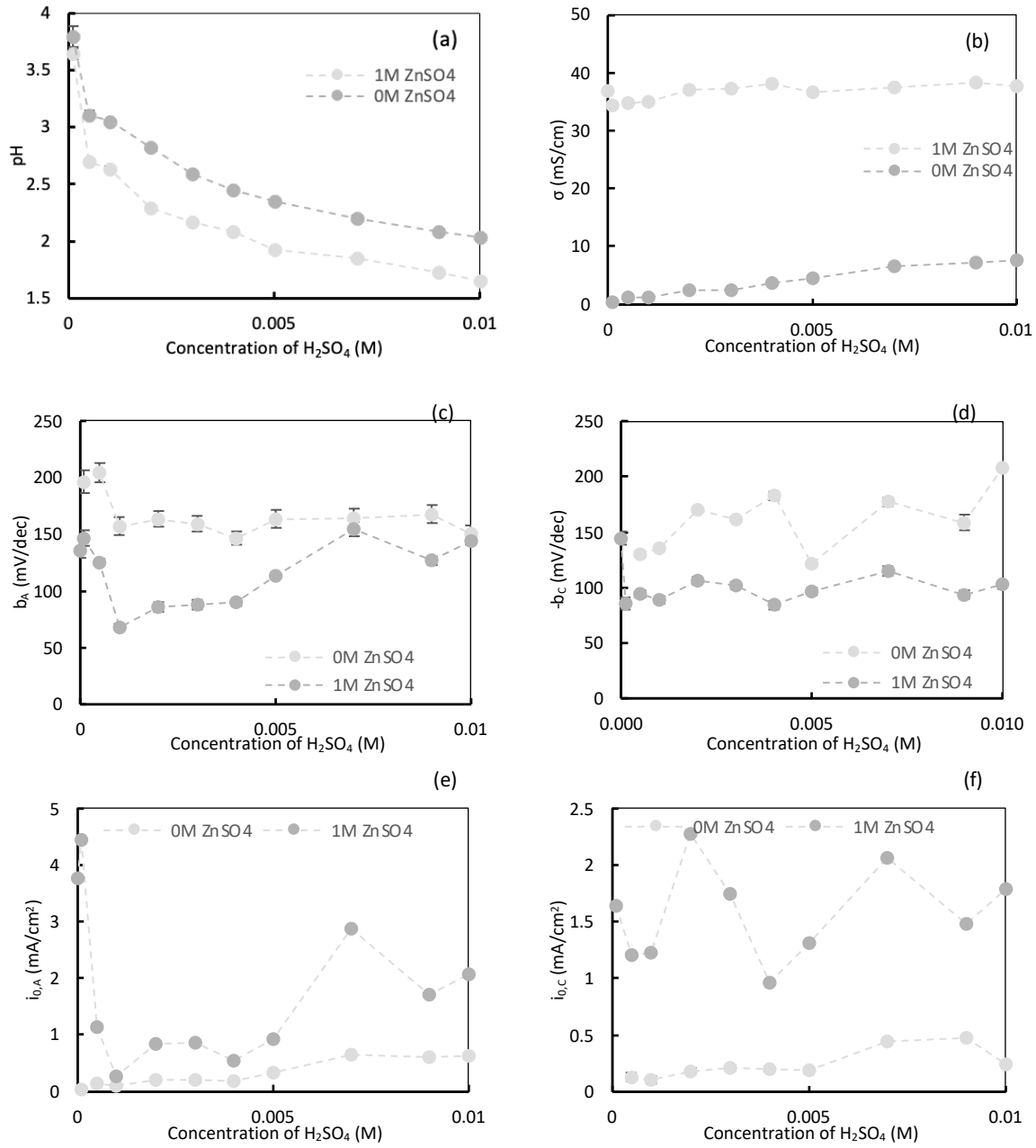

Figure 5. 15 –(a) pH (b) conductivity (c) anodic Tafel slope (d) cathodic Tafel slope (e) anodic exchange current density (f) cathodic exchange current density, for different concentrations of H_2SO_4 for solutions containing 0 M and 1 M of $ZnSO_4$. Inclusion of error bars in all figures, where dotted lines are used as a visual graphical aid.

5.2.5 Methanesulfonic Acid Media

Similarly with the other acidic electrolytes, the WE was placed in 0.1 M of CH_4O_3S and its surface was observed for 5 minutes, during which bubbles formed indicating that the zinc was dissolving spontaneously, and this acid concentration was too strong.

This process was repeated using a 10-fold dilution (0.01 M) until no bubbles were visible. Five concentrations of CH_4O_3S were tested – 0.001, 0.003, 0.005, 0.007 and 0.01 M – containing 0 and 1 M of $ZnSO_4$. The results of the LV studies are shown in Figure 5. 16 , and similarly to the sulphuric media, there was no correlation noticeable.

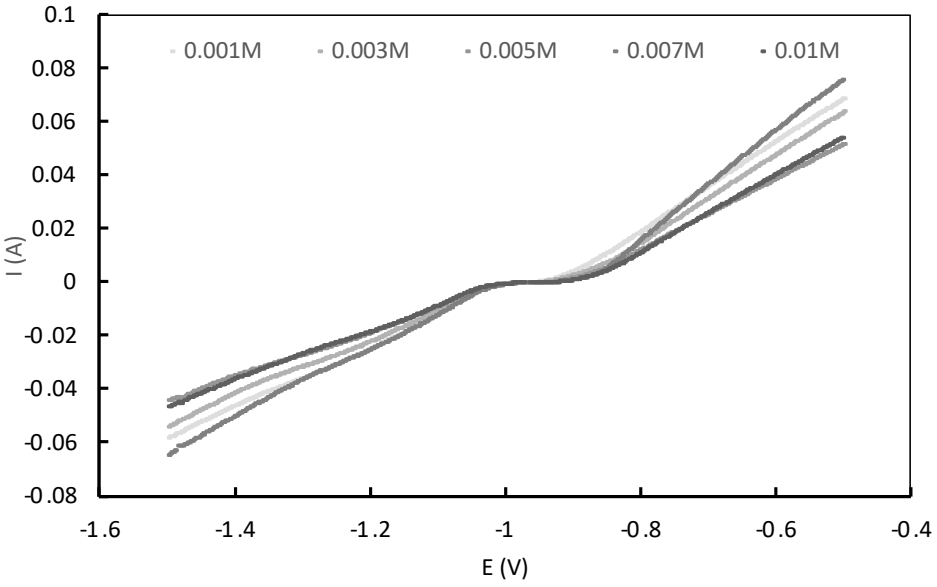

Figure 5. 16 – LV studies for electrolytes containing 1 M $ZnSO_4$ in different concentrations of CH_4O_3S

The pH, conductivity, and Tafel analysis results are shown in Figure 5. 17. For pure solutions and increasing acid concentration, the pH decreased, the conductivity remained constant, b_A generally decreased and $i_{0,A}$ increased.

Tests with 1 M $ZnSO_4$ and increasing acid concentration showed decreasing pH , and a fairly constant conductivity (value much larger than pure acid case). Both b_A and $-b_C$ reduced initially and tended to level off, while the $i_{0,A}$, reduced sharply and $i_{0,C}$ fluctuated showing no apparent trend.

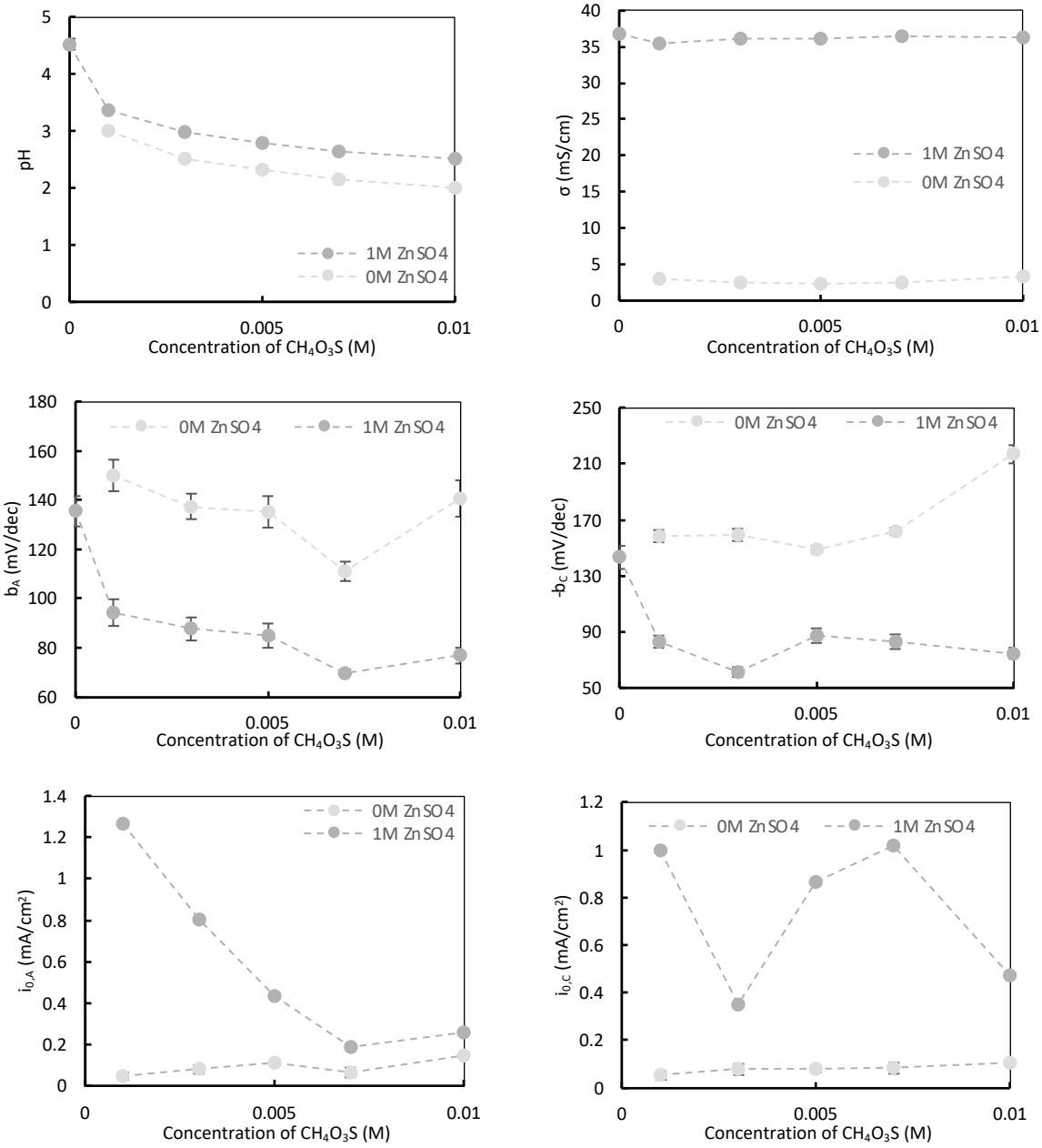

Figure 5. 17 – (a) pH (b) conductivity (c) anodic Tafel slope (d) cathodic Tafel slope (e) anodic exchange current density (f) cathodic exchange current density, for different concentrations of CH_4O_3S for solutions containing 0 M and 1 M of $ZnSO_4$. Inclusion of error bars in all figures, where dotted lines are used as a visual graphical aid

5.2.6 Sodium Hydroxide Media

To investigate the effect of alkali media on the anodic half-cell reaction, varying concentrations of NaOH were tested. Initially, a 1 M NaOH solution was created and further diluted – 0.5, 0.25, 0.1, 0.01, 0.001, 0.0001, 0.00001 and 0.000001 M.

A cathodic, followed by an anodic, LV study was completed with adjusted voltage limits due to a decrease in the OCP (-1.4 V), where the WE was polished between concentrations. Mass transfer limitations were exhibited in the cathodic cycle, as expected due to no zinc being present in the

electrolyte to be reduced. In the anodic study, unusual behaviour was observed; a change in the working electrode surface is likely to have taken place due to the significant drop in current (Figure 5. 18(a)).

From a Pourbaix diagram for zinc (Appendix B.3) (35), it could be assumed a passive layer of $Zn(OH)_2$ had formed on the surface. The same behaviour in the anodic LV study was found for concentrations of 0. 5 and 0.25 M of NaOH.

Further dilutions – 0.1 M and 0.01 M NaOH – were studied, however the system failed to stabilise. Attempts to clean the WE with 0.1 M HCl and polishing it made no change as the system remained unstable in a 300s OCP experiment (Figure 5. 18(b)). Thus, concluding a film was forming on the WE surface creating a passive layer, which makes the electrolyte unsuitable for a battery, as the internal resistance of the cell increases dramatically.

It was found the system was stable for 0.001 M of NaOH, therefore an anodic LV study was completed. A 10-fold dilution was prepared an additional 3 times, with an anodic LV study run for each. The pH and concentration of each solution, as well as the Tafel parameters are shown in Figure 5. 19.

Both pH and conductivity increased for increasing concentrations of NaOH, which was expected with more OH^- ions. The b_A values were relatively constant with $i_{0,A}$ displaying an increase.

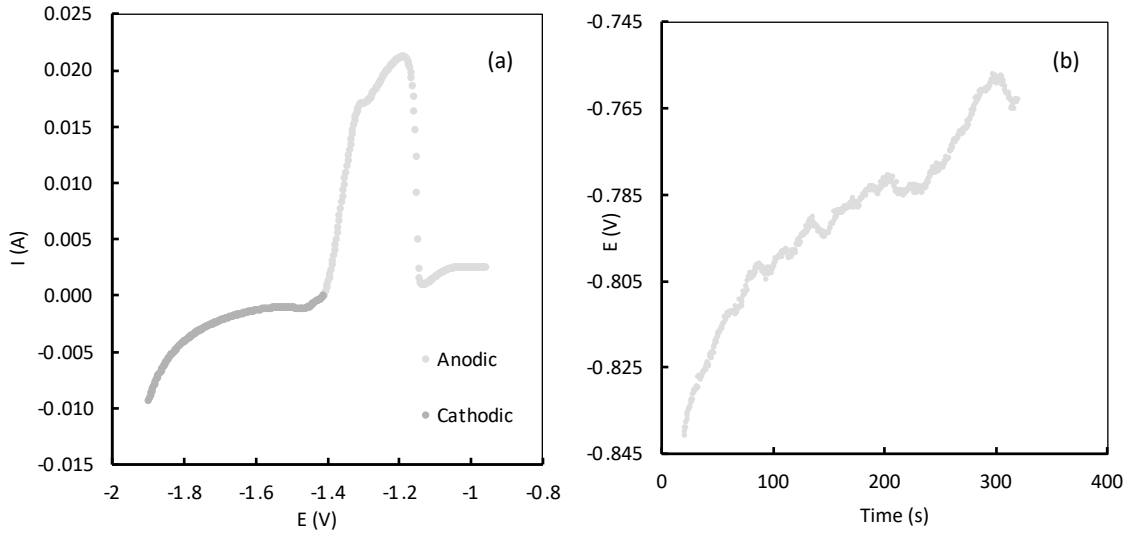

Figure 5. 18 – (a) LV study for 1 M NaOH solution, (b) OCP study for 0.01 M NaOH and water measured for 300 seconds

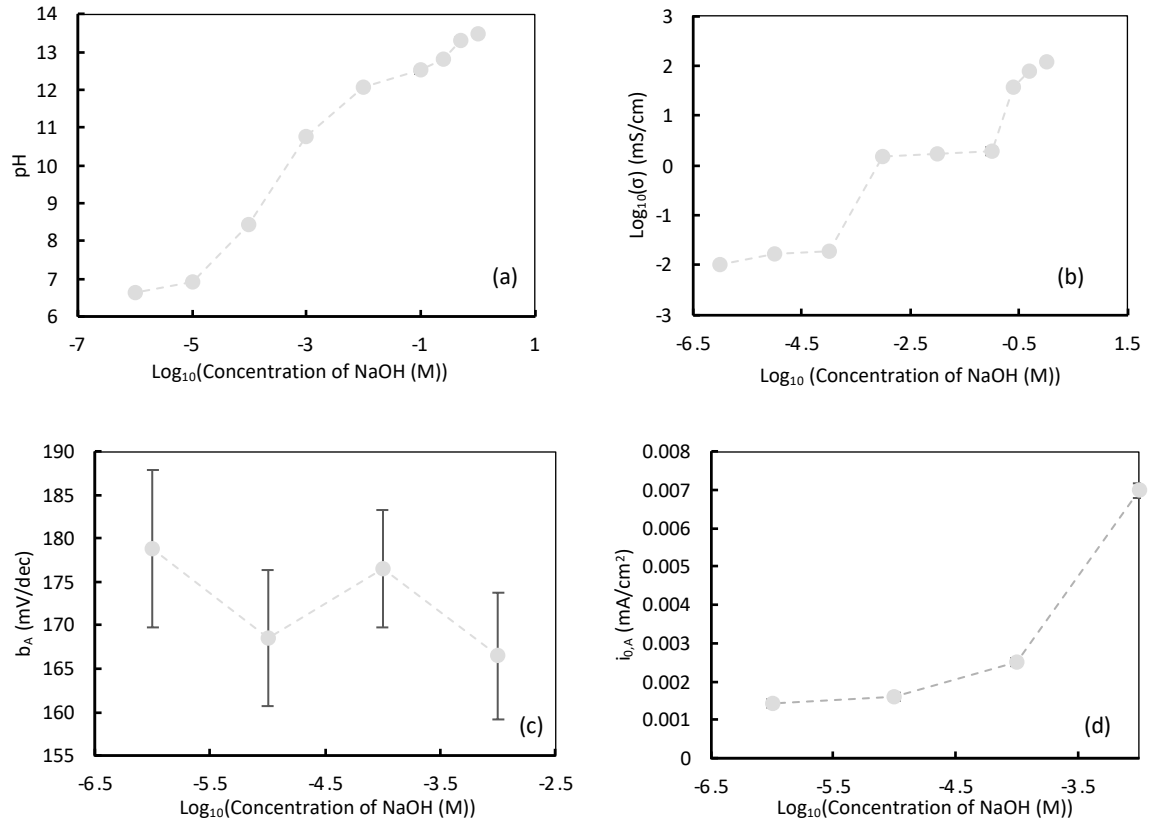

Figure 5. 19 – (a) pH (b) conductivity (c) anodic Tafel slope (d) anodic exchange current density, for varying concentrations of NaOH. Dotted line used as a visualise aid

Using 100 ml of the 1 M of NaOH solution, an attempt was made to dissolve 1 M of $ZnCl_2$, however a white precipitate formed (Figure 5. 20), which was thought to be zinc hydroxide ($Zn(OH)_2$) (36). This was repeated using 1 M $ZnSO_4$ with the same outcome. The pH of NaOH which could be used was calculated using Eq. 8 with a solubility constant (K_{sp}) for zinc hydroxide of $1.74x10^{-17}$ (at 25°C) (37). The pH at which the components would dissolve without the formation of the precipitate fell beyond the alkaline range (the pH was calculated < 7), therefore no further experiments were conducted.

$$K_{sp} = [Zn^{2+}][OH^{-}]^2 \qquad \text{Eq. 8}$$

Where K_{sp} is the solubility constant of $ZnOH_2$ at 25°C, $[Zn^{2+}]$ is the concentration of Zn^{2+} ions in the solution and $[OH^-]$ is the concentration of OH^- the solution.

Figure 5. 20 – Experimental pictures of $Zn(OH)_2$ precipitation in a 100 ml 1 M NaOH – 1M $ZnCl_2$ solution

5.2.7 Sodium Chloride Media

Five concentrations of NaCl and water were tested – 3.3, 3, 2, 1 and 0.5 M (based on the solubility of NaCl) – where an anodic and cathodic LV study were run for each. This was repeated for solutions containing 1 M of $ZnCl_2$. The results are shown in Figure 5. 21.

For electrolytes of pure NaCl, and with increasing concentration of NaCl, the pH was relatively constant, conductivity increased and b_A increased to a maximum at 2 M then reduced. The $i_{0,A}$ remained relatively constant and was small. A literature source recorded b_A equal to 25 and 30 mV/dec for concentrations of 1 (pH 3.8) and 0.1 M (pH 5.3) NaCl (32). The b_A values displayed are of a different magnitude, but the NaCl had a small effect on b_A which is coherent.

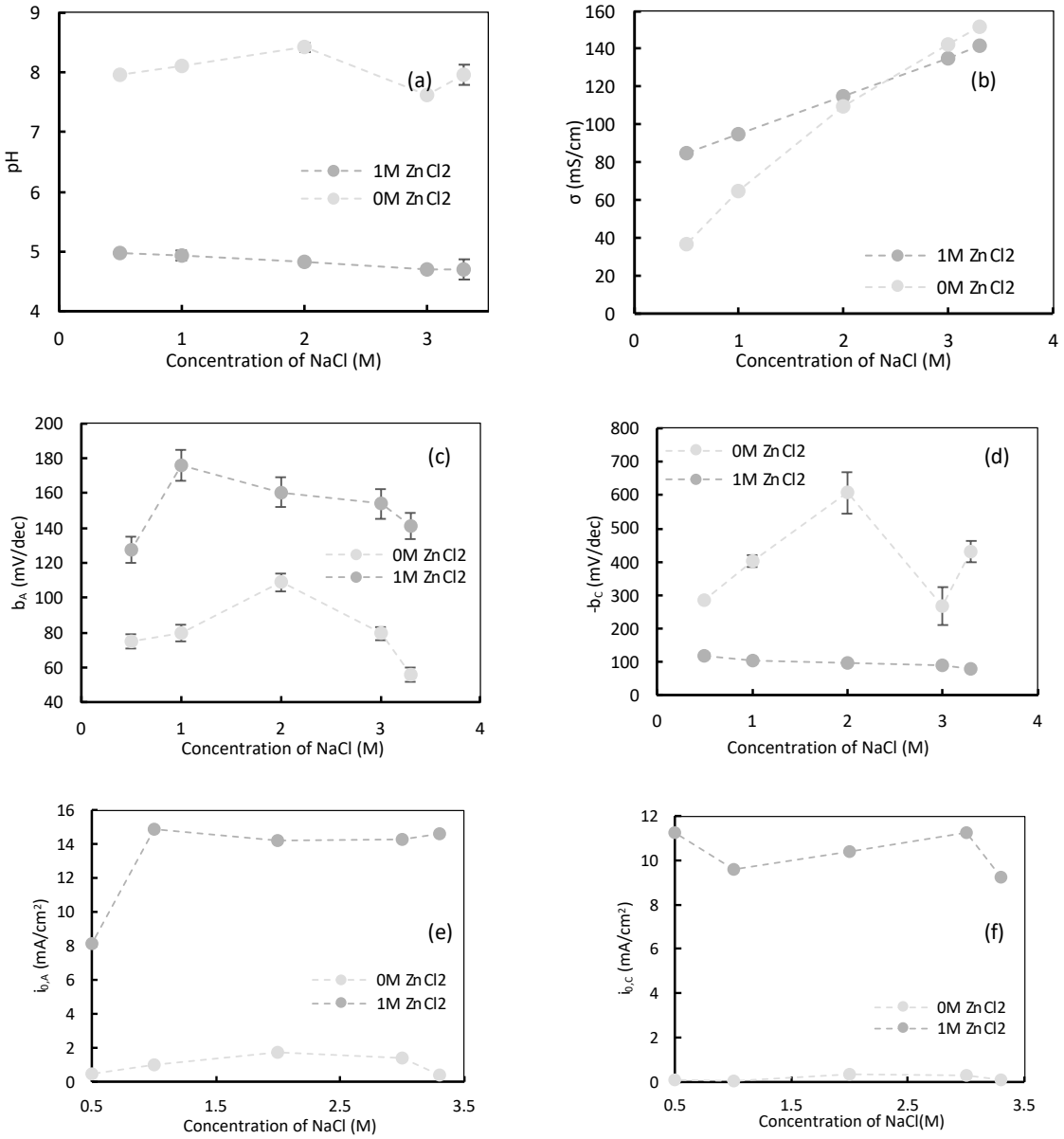

Figure 5. 21 –(a) pH (b) conductivity (c) anodic Tafel slope (d) cathodic Tafel slope (e) anodic exchange current density (f) cathodic exchange current density, for different concentrations of NaCl for solutions containing 0 M and 1 M of $ZnCl_2$. Inclusion of error bars in all figures, where dotted lines are used as a visual graphical aid.

For the $ZnCl_2$ electrolyte studies the pH remained relatively constant, the conductivity increased, b_A decreased, $-b_C$ reduced slightly, and both $i_{0,A}$ and $i_{0,C}$ remained relatively constant for increasing concentration of NaCl.

Aside from an increase in the electrolyte conductivity at greater concentrations of NaCl, the kinetic parameters are seen to be unaffected by the concentration of NaCl. Greater concentrations of NaCl for solutions containing 1 M $ZnCl_2$ are favourable due to their high conductivity, low anodic Tafel slope and high anodic exchange current density.

5.2.8 Sodium Sulphate Media

Na_2SO_4 was found in literature to be less soluble than NaCl in water (38), hence the greatest concentration tested of Na_2SO_4 was 1 M. The five concentrations of Na_2SO_4 and water tested were 1, 0.75, 0.5, 0.25 and 0.1 M - where an anodic and cathodic LV study were run for each. This was repeated with the addition of 1 M $ZnSO_4$. The results measured and determined are presented in Figure 5. 22.

For electrolytes of pure Na_2SO_4, for increasing concentration of Na_2SO_4, the pH remained constant, the conductivity increased, b_A decreased and $i_{0,A}$ increased - the desired combination for the electrochemical parameters.

For the electrolytes containing $ZnSO_4$, for increasing concentration of Na_2SO_4, the pH remained relatively constant, the conductivity increased, b_A decreased and $-b_C$ remained constant, $i_{0,A}$ decreased, with the opposite for $i_{0,C.}$ The increasing conductivity and reducing b_A supports the selection of this electrolyte. Although $i_{0,A}$ decreased, its magnitude is suitable in comparison to other electrolytes tested.

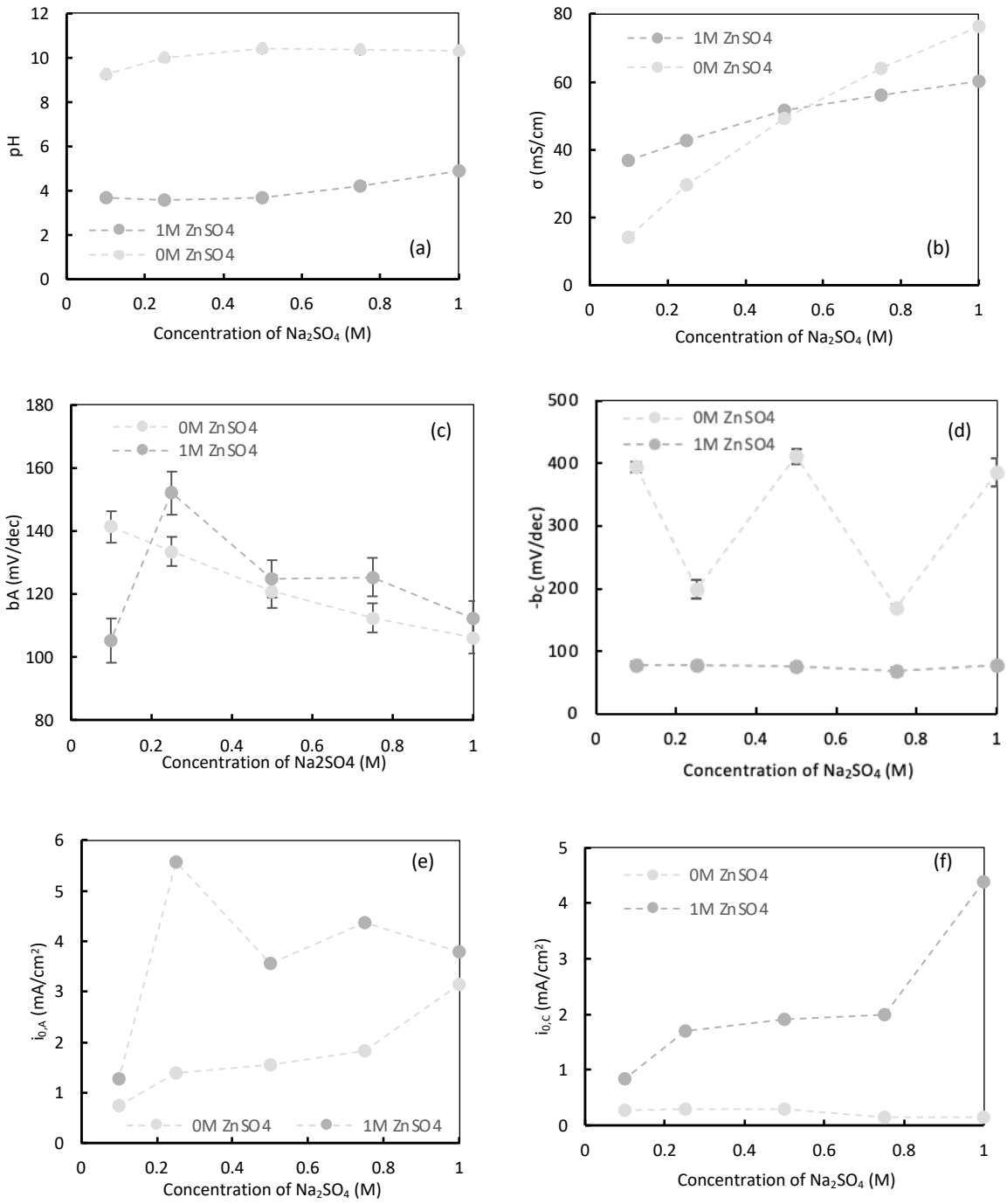

Figure 5. 22 -(a) pH (b) conductivity (c) anodic Tafel slope (d) cathodic Tafel slope (e) anodic exchange current density (f) cathodic exchange current density, for different concentrations of Na_2SO_4 for solutions containing 0 M and 1 M of $ZnSO_4$. Inclusion of error bars in all figures, where dotted lines are used as a visual graphical aid

5.3 Selection of Electrolyte

The electrolyte selection considered the two states of the cell: "fully charged" (0 M $ZnCl_2$ or $ZnSO_4$) and "partially discharged" (1 M of $ZnSO_4$ or $ZnCl_2$) for the purpose of being able to evaluate the reaction kinetics of the cell optimal at the start of the cell's use and after dissolution of the zinc electrode.

The selection of the electrolyte to optimise the reaction kinetics and cell operation were based on 3 parameters – conductivity, Tafel slope and exchange current density. For solutions containing Zn^{2+} ions, both the anodic and cathodic parameters were analysed to gain an understanding of both the dissolution and deposition reactions occurring depending on whether the cell is charging (deposition) or discharging (dissolution).

For greater conductivity lower resistivity is required. A lower Tafel slope is desired as by its definition, a lower Tafel slope translates to less voltage required for a given current increase. An electrolyte which yields a larger exchange current density is favoured as this implies faster reaction kinetics and therefore lower voltage losses associated with the reaction activation energy. To select the most optimal electrolyte, the optimal or average value (independent of the concentration) for each electrolyte for the different parameters were plotted. The optimal value – lowest b, and greatest σ and i_0 – was selected for the plot when the parameter varied with the electrolyte concentration.

"Fully charged" cell conditions

From Figure 5. 23(a), the electrolyte NaCl has a significantly higher conductivity (lower resistivity) in comparison to the other electrolytes tested. Coherent with literature, soluble salts are good conductors and the more ions they dissociate into, the greater the conductivity. For NaCl, the greatest concentration tested equalled the highest conductivity.

Figures 5.23 (b) and (c), show the anodic kinetic parameters listed with their optimal concentration of electrolyte. For the anodic reaction, NaCl appears most favourable due to its high σ, low b_A and relatively high $i_{0,A.}$

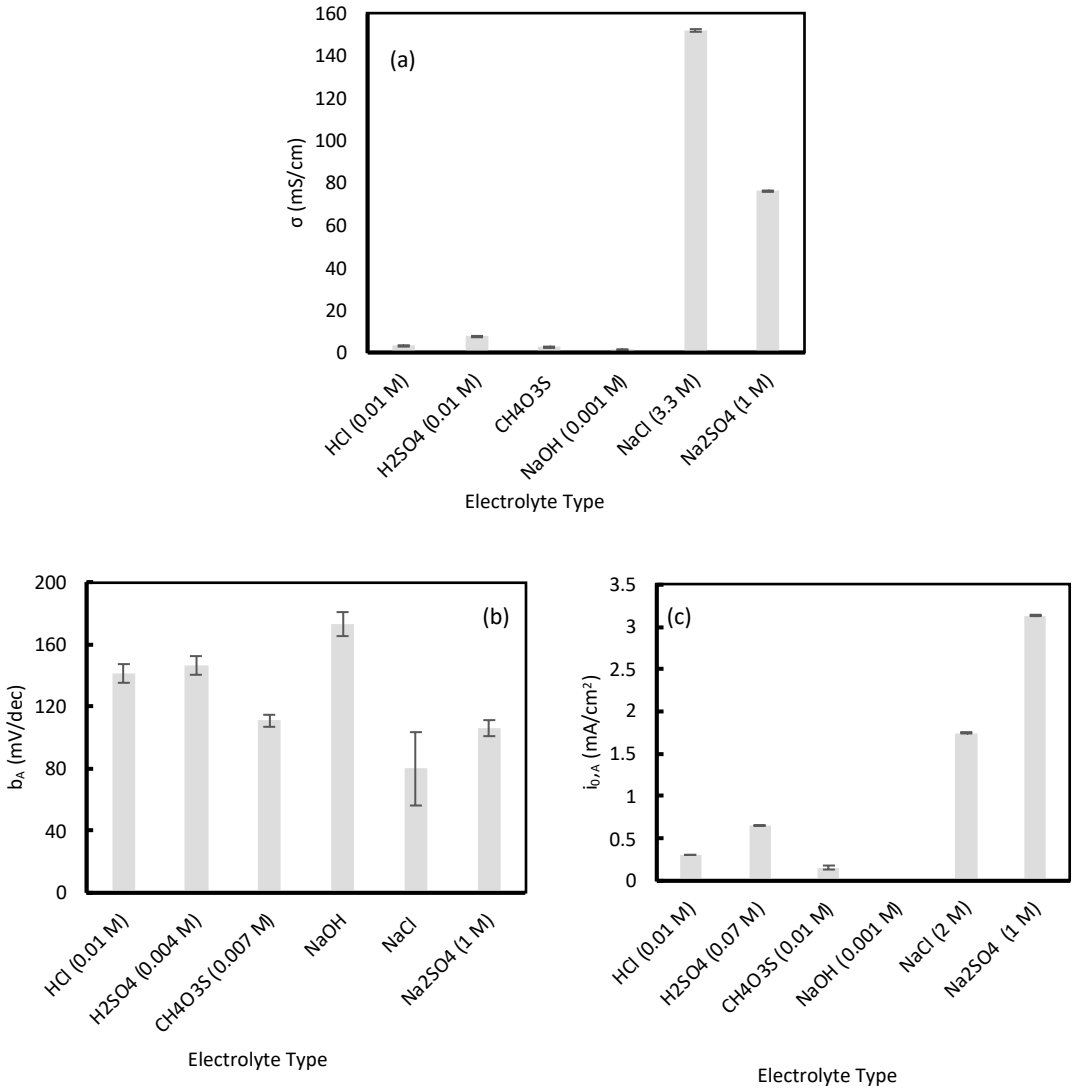

Figure 5. 23 –(a) Conductivity of electrolytes tested containing no Zn^{2+} ions, reaction kinetic parameters for electrolytes containing no Zn2+ ions (b) anodic Tafel slope and (c) anodic exchange current density

'Partially discharged' cell conditions

Similar to the 'fully charged' cell conditions, NaCl measured the greatest conductivity (see Figure 5. 24(a)). It is noticeable through comparison of Figures 5.23 and 5.24, that the conductivity increased for acids as the cell operates, however the addition of Zn^{2+} ions to the salt electrolytes decreased their conductivity. Firstly, it can be concluded due to such low acid concentrations being tested, by adding a much greater concentration of Zn^{2+} the electrolyte's conductivity should increase due to more ions being present. This typically holds true for dilute systems, however, can breakdown at high concentrations – like the salt electrolytes tested in this work. At high concentrations, the addition of more ions can cause unusual phenomena to occur e.g., ionic clusters and complex formations, causing its conductivity to reduce.

From Figure 5. 24, the smallest b_A was found in low concentrations of H_2SO_4 (0.001 M) and CH_4O_3S (0.007 M). However, with these electrolytes, a trade-off between the two kinetic parameters were apparent since the low b_A also represents low $i_{0,A}$, therefore no media tested favours both parameters. HCl was superior for obtaining the greatest $i_{0,A.}$

For the cathodic reaction, the overpotential losses were smaller for a given current in CH_4O_3S due to the lowest $-b_C$ calculated. Similar to the anodic reaction, HCl produced a large $i_{0,C.}$

Greater concentrations of electrolyte should perform better, which is correct in terms of its conductivity, correlating to more ions. The upper limit of the concentration of acid tested was chemically restricted, because, at higher concentrations of acid the WE was unstable with bubbles forming on its surface. However, the kinetic parameters were seen to be independent of the concentration of electrolyte, therefore the comparisons remained valid. Time limitations prevented further studies, in which tertiary electrolyte systems were planned to be tested with a salt, solute and acid electrolyte, enabling the investigation of the electrolyte pH characteristics without the large conductivity difference.

A notable observation which was seen between the two cell types was the appearance of the WE after completion of the LV. Experiments containing no initial Zn^{2+} ions retained its shiny-mirror like surface, only losing its shine slightly. However, in electrolytes, specifically acidic, containing Zn^{2+} ions, the WE surface appeared to have something formed on it, with a notable change in appearance (Figure 5. 25). From a literature study, it was outlined in acidic electrolytes (pH 4 - 6) the formation of non-passivating porous oxide films can form (39) which supports the noticeable change seen .

From the electrolytes tested, the salt medias, specifically NaCl, an optimal solution for the “fully charged” cell, and fairly suitable solution for the “partially discharged” cell was apparent. Selection for the latter proved challenging due to the trade-off between the Tafel slope and exchange current density. A literature report investigated the electrolyte concentration on battery performance using zinc nitrate, potassium chloride and sodium chloride. The study concluded sodium chloride produced the greatest power density (40) supporting its optimal use.

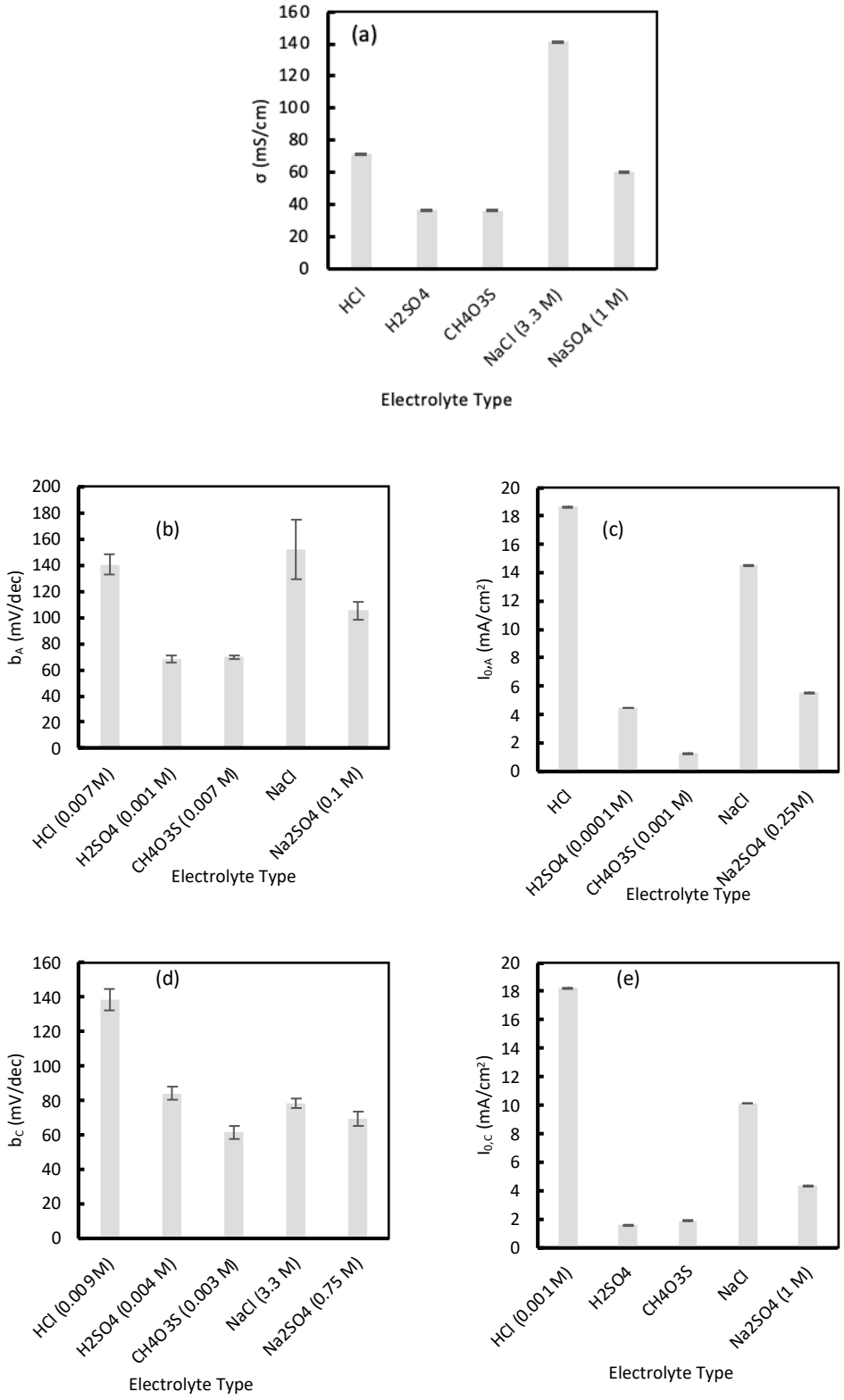

Figure 5. 24 – (a) Conductivity of electrolytes tested containing 1 M of Zn^{2+} ions , Reaction kinetic parameters for electrolytes containing 1 M Zn^{2+} ions (b) anodic Tafel slope, (c) anodic exchange current density, (d) cathodic Tafel slope, (e) cathodic exchange current density

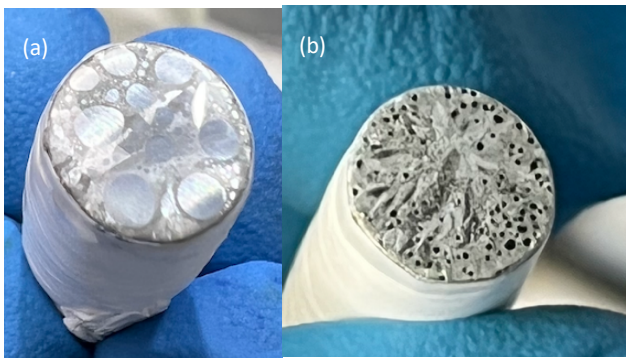

Figure 5. 25 - Changes to WE surface after completion of experiment containing (a) 1 M of $ZnSO_4$ in 0.01 M CH_4O_3S (b) 1 M $ZnCl_2$ in 0.01 M HCl

5.4 Difficulties Associated with the Results

Identifying the Linear Tafel region

The key difficulty with obtaining accurate kinetic parameters corresponding to the dissolution and deposition of zinc was the selection of the linear Tafel region. The Differential Tafel plot (DTP) method, mentioned in literature (22), was employed, where the differential of the Tafel equation was plotted against overpotential. This approach was suggested due to the differential plot being more sensitive, however it suggested the overpotential should be greater than 250 mV (an example of a DTP is shown in Appendix B.4) and therefore was unsuitable for this system.

Maintaining consistency and ensuring the selection of data was in similar regions for each experiment, the starting point originated at an overpotential of 50 mV. A trade-off between linearity and number of data plots selected was made using personal judgement. This is shown in Figure 5. 26, where a greater inclusion of data points shows a more curved line. It conveys how a singular point impacts the slope and intercept of the line, and therefore the kinetic parameters.

Although uncertainties are calculated for the Tafel parameters, the error is only associated with the linear data selected for the plot. It does not account for errors associated with the selection of data points, which is not within the scope of this project.

Limitations of this work

Ways to improve the findings of this work include:

- Completion of additional experiments at more concentration intervals to better analyse the trends. Specifically, in experiments where fluctuations were apparent. This would help to negate possible experimental and analytical error.
- Applying the KL analysis to all electrolyte types to confirm it is not viable for this work. More voltage points would be selected, as well as ensuring the current values all appear on the same point of the wave (e.g., the peak or trough).

- Constructing a more reliable experimental structure, as due to the requirements of polishing the WE and cleaning/changing the electrolyte in the Luggin capillary, the position of the components of the cell may have changed. Despite efforts to maintain consistency, error in the electrode surface and position is possible due to it not being identical.

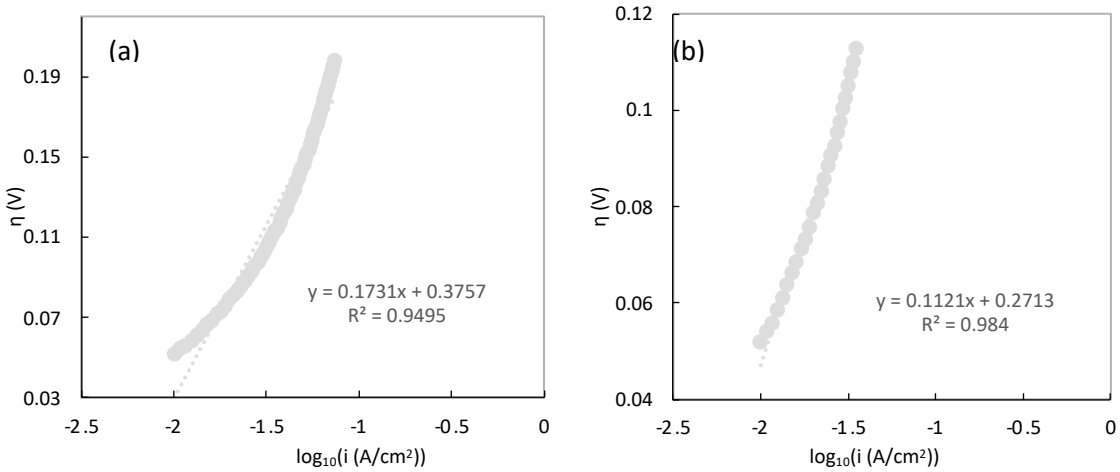

Figure 5. 26 - Example of anodic TP highlighting the sensitivity to the linear zone selected. (a) displays the plot containing 60 data points for an overpotential ranging from 52 mV to 198 mV, (b) displays the plot containing 26 data points for an overpotential ranging from 52 mV to 113 mV

Areas of Future work

With a longer project period, further objectives could involve:

- Developing a program/computer script on MATLAB® or Python® to determine the Tafel parameters more efficiently. The time saved would allow more concentrations to be tested . Likewise for the KL analysis, which would facilitate the selection of more voltage points to better represent the data.
- Investigating the effect of other parameters on the cell performance, namely, temperature.
- Study the chemical measurements by determining the chemical reaction parameters to compare with those found.

I would have liked to have continued this process for tertiary electrolytes, e.g., using large concentrations of salt, small quantity of acid and corresponding solute. Acidic pH electrolytes conductivity was limited due to the maximum concentration which could be tested before the electrode chemically degrades. The salt in the electrolyte would provide a higher conductivity, while the small addition of acid would enable the pH level to be reduced without harming the electrode. Additionally repeating this process for the cathodic half-cell (i.e., copper) would have been interesting, then from both half-cell findings, the optimal electrolyte for each could be employed in the full battery to ultimately optimise the Daniell cell. Furthermore, additional components of the

Daniell cell could be optimised, e.g., operating temperature, cell geometries and sizes, composition of salt bridges and separators.

5.5 Significance of the Results on the Organisation

The completion of this project has opened a new avenue of research for the development of Zn/Cu batteries. As the investigation focused on the performance of the Zn half-cell reaction in varying electrolytes, a similar process could be repeated for the Cu half-cell, thus full Daniell cell optimisation would be obtained.

Chapter 6. Conclusions

In conclusion, a reproducible experimental procedure was proposed after the optimisation of the method. A voltage range of -1.5 to -0.5 V and a scan rate of 10 mV/s were selected. Nitrogenation was found to be unnecessary, and an optimal EIS perturbation amplitude of 15 mV was used.

The concentration of active material in the aqueous electrolytes containing $ZnCl_2$ or $ZnSO_4$, was found to impact the reaction kinetics, therefore a fixed concentration was used for testing the different electrolytes. 0 M and 1 M of active material was used to assess the performance of the cell in its "fully charged'' and "partially discharged" states.

For the "fully charged" cell:

- NaCl electrolytes had the greatest conductivity (152 ± 0.4 mS/cm) of the electrolytes tested.
- For the anodic reaction, the lowest b_A (80 ± 24 mV/dec) was calculated in NaCl, with similar magnitudes calculated for CH_4O_3S and $NaSO_4$. The $NaSO_4$ electrolyte produced the greatest $i_{0,A}$ (3.1 ± 0.01 mA/cm^2)
- In summary, NaCl was found most favourable due to its high σ, low b_A and relatively high $i_{0,A}$.

For the "partially discharged" cell:

- NaCl was also shown to have the greatest cell conductivity (142 ± 0.1 mS/cm).
- For the anodic reaction, electrolyte medias, H_2SO_4 and CH_4O_3S, facilitated the lowest b_A (69 ± 3 and 70 ± 1 mV/dec, respectively). A trade-off between the two kinetic parameters were conveyed, where electrolyte medias with low b_A presented also a low $I_{0,A}$ and vice versa. HCL was found to produce the greatest $i_{0,A}$ (18 ± 0.01 mA/cm^2)
- For the cathodic reaction, CH_4O_3S produced the lowest $-b_C$.(62 ± 4 mV/dec), and HCl had the highest $i_{0,C}$ (18 ± 0.01 mA/cm^2)
- In summary, no favourable electrolyte was apparent.

Comparison of the two cell states concluded with difficultly in identifying the out-right optimal electrolyte. From an overview, NaCl appears to best support the cell types due to its high conductivity, and relativity advantageous kinetic parameters (high i_0 and low b).

References

1. Fossil Fuels | EESI. Available from: https://www.eesi.org/topics/fossil-fuels/description
2. History Of Batteries: A Timeline. News about Energy Storage, Batteries, Climate Change and the Environment. 2014. Available from: https://www.upsbatterycenter.com/blog/history-batteries-timeline/
3. HBU-103: Global Battery Markets. Battery University. 2010. Available from: https://batteryuniversity.com/article/bu-103-global-battery-markets
4. John B. Goodenough - The Inventor of the Li-ion Battery. Available from: https://www.fuergy.com/blog/john-b-goodenough-the-inventor-of-the-li-ion-battery
5. Löchte A. Battery management of rechargeable zinc-air batteries. Universidad de Granada; 2021. Available from: https://digibug.ugr.es/handle/10481/72051
6. Daniell Cell - MagLab. Available from: https://nationalmaglab.org/education/magnet-academy/watchplay/interactive/daniell-cell
7. ShanghaiRanking-Univiersities. Available from: https://www.shanghairanking.com/institution/polytechnic-university-of-valencia
8. Noticia UPV: The UPV ranks as the best university in Spain to study Telecommunications Engineering and Mechanical Engineering | Universitat Politècnica de València. Available from: https://www.upv.es/noticias-upv/noticia-12959-ranking-de-sha-en.html
9. Hao J et al. Deeply understanding the Zn anode behaviour and corresponding improvement strategies in different aqueous Zn-based batteries. Energy Environ Sci. 2020 Nov 12;13(11):3917–49.
10. Dong X et al. Re-building Daniell Cell with a Li-ion exchange Film. Sci Rep. 2014 Nov 5;4(1):6916.
11. Trócoli R, La Mantia F. An Aqueous Zinc-Ion Battery Based on Copper Hexacyanoferrate. ChemSusChem. 2015;8(3):481–5.
12. Mypati S et al. A novel rechargeable zinc–copper battery without a separator. J Energy Storage. 2021 Oct 1;42:103109.
13. Jameson A et al. A rechargeable zinc copper battery using a selective cation exchange membrane. J Power Sources. 2020 Mar 31;453:227873.
14. Mainar AR et al. An overview of progress in electrolytes for secondary zinc-air batteries and other storage systems based on zinc. J Energy Storage. 2018 Feb 1;15:304–28.
15. Mallick S, Raj CR. Aqueous Rechargeable Zn-ion Batteries: Strategies for Improving the Energy Storage Performance. ChemSusChem. 2021;14(9):1987–2022.

16. Shin J et al. Aqueous zinc ion batteries: focus on zinc metal anodes. Chem Sci. 2020;11(8):2028–44.
17. Shi J et al. Ultrahigh Coulombic Efficiency and Long-life Aqueous Zn Anodes Enabled by Electrolyte Additive of Acetonitrile. Electrochimica Acta. 2020 Aug 1;358:136937.
18. Nernst Equation. Chemistry LibreTexts. 2013. Available from: https://chem.libretexts.org/Bookshelves/Analytical_Chemistry/Supplemental_Modules_(Analytical_Chemistry)/Electrochemistry/Nernst_Equation
19. 6.8A: Electrical Conductivity and Resistivity. Chemistry LibreTexts. 2013 Available from: https://chem.libretexts.org/Bookshelves/Inorganic_Chemistry/Map%3A_Inorganic_Chemistry_(Housecroft)/06%3A_Structures_and_energetics_of_metallic_and_ionic_solids/6.08%3A_Bonding_in_Metals_and_Semicondoctors/6.8A%3A_Electrical_Conductivity_and_Resistivity
20. Fang Y-H, Liu Z-P. Tafel Kinetics of Electrocatalytic Reactions: From Experiment to First-Principles. ACS Catal. 2014 Dec 5;4(12):4364–76.
21. Verification of Tafel Equation (Theory) : Physical Chemistry Virtual Lab : Chemical Sciences : Amrita Vishwa Vidyapeetham Virtual Lab . Available from: https://vlab.amrita.edu/?sub=2&brch=190&sim=605&cnt=1
22. Khadke P, Tichter T, Boettcher T, Muench F, Ensinger W, Roth C. A simple and effective method for the accurate extraction of kinetic parameters using differential Tafel plots. Sci Rep. 2021 Apr 26;11(1):8974.
23. Thermodynamics and kinetics. Available from: https://www.doitpoms.ac.uk/tlplib/batteries/thermodynamics.php
24. Leung PK et al. Zinc deposition and dissolution in methanesulfonic acid onto a carbon composite electrode as the negative electrode reactions in a hybrid redox flow battery. Electrochimica Acta. 2011 Jul 15;56(18):6536–46.
25. Elgrishi N et al. A Practical Beginner's Guide to Cyclic Voltammetry. J Chem Educ. 2018 Feb 13;95(2):197–206
26. Rotating Ring Disk Electrode Fundamentals. Pine Research Instrumentation Store. 2019. Available from: https://pineresearch.com/shop/kb/theory/hydrodynamic-electrochemistry/rotating-electrode-theory/
27. Carrillo Abad J et al. Electrochemical recovery of zinc from the spent pickling solutions coming from hot dip galvanizing industries. Galvanostatic operation. In: International Journal of Electrochemical Science. Electrochemical Science Group; 2012 p. 5442–56. Available from: https://riunet.upv.es/handle/10251/63344

28. Giner-Sanz JJ et al. Harmonic Analysis Based Method for Perturbation Amplitude Optimization for EIS Measurements. J Electrochem Soc. 2017;164(13):H918–24.
29. Jorné J et al. The zinc-chlorine battery: half-cell overpotential measurements. J Appl Electrochem. 1979 Sep 1;9(5):573–9.
30. Aikens DA. Electrochemical methods, fundamentals and applications. J Chem Educ. 1983 Jan 1;60(1):A25.
31. Peacock JC, Peacock BLDeg. Some Observations the Dissolving of Zinc Chloride and Several Suggested Solvents*. J Am Pharm Assoc 1912. 1918 Aug 1;7(8):689–97.
32. Zhang XG. Corrosion and Electrochemistry of Zinc. Springer Science & Business Media; 2013. 481 p.
33. Oh S-M, Kim S-H. Aqueous zinc sulfate (II) rechargeable cell containing manganese (II) salt and carbon powder. US6187475B1, 2001. Available from: https://patents.google.com/patent/US6187475B1/en
34. Guerra E. Evaluation of zinc electrodeposition kinetics from acidic zinc sulfate solutions using a UPD modified platinum substrate. University of British Columbia; 2003 Available from: https://open.library.ubc.ca/soa/cIRcle/collections/ubctheses/831/items/1.0078683
35. McCafferty E. English: a simplified pourbaix diagram of zinc. Available from: https://commons.wikimedia.org/wiki/File:Porbaix_diagram_of_Zn.png
36. ZnCl2 + 2 NaOH → Zn(OH)2 + 2 NaCl - Balanced equation | Chemical Equations online! Available from: https://chemequations.com/en/?s=ZnCl2+%2B+NaOH+%3D+Zn%28OH%292+%2B+NaCl
37. Reichle RA et al.: Solubility Product and Hydroxy-complex Stability Constants from 12.5–75 °C. Can J Chem. 1975 Dec 15;53(24):3841–5.
38. PubChem. Sodium sulfate Available from: https://pubchem.ncbi.nlm.nih.gov/compound/24436
39. Hosseini S et al. Current status and technical challenges of electrolytes in zinc–air batteries: An in-depth review. Chem Eng J. 2021 Mar;408:127241.
40. Gmyrek KG. Effect of Electrolyte Concentration on the Performance of Batteries. 2014. Available from: https://digitalrepository.salemstate.edu/handle/20.500.13013/734
41. Levich Study (RDE). Pine Research Instrumentation Store. 2019. Available from: https://pineresearch.com/shop/kb/theory/hydrodynamic-electrochemistry/levich-study-rde/

42. Koutecky-Levich Analysis (RDE) Pine Research Instrumentation Store. 2019. Available from: https://pineresearch.com/shop/kb/theory/hydrodynamic-electrochemistry/koutecky-levich-analysis/

43. The Diffusion Coefficient of Zinc Sulfate in Dilute Aqueous Solution at 25° | Journal of the American Chemical Society. Available from: https://pubs.acs.org/doi/10.1021/ja01152a063

44. Bratsch SG. Standard Electrode Potentials and Temperature Coefficients in Water at 298.15 K. J Phys Chem Ref Data. 1989 Jan;18(1):1–21.

Appendices

APPENDIX A

Appendix A.1 – Images of experimental set-up of cell

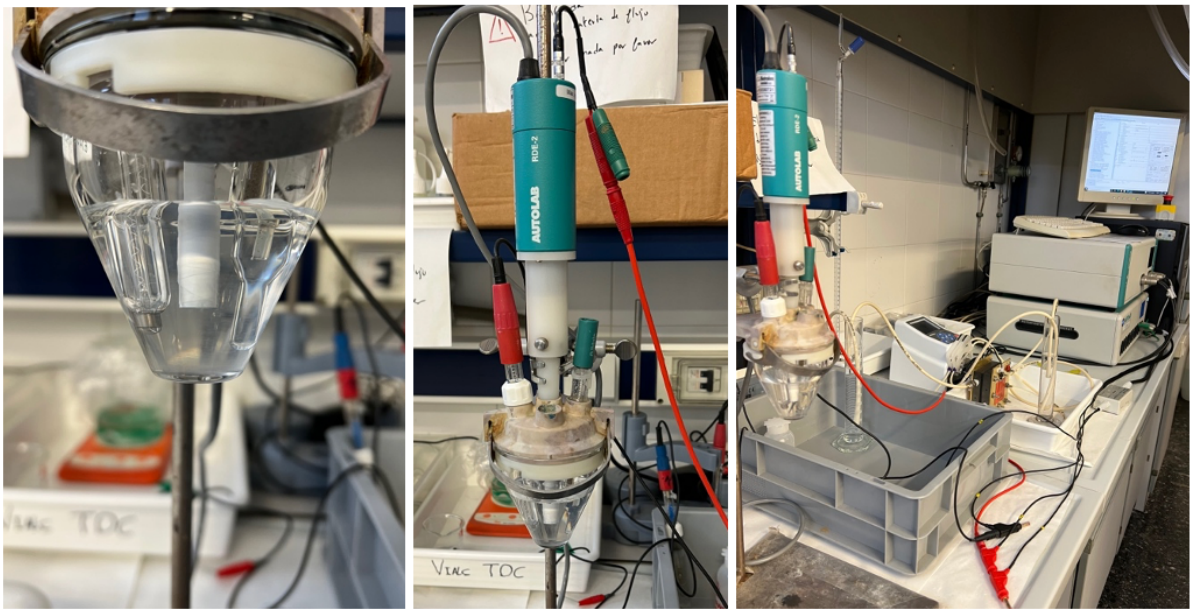

Figure A. 1 – Original experimental set up for anodic half-cell. (a) cell containing electrolyte and the three electrodes: (starting from the left) counter, working and reference. (b) larger view of cell (c) connection of half-cell to the potentiostat

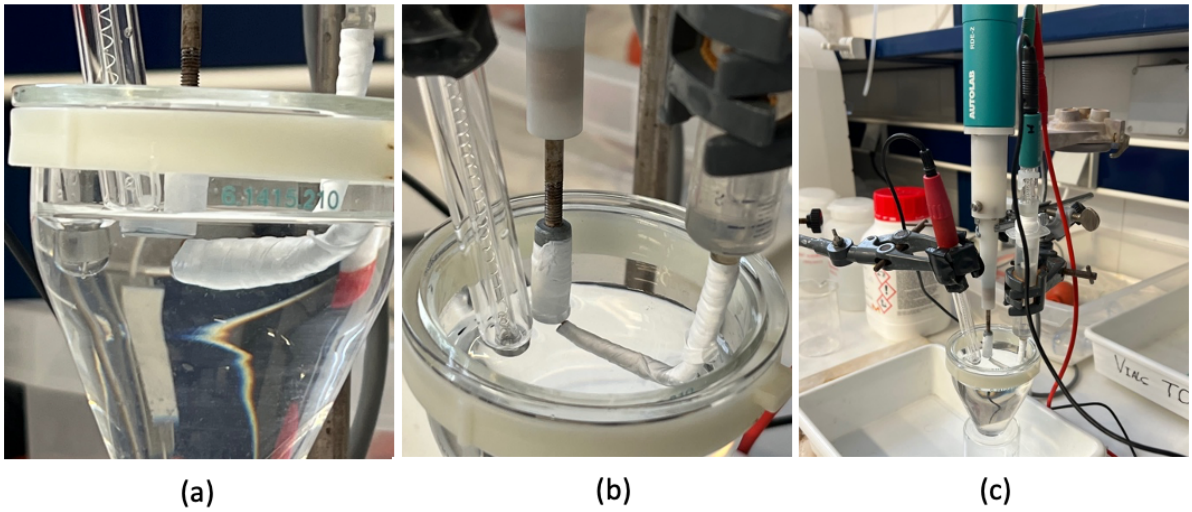

Figure A. 2 – New experimental set-up with the addition of the Luggin Capillary. In (b) the electrode on the LHS remains the counter electrode, the middle is the working electrode and the RHS shows the reference electrode inserted into the Luggin tube filled with the electrolyte solution

Appendix A.2 – Polishing of Working electrode

To obtain a shiny, mirror-like surface for the working electrode, the following steps were taken:

1. With water, the roughest sandpaper (P240) was placed on a mechanical rotating plate. The surface of the electrode to be polished was firmly placed on the wet rotating paper to obtain straight parallel lines all going in the same direction.
2. The sandpaper was replaced with a less rough type (P500), where the process was repeated however the electrode was rotated by 90, to obtain perpendicular parallel lines.
3. To finish, the least rough sandpaper (P4000) was used to remove the lines present on the electrode surface to achieve the desired mirror-like surface. The electrode was repeatedly rotated until no lines were visible on the surface and your reflection could be seen.
4. After the desired surface was achieved, the WE was rinsed with DI water, dried and carefully wrapped in Nafion enabling only the circular face to be active in the reaction.

Appendix A.3 – Tafel analysis: worked example

The steps taken to obtain the Tafel slope and exchange current density, including their errors, are presented below for the electrolyte example of 0.05 M $ZnSO_4$ in water.

1. To start the raw data of the 'best' cycle of the CV study is pasted into excel. For LV studies, this was much simpler as the two branches were plotted with no additional steps required. For this specific example, the raw data collected was plotted and shown Figure A. 3.

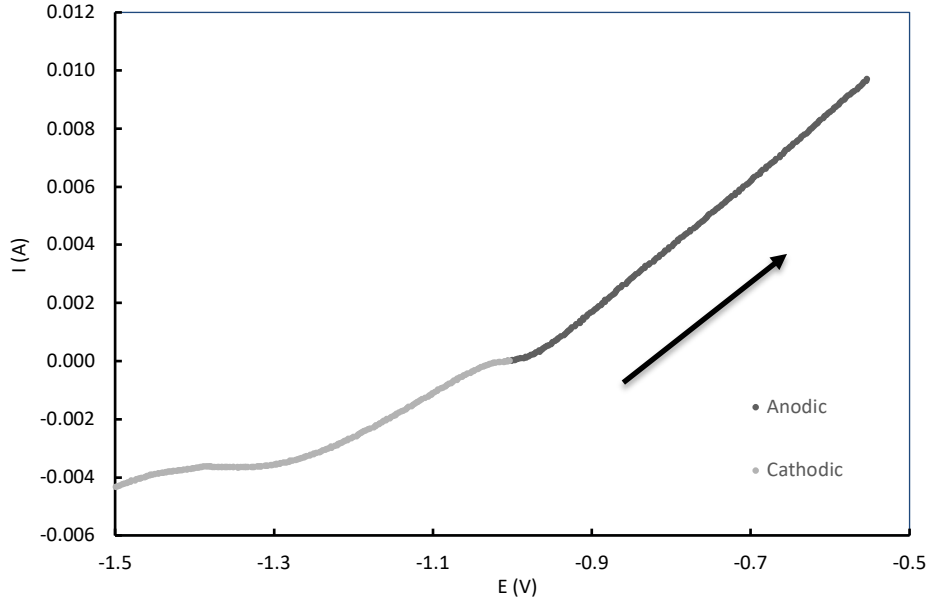

Figure A. 3 – Voltage against current for aqueous electrolyte containing 0.05 M $ZnSO_4$

2. To calculate the current density, each measured current data point was divided by the area of the WE surface, calculated using $A = \pi r^2$ where A is the surface area of the WE and r is the radius of the WE.
3. The equilibrium potential was calculated by using linear interpolation for the data points where the current changed from negative to positive.

   This equilibrium potential was subtracted from each voltage point and plotted against its corresponding current density, see Figure A. 4, where it can now be seen the data points go through the origin.

4. The logarithm of the current density was plotted against the overpotential to construct a Tafel plot, see Figure A. 5.

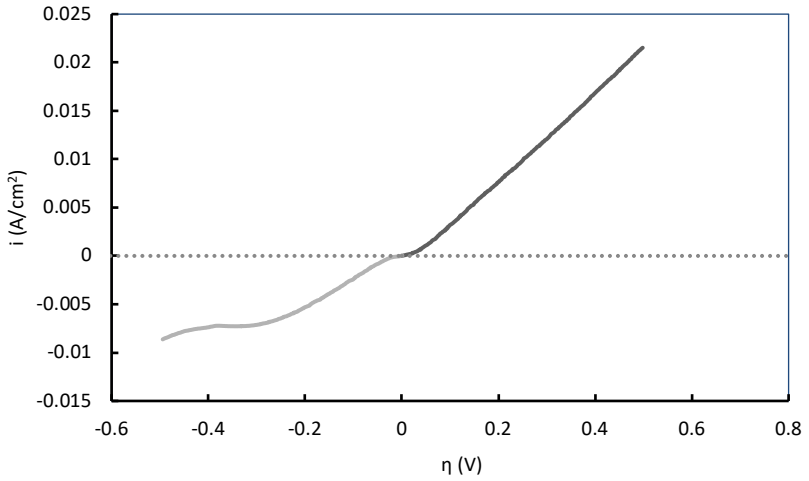

Figure A. 4 – Overpotential against current for aqueous electrolyte containing 0.05 M $ZnSO_4$

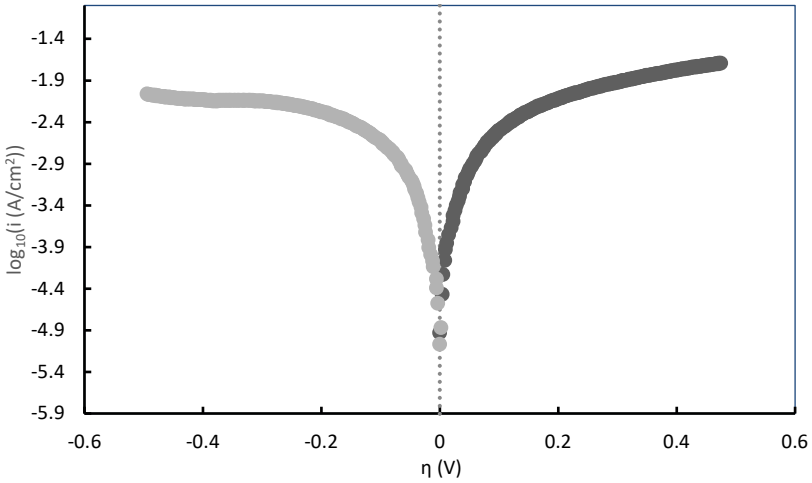

Figure A. 5 - Tafel plot for aqueous electrolyte containing 0.05 M $ZnSO_4$

5. The anodic and cathodic data was plotted separately to select the 'linear' zone of the Tafel plot for the dissolution and deposition of Zn. A linear trendline was added where the range of data points selected were adjusted until the data was linear.
6. If mass transfer limitations were shown in the original current vs voltage plot, or in the Tafel plot, a correction was made to the current. In all experiments completed, mass transfer limitations were only shown for the cathodic region. It was assumed the limiting current was equal to the minimum current density measured. The kinetic current (i_k) was found as stated in Section **Error! Reference source not found.**. The logarithm of the kinetic current was taken and plotted against the over potential. The anodic, cathodic, and corrected cathodic linear zone of the Tafel plot is shown in Figure A. 6.

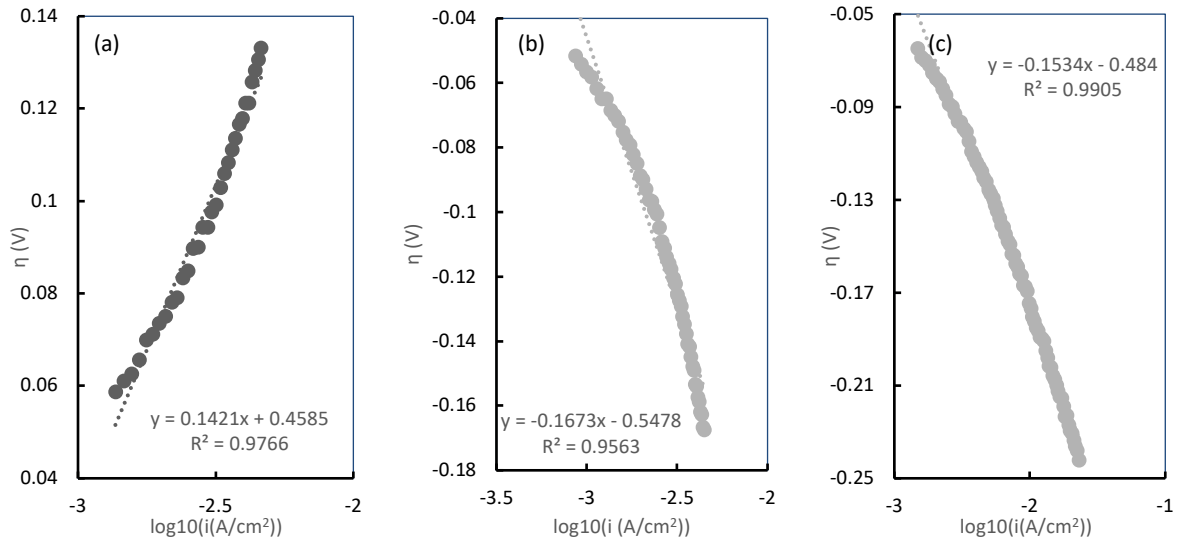

Figure A. 6 –(a)Anodic, (b)cathodic, and (c) corrected cathodic linear zone of the Tafel plot for aqueous electrolyte containing 0.05 M $ZnSO_4$

7. A 95% confidence interval of the linear data to the trendline was estimated using the LINEST Excel function, with the errors produced multiplied by a factor of 2. An example of how the Tafel slope and exchange current density was estimated from the equation of line is shown below:

$$\eta = a + b\log(i)$$

$$\eta = (\pm)\frac{2.303RT}{\alpha Fn} log_{10}(i_0) + (\pm)\frac{2.303RT}{\alpha Fn} log_{10}(\mathrm{i})$$

$$\eta = (\pm)b\ log_{10}(i_0) + (\pm)b\ log_{10}(\mathrm{i})$$

Hence, it can be seen the gradient is equal to b (the Tafel slope) = $(\pm)\frac{2.303RT}{\alpha Fn}$ and the intercept equals a = $(\pm)\frac{2.303RT}{\alpha Fn}\log(i_0)$.

Using the straight-line equation for the anodic region shown above, the anodic kinetic parameters were found as shown below:

$$y = 0.4585 + 0.1421x$$
$$\eta = (\pm)b\ log_{10}(i_0) + (\pm)b\ log_{10}(\mathrm{i})$$

b = 0.1421 V/dec = 142.1 mV/dec

$i_0 = 10^{(0.4585/-0.1421)}$ = 0.00059347 A/cm² = 0.5934 (± 0.0001) mA/cm²

Appendix A.4 – Levich and Koutecky-Levich Analysis

Underlying theory

The current signal recorded during an electrochemical experiment is easily disturbed by the convection of molecules and ions as a result of bulk movement of the solution. Control of solution movements is critical to electrochemical experiment design, where the issue of convection cannot be negated. To overcome this, a rotating disk electrode (RDE) is used to enable the steady-state mass transport regime to be reached (26).

The general theory describing mass transport at a rotating disk electrode (RDE) was developed by Benjamin Levich. He was the first to develop a mathematic expression of convection and diffusion with a rotating disk electrode (see below). Levich published this theory in 1952, which caused research expansion of using a RDE as a tool to query electrochemical reaction kinetics (41).

$$I_l = 0.620nFAD_o^{\frac{2}{3}}\nu^{-\frac{1}{6}}\omega^{\frac{1}{2}}C_o$$

$$I_l = 0.620nFAD_R^{\frac{2}{3}}\nu^{-\frac{1}{6}}\omega^{\frac{1}{2}}C_R$$

Where I_l is the limiting current, A is the electrode area, D_o and D_R are the diffusion coefficient of the oxidised and reduced form, ν is the kinematic viscosity of the solution, ω is the angular rotational speed, with all other symbols the same as previously defined. The constant (0.620) has units of $rad^{-1/2}$.

Conducting voltammetry studies using an RDE at various rotation rates (known as a Levich study) enables mass transfer limitations and slow reaction kinetics to be analysed. The current is limited by how fast the reactants can arrive or leave the surface of the electrode. This maximum current known as the limiting current. Increasing the rotational speed of the electrode, increases the rate at which the material arrives/leaves at the electrode surface hence I_{lim} increases with increase in rotation rate (26).

To determine the mass transport parameters (e.g., diffusion coefficient) and the kinetic parameters (e.g., standard rate constant), a Levich plot can be used (see Figure A. 7a). This involves plotting the peak current against its corresponding rotational speeds. Alternatively, the Koutecky-Levich (KL) equation (see below) can be used, which too expresses the electric current at the electrode to the reaction kinetics and mass transport. By plotting the reciprocal of the limiting current against the reciprocal square root of the angular rotational speed, a Koutecky-Levich plot is created (see Figure A. 7b).

$$\frac{1}{I_l} = \left(\frac{1}{0.620nFAD^{\frac{2}{3}}\nu^{-\frac{1}{6}}C}\right)\omega^{-\frac{1}{2}}$$

For a simple and reversible electrochemical half-reaction, the plateaus shown in the i-E plot will occur regardless of the ω. In a Levich plot, the I_l should vary linearly with $\omega^{1/2}$ going through the origin. This is only applicable to the limiting current; therefore, a KL plot is alternatively used. Also, for a simple, reversible half reaction, the data in a KL plot should form a straight line which intercepts the vertical axis at zero (41).

At high overpotentials there are no kinetic limitations, hence only mass transport limits the current, so the usual Levich behaviour applies. However, at lower overpotentials, the extrapolation to the vertical axis produces non-zero intercepts highlighting a kinetic limitation meaning if mass transport was infinite (i.e., infinite rotation rate) the half-reaction would still be limited by the slow kinetics at the electrode surface. If the line in a KL plot crosses the y-axis above zero, it implies the half-reaction is limited by slow kinetics opposed to mass transport. The use of Levich and KL plots enable mass transfer and kinetic parameters to be found for the system, e.g., kinetic current, diffusivity of species, standard rate constant, from the linear line (42).

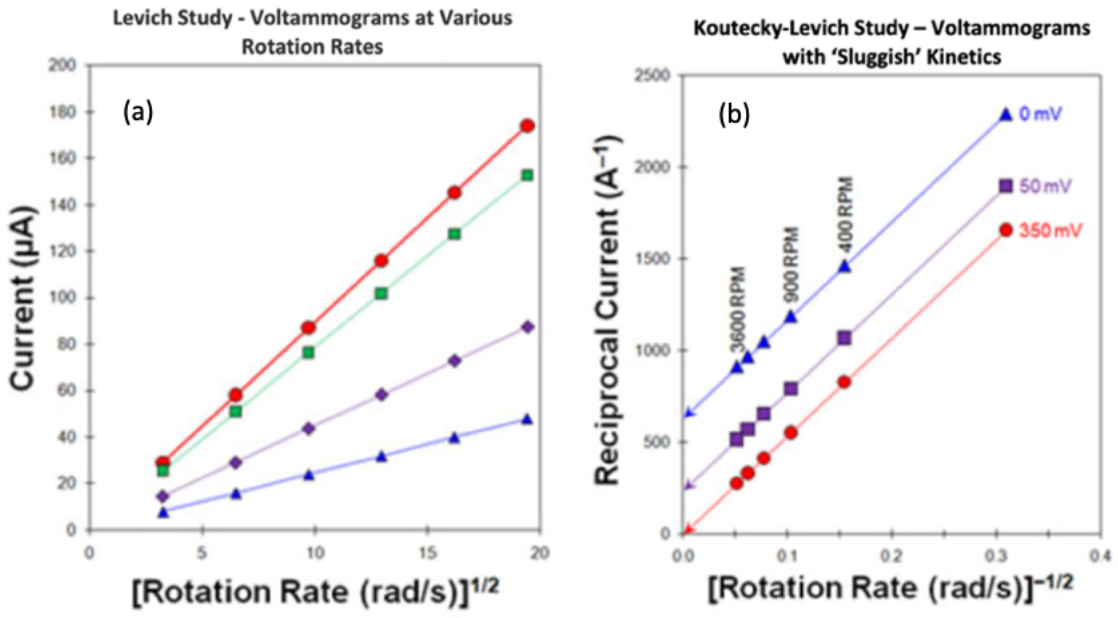

Figure A. 7 - Example of Levich and Koutecky-Levich plots (41)

Application of analysis

The method used to apply the Levich, however focused on the Koutecky-Levich analysis, has been summarised in Figure A. 8. The selection of 5 voltage points was decided as it was deemed appropriate to provide an admissible representation of the data collected mindful of the time needed to manually select the current at the stated voltage range for each rotational speed.

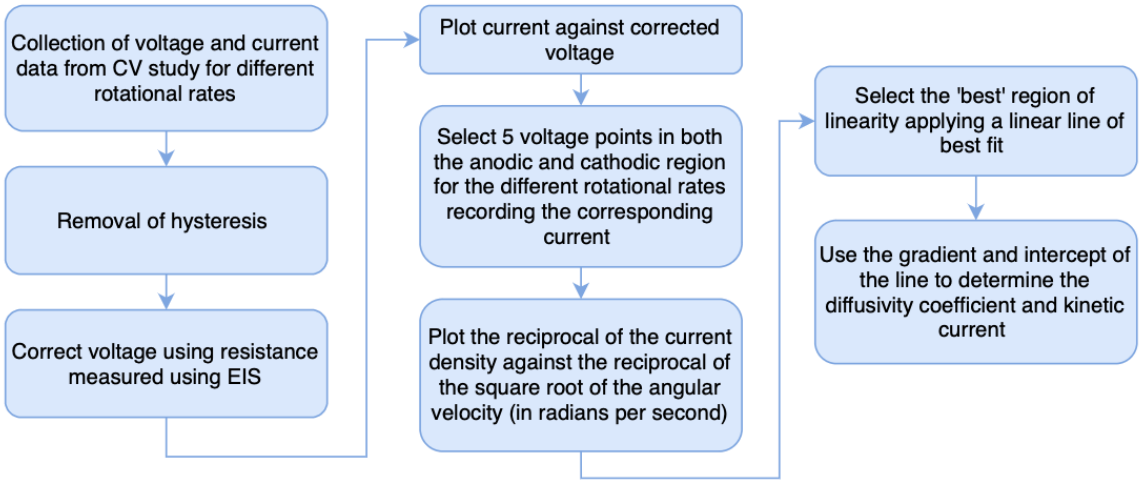

Figure A. 8 - Simplified flowchart outlining the method used to obtain reaction kinetic parameters using the Koutecky-Levich analysis

Results

Four concentrations of aqueous – $ZnCl_2$ electrolytes were tested - 0.1, 0.5, 0.75 and 1 M, with rotational speeds of 250, 500, 750, 1000, 1250 and 1500 rpm.

A Levich plot (Figure A. 9) for the aqueous electrolyte containing 0.1 M $ZnCl_2$, displays the results for the 5 anodic selected voltage points. The data does not go through the origin highlighting the reaction occurring is not within the limiting zone indicating the Levich analysis is not suitable for this system. As a result, KL plots was constructed for the 'most linear' data with the same electrolyte provided as an example, see Figure A. 10.

From literature, it was expected the lines on the KL plots would have approximately similar slopes and the data points should be parallel (41, 42). This is not the case in this instance. This caused the diffusivity coefficients to vary with voltage. As a result, the value of the diffusivity coefficients and kinetic currents for the varying electrolyte concentrations (see Figure A. 11 and A.12) carry little validity.

The diffusivity of $ZnCl_2$ for similar systems was not found in literature, however the diffusivity coefficient of 0.001 and 0.005 M of $ZnSO_4$ at 25°C was found equal to 0.721×10^5 and 0.644×10^5 cm^2/s

(43). Although difference in the sulphate and chloride ions, it was observed for greater concentrations of zinc containing electrolytes, the diffusivity decreases – this is coherent with the findings from this experiment at more negative or more positive voltage points.

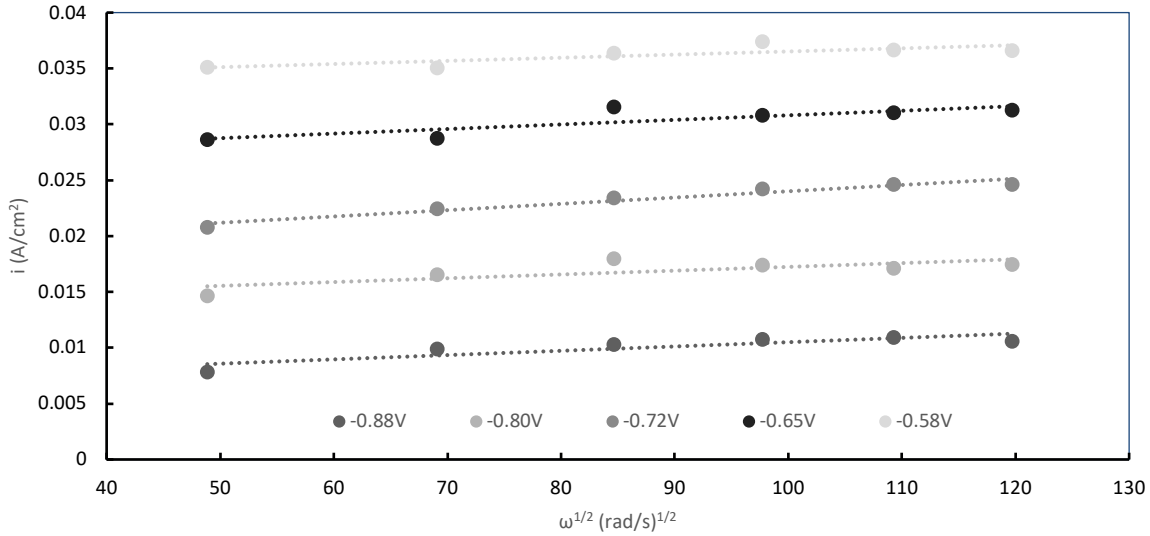

Figure A. 9 - Levich plot for the anodic data of 0.1 M $ZnCl_2$

The validity in accurately representing the system using KL analysis was compromised due to its time-consuming nature impacting the number of voltage points selected which prevented precise conclusions to be drawn. The waves due to electrode wobbling displayed on the CV using the RDE creating challenges as it was unknown if the data point selected was on the same part of the wave. Due to the large uncertainty in the KL analysis approach, it was concluded the Tafel analysis would be best used to determine the kinetic parameters, both with respect to accuracy and time.

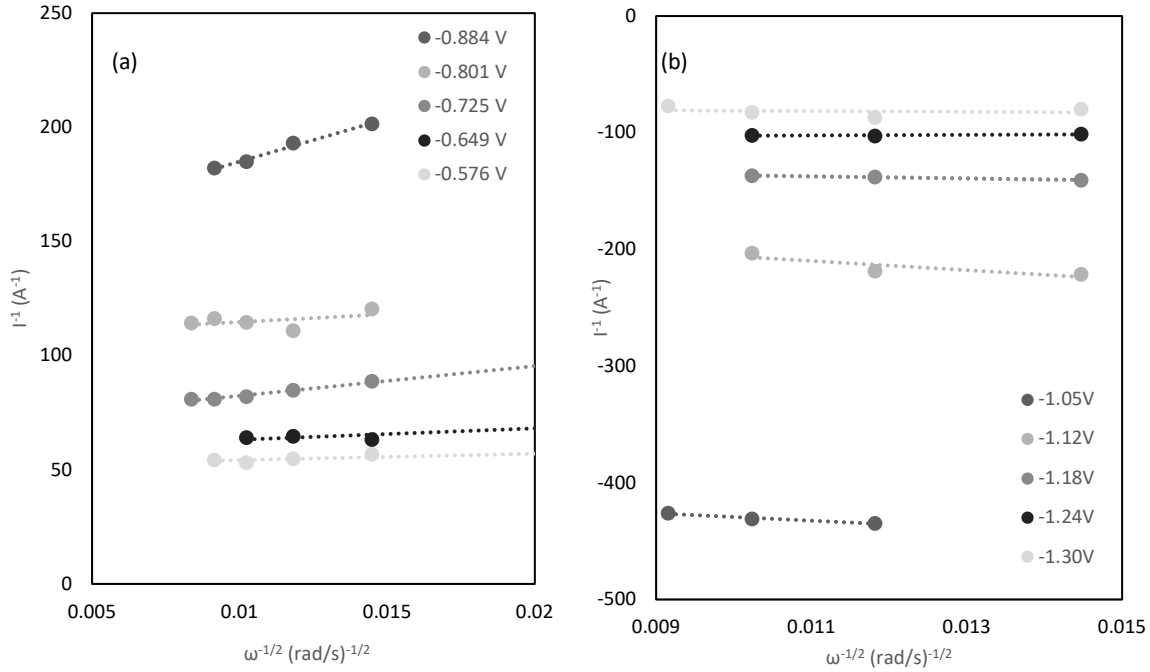

Figure A. 10 – (a) Anodic Koutecky-Levich plot for 0.1 M $ZnCl_2$.(b) Cathodic Koutecky-Levich plot for 0.1 M $ZnCl_2$.

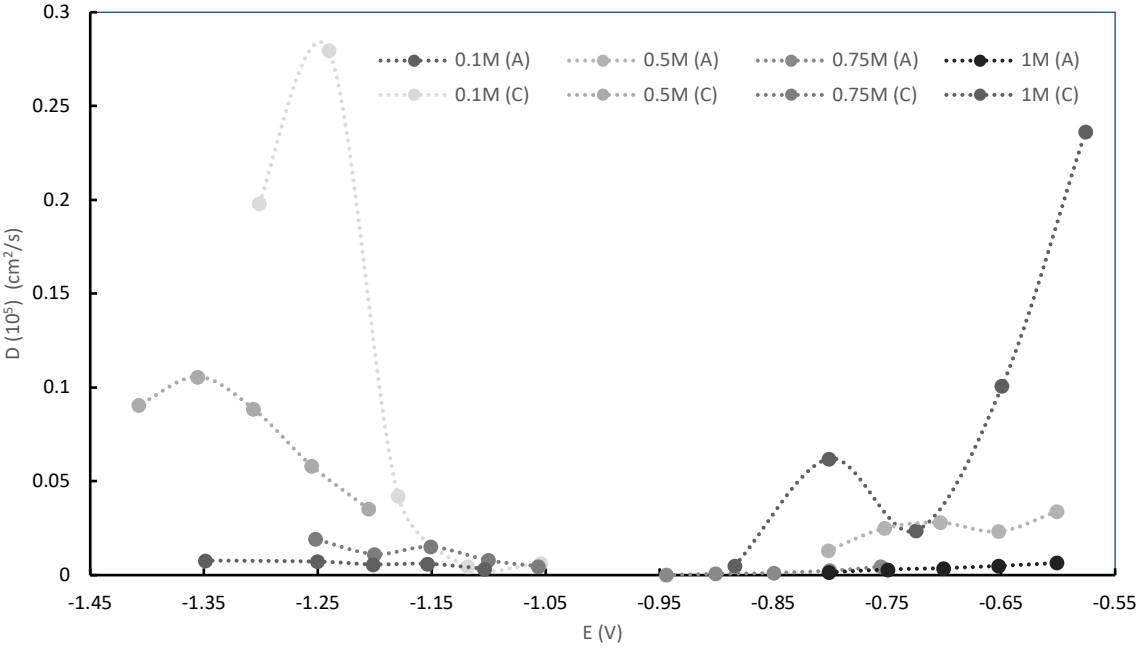

Figure A. 11 - Diffusivity coefficients for Zn for varying concentrations of $ZnCl_2$ in water electrolytes.

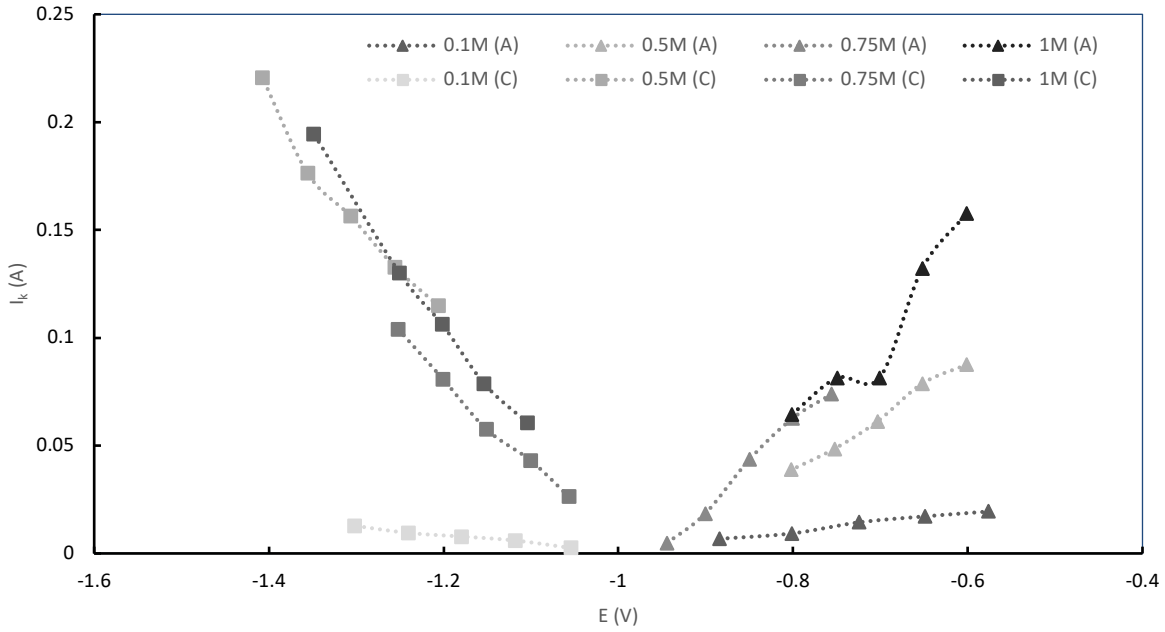

Figure A. 12 - Kinetic current for Zn for varying concentrations of $ZnCl_2$ in water electrolytes.

Worked example for the aqueous electrolyte containing 1 M $ZnCl_2$

The steps taken to apply the Levich and Koutecky-Levich are presented below for the electrolyte example of 1 M $ZnCl_2$ in water.

1. For each of the rotational rates tested – for this example, 0 rpm, 250 rpm, 500 rpm, 750 rpm, 1000 rpm, 1250 rpm, 1500 rpm – the 1st cycle of each CV study were copied into an Excel file.
2. In the next tab of the Excel file, the hysteresis of each cycle was removed in the same way it was done for the Tafel analysis.
3. Five voltage points were selected in both the anodic and cathodic region for all rotational speeds. The current corresponding to the voltage points selected were copied into another Excel tab for further processing. Figure A. 13 displays the process for selecting 5 voltage points and the corresponding current.

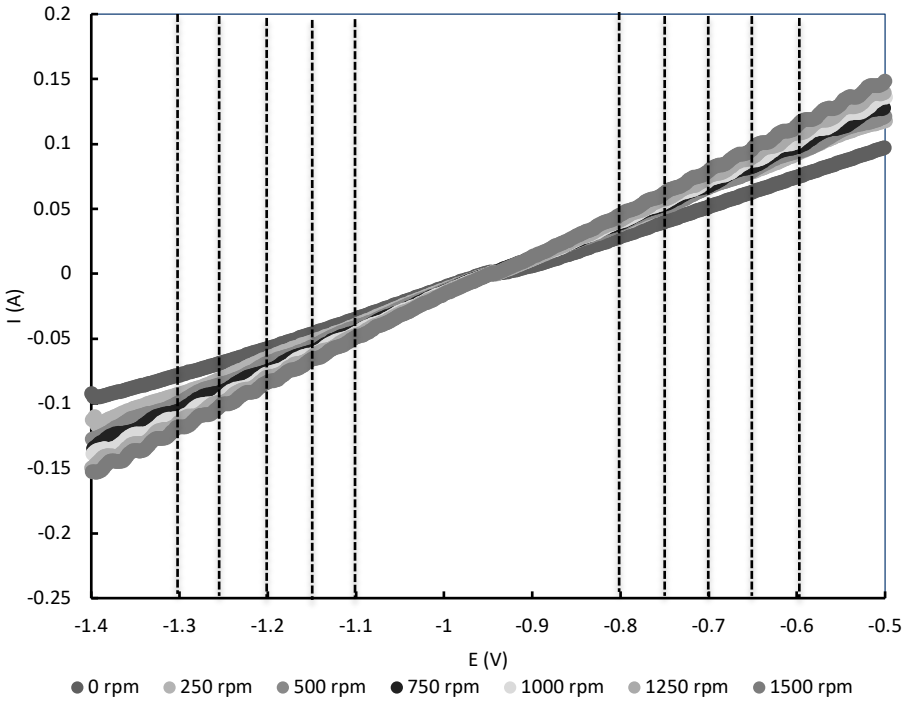

Figure A. 13 – Selection of 5 voltage points (see dotted vertical lines) from raw data for RDE CV studies for an aqueous electrolyte containing 1 M $ZnCl_2$.

4. A table was created for each voltage point, listing the current for each rotational speed. A Levich plot was created by plotting the current against the square root of the rotational rate, see Figure A. 14. From the Levich equation, the limiting current should increase linearly with the square root of the rotation rate (with a slope of $0.620nFAD^{2/3}v^{-1/6}C$ where n is the number of electrons, F is Faraday's constant, A is the surface area of the WE, D is the diffusivity coefficient, v is the kinematic viscosity of the electrolyte and C is the concentration of the electrolyte). It is evident from the Figure A. 14; the lines of the five selected voltage points do not appear linear. This analysis is based on the limiting current therefore does not apply to systems experiencing mass transfer limitations or sluggish kinetics.

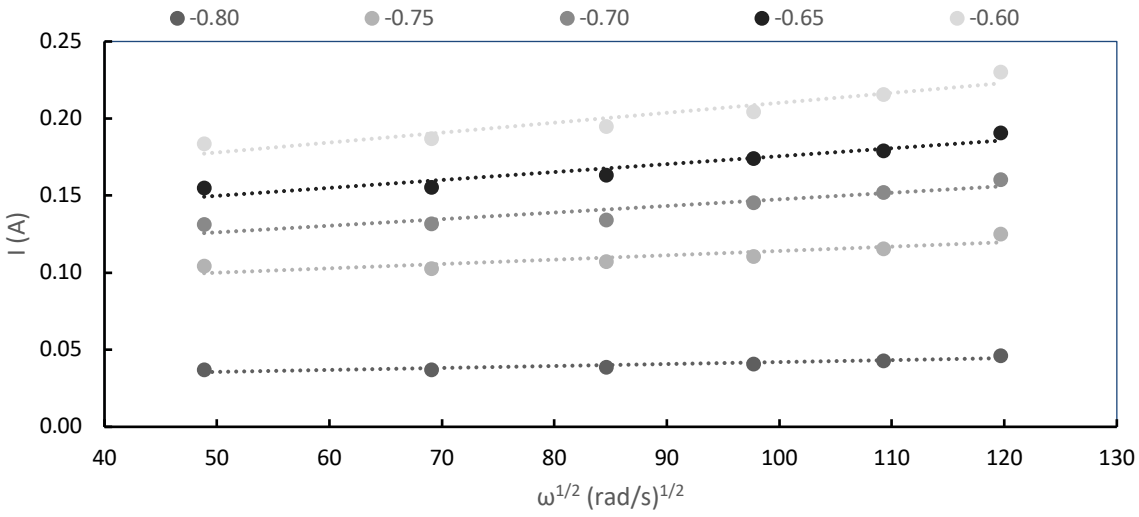

Figure A. 14 – Anodic Levich plot for an aqueous electrolyte containing 1M $ZnCl_2$, using voltage points of -0.8, -0.75, -0.7, -0.65 and -0.6 V

5. The current density was estimated by dividing the current by the surface area of the working electrode ($A=\pi r^2$). To create the Koutecky-Levich plot, the reciprocal current was plotted against the reciprocal square root of the rotational rate. This is applicable to systems with a simple reversible half reaction. The data should fall as straight parallel lines and cross the y-axis at 0. The KL plot, for this example see Figure A. 15, where it can be seen each of the voltage lines are not parallel nor have a 0 y-intercept. This highly suggests the half-reaction is limited by sluggish kinetics rather than by mass transport limitations.

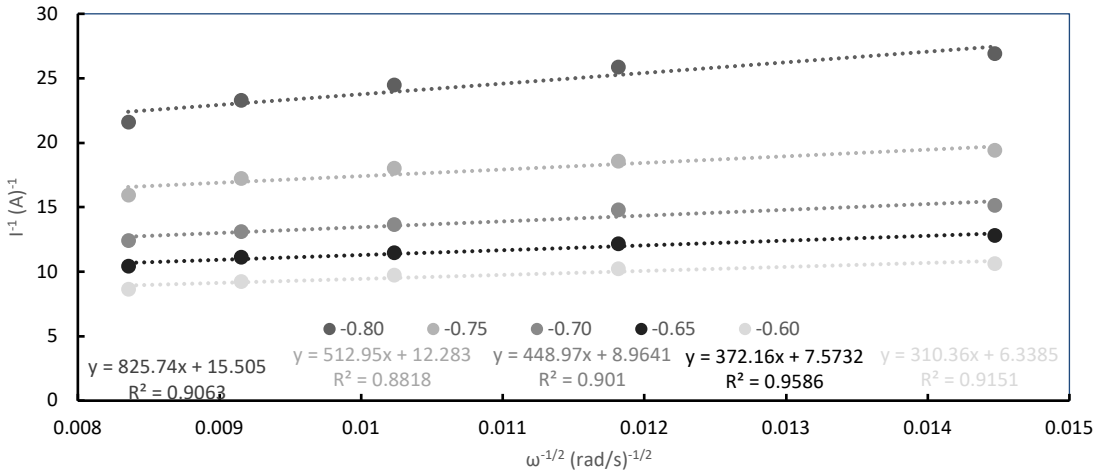

Figure A. 15 - KL Plot for an aqueous electrolyte containing 1 M $ZnCl_2$, using voltage points of -0.8, -0.75, -0.7, -0.65 and -0.6 V

6. Using the trendline linear equation, the diffusivity coefficient of Zn ions and the kinetic current could be found by relating it to the KL equation:

$$\frac{1}{I_L} = \frac{1}{I} + \left(\frac{1}{0.620nFAD^{\frac{2}{3}}\nu^{-\frac{1}{6}}C}\right)\omega^{-1/2}$$

It can be seen the gradient is equal to $\left(\frac{1}{0.620nFAD^{\frac{2}{3}}\nu^{-\frac{1}{6}}C}\right)$ and the intercept is equal to $1/i_k$. Using the example of the voltage line, 0.8V, where the equation of the trendline is:

$$y = 825.74x + 15.505$$

The other variable within the gradient term is assumed constant, where the following values were set:

$$n = 2$$

$$F = 96486 \text{ mol/C}$$

$$A = 0.794 \text{ cm}^2$$

$$\nu = 0.011386 \text{ cm}^2/\text{s (was assumed equal to water)}$$

$$C = 0.001 \text{ mol/cm}^3$$

Therefore, the constant value equalled 0.00499. The diffusivity was found by diving the constant value by the gradient of the line raised to the power of 3/2, see below:

$$gradient\ of\ line = \frac{constant}{D^{\frac{2}{3}}}$$

$$D = \left(\frac{constant}{gradient\ of\ line}\right)^{3/2}$$

$$D = \left(\frac{0.00499}{825.74}\right)^{3/2} = 1.49 \times 10^{-8}\,\frac{cm^2}{s}$$

The kinetic current can be found by taking the reciprocal of the intercept of the line:

$$i_K = \frac{1}{intercept\ of\ line} = \frac{1}{15.505} = 0.064\ A$$

This process is repeated for each of the voltage points; however, it would be expected the diffusivity coefficient would be the same due to parallel lines having the same gradient.

APPENDIX B

Appendix B.1 – Comparison of CV study with and without Luggin Capillary Tube

Noticeable difference in the resistance of the electrolyte measured by the EIS study before and after the CV encouraged possible change in the experimental set-up to minimise the uncompensated resistance. When reviewing literature, it was apparent many studies used a Luggin capillary (LC) tube to direct the conductive path between the WE and RE to minimise this uncompensated resistance.

A CV study was completed using the new experimental set-up with a previously recorded study containing the same electrolyte (Figure B. 1). It was found the data from each study appeared very similar, where the EIS study with the LC presented a negligible resistance. The inclusion of the LC was used for all future experiments.

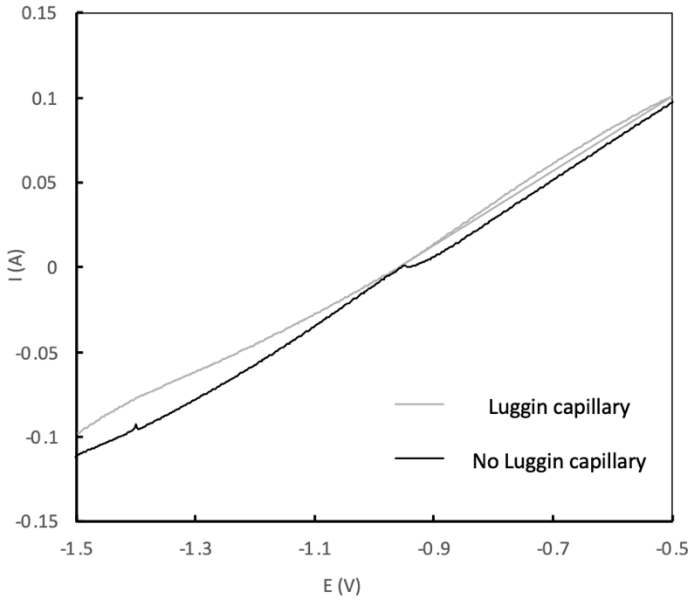

Figure B. 1 - Comparison of CV studies for 1 M $ZnCl_2$ solution with and without the Luggin capillary

Appendix B.2 – OCP experiment using aqueous $ZnCl_2$

Part 1

A 5 M $ZnCl_2$ aqueous solution was initially prepared. It was diluted 29 times - samples 2 to 19 used 45 ml, samples 20 to 25 used 35 ml and samples 26 to 29 used 25 ml of the previous sample solution making up the remaining volume of water – were an OCP experiment measuring the voltage (E_{OCP}) for 300 seconds for approximately 0 current supplied was run for each sample.

The average of the E_{OCP} values recorded for each sample was estimated including a 95% confidence interval and plotted with the theoretical values using the Nernst equation. The temperature of the

electrolyte measured consistently at 20°C during the experiment. The results for each sample is shown in Figure B. 2(a).

The theorectical values calculated using the Nernst equation were found using H_2 as the RE at a temperature of 25°C. A temperature correction obtained from literature (44), see below, and a correction of 0.165 V was subtracted from the Nernst values to change the RE to Ag/AgCl – the same as the experimental values.

$$E_T^o = E_{298}^o + (T - 298.15)\left(\frac{dE^0}{dT}\right)_{298}$$

Where E^0_T is the equilibirum potential as a function of the temperature, E^0_{298} is the equilibirum potential at a temperature of 298K, T is the temperature, $\left(\frac{dE^0}{dT}\right)_{298}$ is the differential of the equilibrium potential at 298K.

The experimental values displayed coherence with the theoretical values estimated using the Nernst equation from a concentration of 0.37 M to 1.03 M. As expected, deviations are shown as the concentration increases, however deviations were also shown at low concentrations.

Part 2

To further investigate the experimental behaviour at lower concentrations, a similar experiment was completed testing 5 different concentrations of $ZnCl_2$: 4, 2, 1, 0.5 and 0.1 M, where the results are shown in Figure B. 2(b). The findings similarly deviate at greater concentrations, however greater similarity to Nernst is seen at lower at concentrations. This suggests a possible contamination at lower concentrations in the previous experiment.

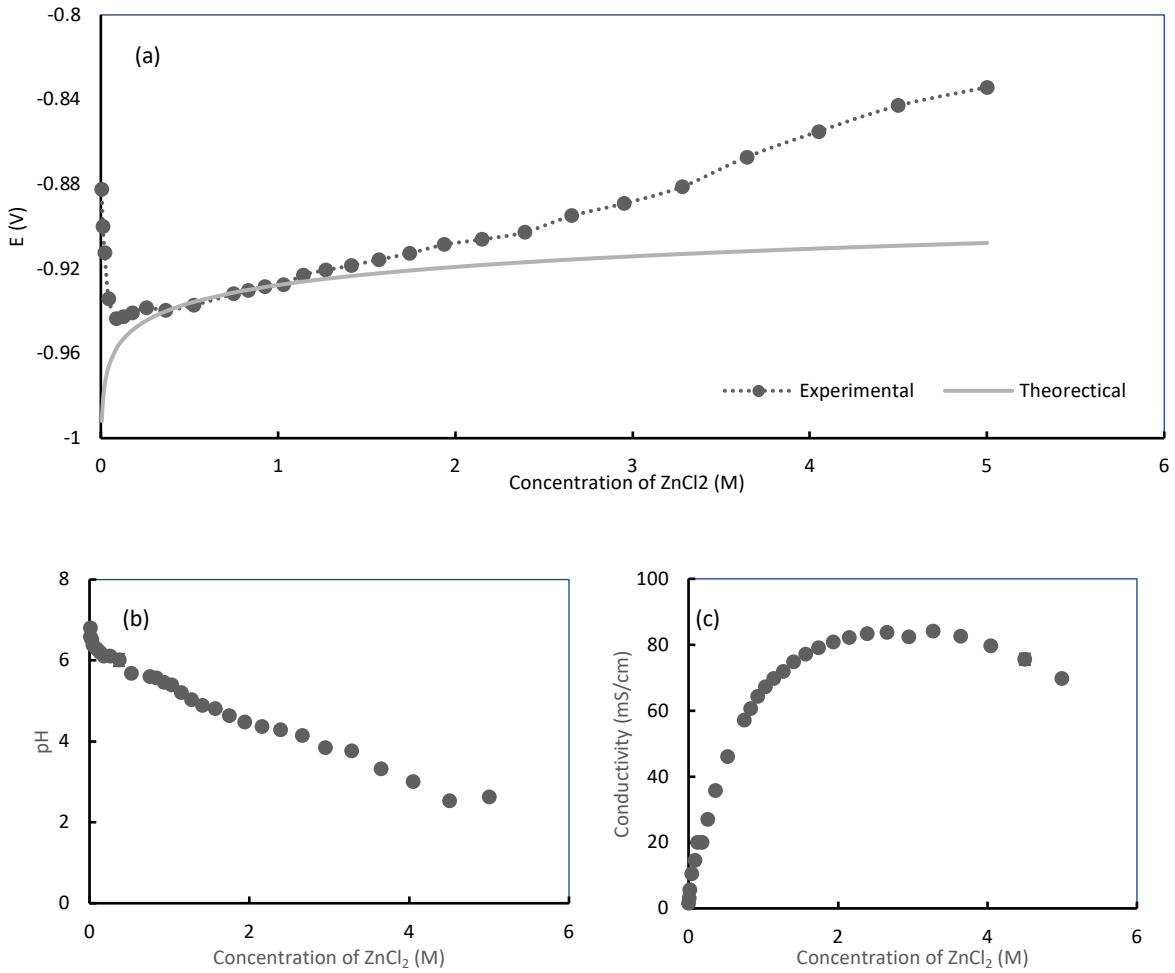

Figure B. 2 – (a) Voltage recorded at a zero current plotted for varying concentrations of aqueous-$ZnCl_2$ electrolytes. Inclusion of theoretical values using the Nernst equation. (b) Variation in pH and (c) conductivity for different concentrations of ZnCl2 and water electrolyte. Inclusion of error bars however the errors are often too small to be seen.

It was noticeable in the preparation of the electrolyte solution, the $ZnCl_2$ power was clumpy suggesting possible moisture being retained within the powder. To investigate this impact on the possible deviation in experimental E_{OCP} to the theoretical value, 8 - 20-gram samples of $ZnCl_2$ were weighed out and placed in an oven at provisionally 120 ^oC, soon increased to 150 ^oC and lastly increased to 200^o C investigate the possible impact in water content present. The samples were left in the oven for over 72-hours at each temperature.

The mass of each dish measured was plotted, see , where it was noticeable the water content present was negligible where extremely small changes in the mass of $ZnCl_2$ were measured for its duration in the oven.

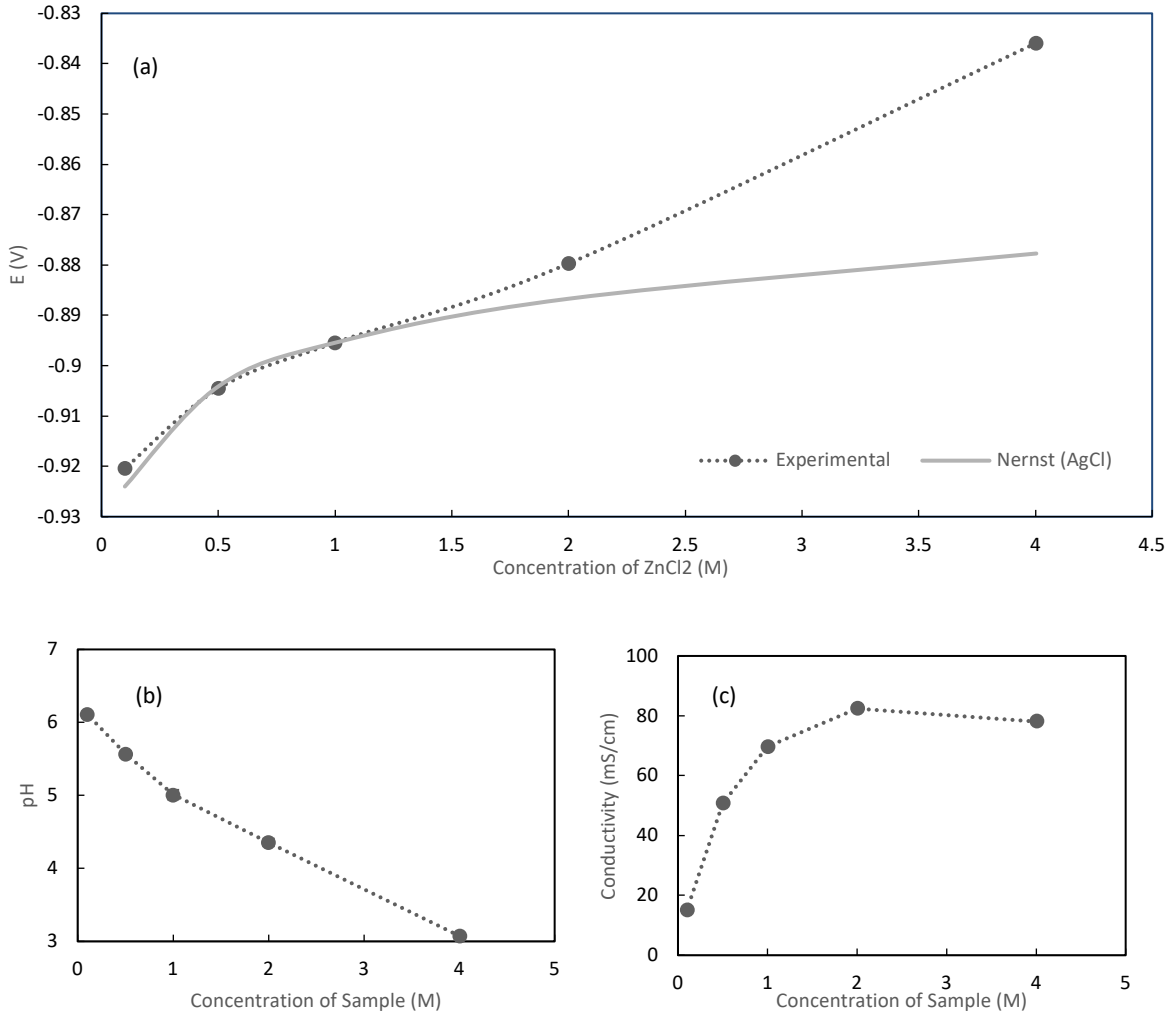

Figure B. 3 -(a) Voltage recorded at a zero current plotted for varying concentrations of aqueous-$ZnCl_2$ electrolytes. Inclusion of theoretical values using the Nernst equation. (b) Variation in pH and (c) conductivity for different concentrations of ZnCl2 and water electrolyte. Inclusion of error bars however the errors are often too small to be seen.

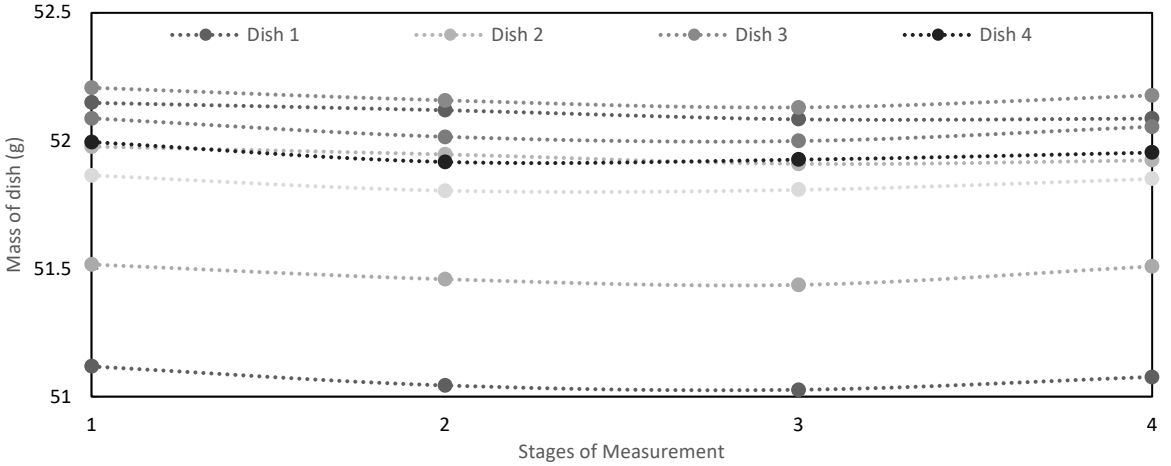

Figure B. 4 - Trend in Mass of dish containing $ZnCl_2$ for 3 measured temperature stages. Stage 1 is the initial weight before placement in the oven, Stage 2 is the mass of dish measured after being in the oven at 120^{o}C, Stage 3 is after being in the oven at 150^{o}C and Stage 4 is after being in the oven at 200^{o}C.

Part 3

It was noticed during the completion of each OCP experiment, the system needed time to stabilise. This raised concern of the stability of the system. As a result, a 100ml aqueous solution containing a 1M of $ZnCl_2$ was created and halved. An OCP test was run for 300 seconds using the first half of the solution. The other half of the solution was tested twice with the results shown a slow steady increase in the OCP value measured. Lastly, the OCP of the solution was measured for 1 hour where the voltage recorded with time is shown in Figure B. 5.

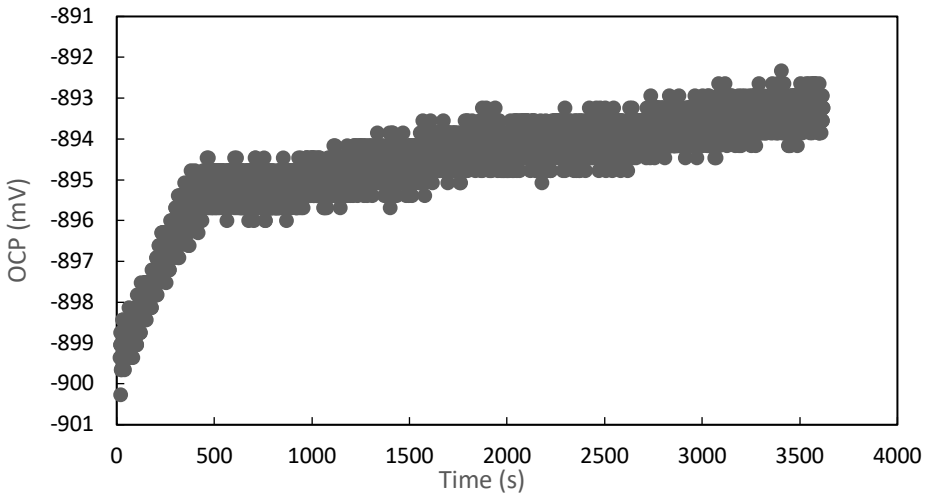

Figure B. 5 – Measured voltage at zero current for 3600 seconds for an 1M of Aqueous $ZnCl_2$ containing electrolyte.

Summary

The average OCP across the three experiments conducted are presented in Table B. 1.

Table B. 1 – Summary of average OCP for the 3 experiments completed.

Experiment No.	Experiment Details	Av. OCP (mV)
1	Solution 1: 50ml solution of a 100ml 1M $ZnCl_2$ and water solution recording the voltage with zero current applied for 300 seconds.	-894.15 ± 0.40
2.1	Solution 2: 50ml solution of a 100ml 1M $ZnCl_2$ and water solution recording the voltage with zero current applied for 300 seconds.	-903.15 ± 0.29
2.2	Solution 2: 50ml solution of a 100ml 1M $ZnCl_2$ and water solution recording the voltage with zero current applied for 300 seconds.	-901.02 ± 0.39

3	Solution 1: 50ml solution of a 100ml 1M $ZnCl_2$ and water solution recording the voltage with zero current applied for 3600 seconds.	-894.59 ± 0.03
Nernst	Theoretical calculation using Nernst equation with reference to AgCl and a temperature of 21°C	-898.23

The OCP was found to fluctuate over time, specifically seen in the Figure B. 5. This could be a result of the extremely small current passing through the zinc causing a very slow electrochemical reaction causing changes to the zinc electrode surface

The OCP values experimentally determined are however of similar scale to the theoretical value obtained using the Nernst equation.

Appendix B.3 – Pourbaix Diagram for Zinc

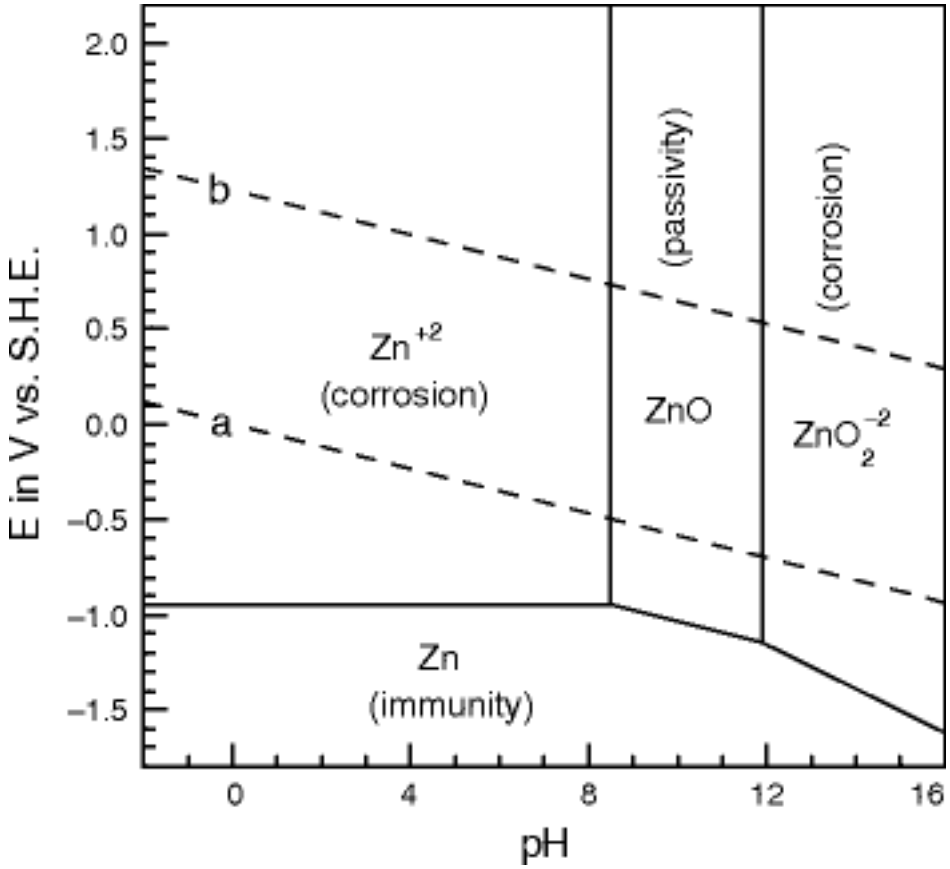

Figure B. 6 -Pourbaix diagram for Zn (40)

Appendix B.4 – Example of DTP for Aqueous electrolyte containing 1 M $ZnCl_2$

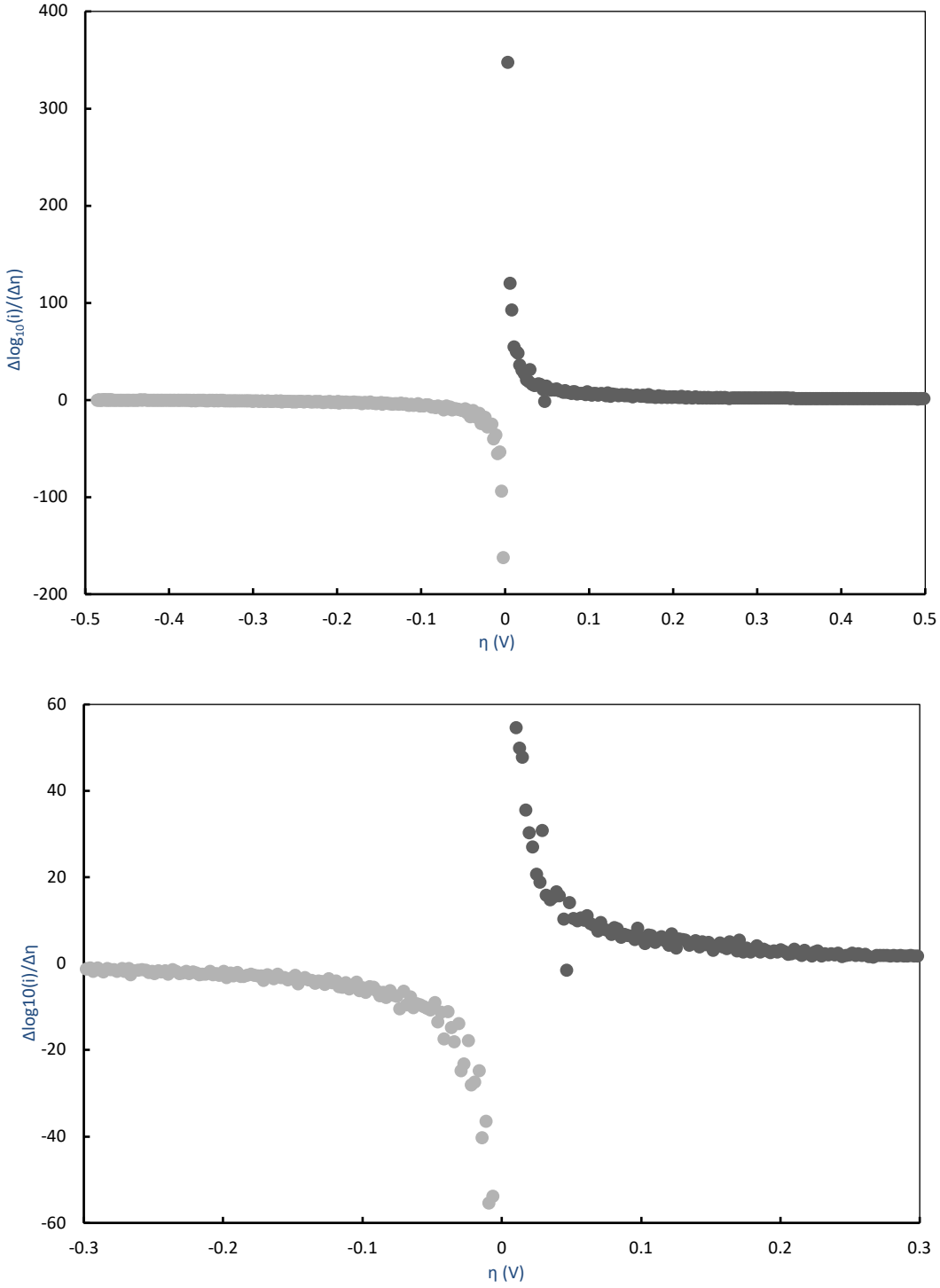

Figure B. 7 –(a) Differential Tafel plot (DTP) for aqueous electrolyte containing 1M $ZnCl_2$, (b) Zoomed in DTP shown in (a)

BUDGET

Chapter 1. Budget

1.1 Budget for the preparation of the Final Degree Project

This chapter outline the budget needed to experimentally carry out this final degree project. It is budgeted for the experiments completed in the laboratory using an anodic half-cell of the Daniell cell, including the materials, machinery and instruments used, and the labour required.

Within the calculation, VAT was estimated equal to 21% and electricity consumption, air conditioning and cleaning were approximated and listed in the final total as general expenses.

The calculation is based on a cell working life of 10 years, where each years contains 250 working days with each day operation of 8 business hours. The industrial benefit is negated since it is academic work.

The following code is used in the calculations:

Code	Description
WO	Workforce
MT	Materials
MA	Machinery and instrumentation

1.1.1 Table of labour prices

Table X outlines the price of the labour needed to complete the work. To calculate the cost of labour, the "Recommendations in the preparation of budgets in R&D&I activities revision 2018" of the Universitat Politècnica de València hae been taken into account.

Table 1 – Projected labour budget

Code	Unit	Description	Amount		
			Cost (€/Hr)	Quantity (Hr)	Total (€)
WO1	Hr	Graduate Chemical Engineer	12.16	600	7296.00
WO2	Hr	Masters Tutor	23.8	20	476.00
WO3	Hr	Masters Professor	40	60	2400.00
Total Cost (€)					10172.00

The budget of labour equates to **ten-thousand one-hundred and seventy-two euros.**

1.1.2 Table of prices of machinery and instrumentation

The machinery and instrumentation are estimated based on depreciation, as opposed to the original purchase cost.

Code	Unit	Description	Amount		
			Cost (€/Hr)	Quantity (Hr)	Total (€)
MA1	Hr	AUTOLAB PGSTAT 302N + Booster 20 A	12	64	768.00
MA2	Hr	pH meter	1.28	64	81.92
MA3	Hr	Conductivity meter	1.28	64	81.92
Total Cost (€)					931.84

The budget of machinery and instrumentation equates to **nine-hundred and thirty-one thousand one hundred and eighty-four cents.**

1.1.3 Table of material prices

The determination of the cost of the material is based on the materials used in this project.

Code	Unit (U)	Description	Amount		
			Cost (€/U)	Quantity (Hr)	Total (€)
MT1	ud	Volumetric flask (1000 mL)	18.88	1	18.88
MT2	ud	Volumetric flask (100 mL)	11.85	1	11.85
MT3	ud	Volumetric flask (50 mL)	5.15	0.5	2.58
MT4	ud	Box of gloves latex (100 units)	9.05	0.5	4.53
MT5	kg	Zinc Chloride (97% ACS)	11.88	2	23.76
MT6	kg	Zinc Sulphate Heptahydrate (99.0-102.0% ACS)	9.14	2.5	22.85
MT7	L	Hydrochloric acid (35.0-36.6%)	8.30	0.2	1.66
MT8	L	Sulphuric acid (96%)	13.97	0.01	0.14
MT9	L	Methansulfonic acid (98%)	134.13	0.1	13.41
MT10	Kg	Sodium Hydroxide	34.49	0.2	6.90

MT11	Kg	Sodium Chloride (99.9% ACS)	7.58	0.5	3.79
MT12	500 g	Sodium Sulphate	5.96	1.5	8.94
MT13	ud	Zinc cylindrical bar electrode	9.39	1	9.39
MT14	ud	Silver/Silver Chloride electrode	40.95	1	40.95
MT15	ud	Platinum electrode	13.74	1	13.74
MT16	ud	Electrochemical cell*	29.41	1	29.41
Total Cost (€)					212.78

The budget of materials equates to **two-hundred and twelve pounds and seventy-eight pence.**

*This includes the wiring, structure (three clamps), glass beaker (200 mL).

1.1.4 Total Budget

Section	Cost (€)
WO	10172
MA	931.84
MT	212.78
General Expenses (10%)	1131.66
VAT (21%)	2614.14
Total	15062.42

The total budget of this project equates to **fifteen-thousand and sixty-two pounds and forty-two pence.**